HEINRICH HEINE
UNIVERSITÄT
DÜSSELDORF

Ultrafast optical spectroscopy of the electron transfer and protein dynamics in Photosystem II

Inaugural-Dissertation

zur Erlangung des Doktorgrades
der Mathematisch-Naturwissenschaftlichen Fakultät
der Heinrich-Heine-Universität Düsseldorf

vorgelegt von

Malwina Szczepaniak
aus Kościan

Düsseldorf/Mülheim an der Ruhr, December 2008

aus dem Max-Planck-Institut für Bioanorganische Chemie, Mülheim an der Ruhr

Gedruckt mit der Genehmigung der
Mathematisch-Naturwissenschaftlichen Fakultät der
Heinrich-Heine-Universität Düsseldorf

Referent:	Prof. Dr. Alfred R. Holzwarth
Koreferent:	Prof. Dr. Georg Pretzler
Tag der mündlichen Prüfung:	28.01.2009

Contents

Abbreviations

β-DM	*n*-dodecyl-β-D-maltoside
Car	β-carotene
Chl	chlorophyll
CS	charge separation
CP	chlorophyll-binding protein
cyt	cytochrome
DAS	decay-associated (emission) spectrum
DCM	4-(dicyanomethylene)-2-methyl-6-(p-dimethylaminostyryl)-4H-pyran
DCMU	3-(3,4-dichlorophenyl)-1,1-dimethylurea
Phe or F	phenylalanine
EET	excitation energy transfer
ET	electron transfer
EPR	electron paramagnetic resonance
FeCN	$K_3[Fe(CN)_6]$
FTIR	Fourier-transform infrared spectroscopy
FWHM	full-width at half-maximum
IRF	instrument response function (=PR)
MES	2-(*N*-morpholino)ethanesulfonic acid
Mn_4Ca	manganese cluster
OD	optical density
OEC	oxygen-evolving complex
OPO	optical parametric oscillator
Pheo	pheophytin *a*
PQ pool	plastoquinone pool
PSI	Photosystem I
PSII	Photosystem II
Q_A	primary quinone electron acceptor
Q_B	secondary quinone electron acceptor
PR	prompt response (= IRF)
RC	reaction center
RP	radical pair
SAES	species-associated (emission) spectrum
SC	streak camera
SPT	single photon timing
TCSPC	time-correlated single photon counting
T. elongatus	*Thermosynechococcus elongatus*
TMH	transmembrane helix
Tyr or Y	tyrosine
TyrD	Tyrosine D of PSII (D2-Y160)
TyrZ	Tyrosine Z of PSII (D1-Y161)
WT	wild type

1 Introduction

1.1 Photosynthesis

Photosynthesis is one of the most important biological processes. Plants, algae and photosynthetic bacteria convert the relatively easily accessible solar energy into chemical energy in the form of organic compounds (for a review on photosynthesis see (*1*), or the following books: (*2*;*3*) and many others, as well as the information present also in the Internet: (*4*)). Oxygenic photosynthetic organisms have the ability to utilize carbon dioxide, release molecular oxygen and produce carbohydrates from CO_2 and H_2O. The most general equation describing oxygenic photosynthesis can be written in the form:

$$CO_2 + H_2O \xrightarrow{\text{light}} O_2 + [CH_2O] \tag{1.1}$$

Photo-induced water splitting together with the associated electron and proton transport steps take place in the thylakoid membrane (Fig. 1-1). There the stepwise electron transfer along the membrane is coupled to pumping of protons across it (Fig. 1-2).

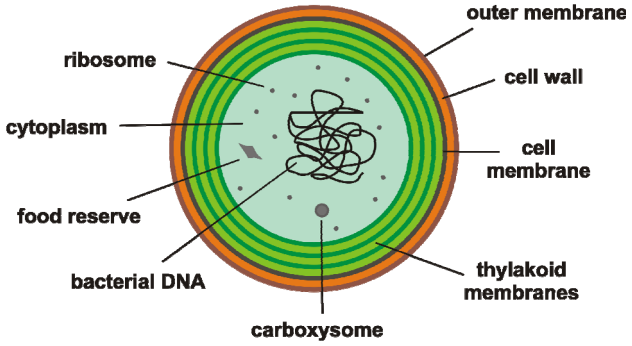

Fig. 1-1 Schematic cyanobacterial cell showing the thylakoid organization.

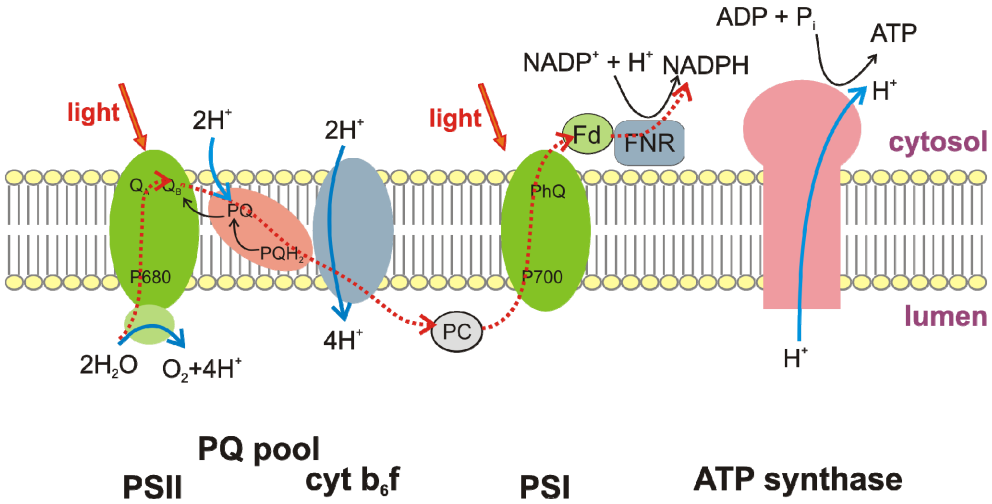

Fig. 1-2 Schematic representation of a thylakoid membrane with shown protein complexes. Electrons are transferred from photosystem II along the membrane through cytochrome b_6f to photosystem I (shown as red dotted line so called Z-scheme). Protons are pumped across the thylakoid membrane (blue solid lines). PQ pool – plastoquinone pool, PC – plastocyanin, Fd – ferredoxin, FNR - Fd:$NADP^+$ oxidoreductase.

1.2 Photosynthetic complexes

Though cyanobacteria have much simpler cell organization than *e.g.* higher plants, they possess full photosynthetic apparatus, embedded in the thylakoid membrane. This membrane embraces a number of protein complexes: the pigment-protein complexes Photosystem I (PSI), Photosystem II (PSII), and the working in between PSII and PSI cytochrome b_6f, as well as the ATP synthase (Fig. 1-2).

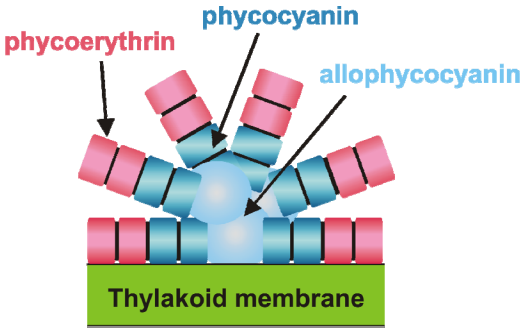

Fig. 1-3 Schematic representation of a cyanobacterial thylakoid membrane with attached phycobiliproteins: allophycocyanin, phycocyanin and phycoerythrin. The figure was adapted from (*5*).

Cyanobacteria use bound to the membrane phycobilisomes to harvest light and deliver it to the reaction centers (Fig. 1-3). The antenna complexes are composed of a number of water-soluble proteins, so-called phycobiliproteins, which bind the chromophores capable of absorbing light in the spectral range (500-650 nm) – the phycobilins. This spectral range is essentially inaccessible to the basic light-harvesting pigments – chlorophylls. Due to their specific architecture, phycobiliproteins deliver solar energy very efficiently to the antenna chlorophylls of PSI and PSII. Subsequently the energy is transferred to the reaction centers (RCs) of PSI and PSII, where it is utilized in the redox reactions, finally leading to O_2, ATP and NADPH production.

There are also other pigments, except for chlorophylls and phycobilins, present in the cyanobacterial photosynthetic apparatus. Carotenoids play a dual role: apart from their light harvesting function, they protect the photosynthetic complexes from the dangerous triplet state of chlorophylls and the subsequently formed reactive oxygen species (called ROS), like *e.g.* singlet oxygen.

The photons captured by the extended antenna system are delivered to the RCs, where their energy is utilized for the charge separation process and the electron transfer to the secondary electron acceptors. In case of PSII the primary electron donor is reduced *via* TyrZ by the manganese cluster. The latter is involved in the water oxidation process. The electron acceptor, quinone Q_B is loosely bound to its binding pocket, and after double electron delivery and double protonation leaves its site and enters the plastoquinone pool. Q_BH_2 delivers electrons to cytochrome b_6f, and gets deprotonated. The protons of Q_BH_2 are released on the lumenal side of the membrane, while the electrons are further transported by plastocyanin, a soluble protein, to PSI. The electrons are used for the reduction of P700 (primary electron donor in PSI), which was beforehand oxidized in a charge separation process upon

illumination. PSI passes electrons to a Fe-S protein, called ferredoxin, and then to the Fd:$NADP^+$ oxidoreductase, where NADPH is released. During the water oxidation and the electron transport through the cytochrome b_6f complex, protons are released on the luminal side of the thylakoid membrane. This results in generation of a proton gradient across the membrane necessary for the production of ATP by another protein complex embedded in the thylakoid membrane, the ATP-synthase (*2;6*).

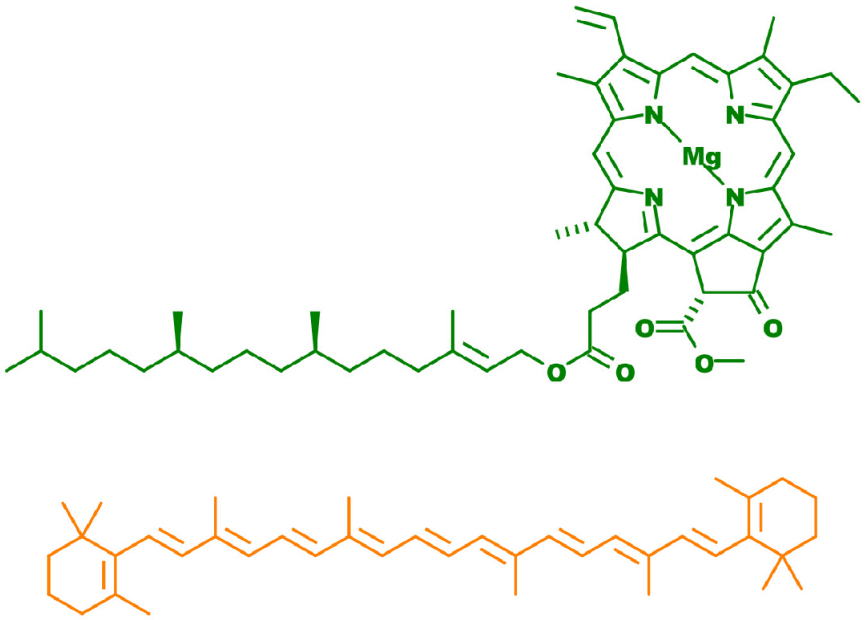

Fig. 1-4 Structures of the most abundant photosynthetic pigments found in PSII: *(top panel)* chlorophyll *a* and *(bottom panel)* β-carotene.

1.3 Photosystem II core complex

The minimal PSII preparation capable of oxygen evolution is the PSII core complex. Its structure has been recently determined to high resolution (from 3.5 down to 3.0 Å) (*7;8*) (for a review on PSII structure and functions see (*9;10*)). In higher plants, algae and cyanobacteria PSII forms homodimeric structures, with 20 protein subunits and 77 cofactors: among them 35 chlorophylls *a* (Chls), 2 pheophytins *a* (Pheos), 11 β-carotenes (Cars) and 2 quinones (Q) per monomer (Fig. 1-4, Fig. 1-5 and Fig. 1-10).

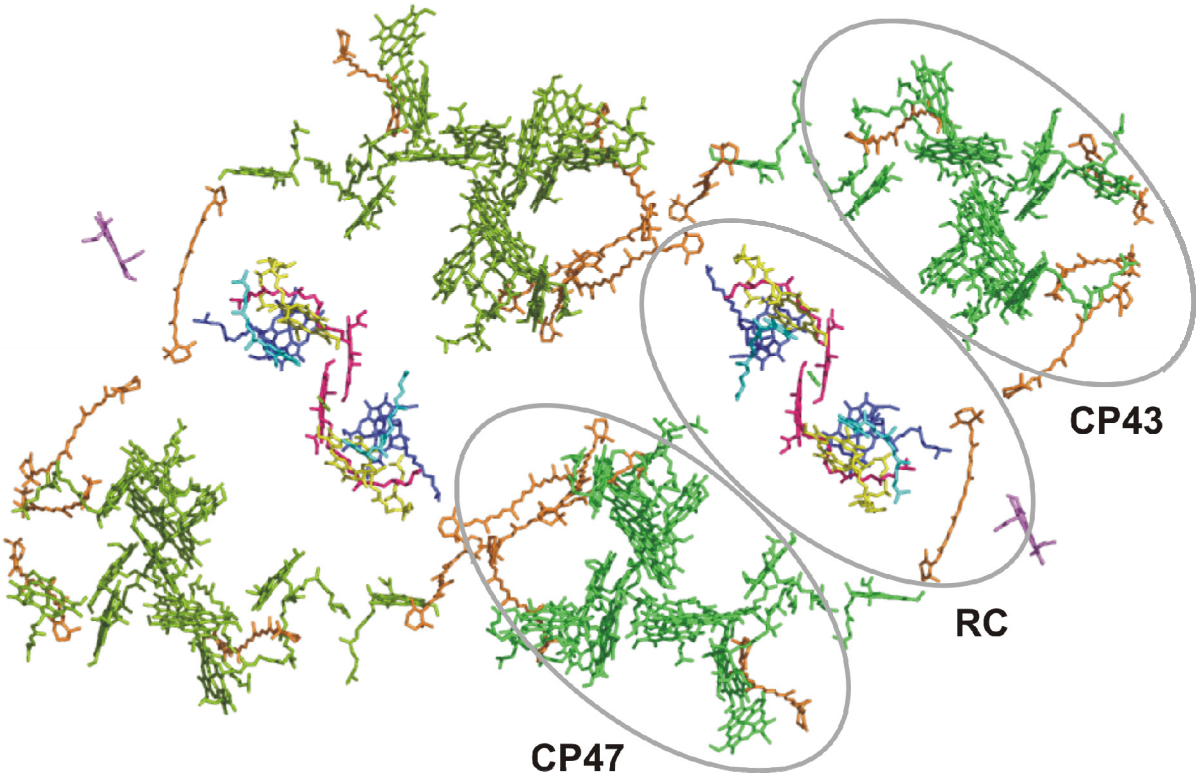

Fig. 1-5 PSII core dimer pigments, shown without the protein matrix (top view). In each monomer the antenna Chls are shown in green, Cars in orange, the RC Chls: P_{D1} and P_{D2} in magenta and Chl_{accD1} and Chl_{accD2} in blue, pheophytins $Pheo_{D1}$ and $Pheo_{D2}$ in yellow, quinones Q_A and Q_B in cyan, and cyt *b-559* in violet. The antenna complexes, CP43 and CP47, and the RC of one monomer are shown with grey elipses. The figure was prepared on the basis of the file 2AXT.pdb (*8*).

1.3.1 PSII structure

Reaction center

The RC is the central part of the PSII core monomer, surrounded by the antenna complexes, CP43 and CP47. It consists mainly of two polypeptide chains D1 and D2 (see Fig. 1-6); each of them comprises five transmembrane helices (TMH). RC binds 6 Chls (two historically called "primary donor" Chls, P_{D1} and P_{D2}, two accessory Chls, Chl_{accD1} and Chl_{accD2}, and finally two peripheral Chls, $Chlz_{D1}$ and $Chlz_{D2}$), 2 Pheos ($Pheo_{D1}$ and $Pheo_{D2}$), 2 quinones (Q_A and Q_B), and 2 Cars (Car_{D1} and Car_{D2}) arranged in the pseudo-C2 symmetry (Fig. 1-7). In addition, the X-ray structure reveals the manganese cluster (Mn_4Ca), a non-haem iron, 1 to 2 bicarbonates, and 2 cytochromes: cyt *b-559* and cyt *c-550* (*8;9*).

The D1 side cofactors (bound to the D1 protein P_{D1}, Chl_{accD1}, $Pheo_{D1}$, and Q_B and additionally bound to the D2 subunit Q_A) take $_{active}$ part in the electron transfer process, while the D2 side of the RC is inactive under physiological conditions (see section 1.3.2). TyrZ delivers electrons to the oxidized P_{D1}^+, and afterward is reduced by the Mn_4Ca cluster, which splits water to dioxygen. The actual role of TyrD is still unclear, however various redox and electrostatic functions of TyrD have been postulated: due to some electrostatic interaction it probably can direct the charge separation on the D1 side of the RC, it can also get oxidized by P_{D1}^+, but on a much longer time scale than TyrZ (*11*). The remaining cofactors, cyt *b-559*, both

peripheral chlorophylls ($Chlz_{D1}$ and $Chlz_{D2}$), and Car_{D2} are supposedly involved in an alternative cyclic electron transfer induced in case the oxygen evolution is blocked (*e.g.* at low temperatures or when the usual reduction pathway of P_{D1}^{+} is blocked). In this alternative electron transfer pathway Car_{D2} donates an electron to P_{D1}^{+}, whereas cyt b-559 and $Chlz_{D1}$ are able to donate electrons to Car_{D2}^{+} (*12-14*). On the basis of the structural arrangement, Car_{D1} is not considered as an element of the secondary electron transfer pathway, rather its function is associated with the transfer and/or quenching of the $Chlz_{D1}$ triplet states and the quenching of singlet oxygen (*8*). Hence, the D1 branch of the PSII RC is directly involved in the absorbed light energy utilization and water splitting, whereas the D2 side takes part in the protection against photodamage.

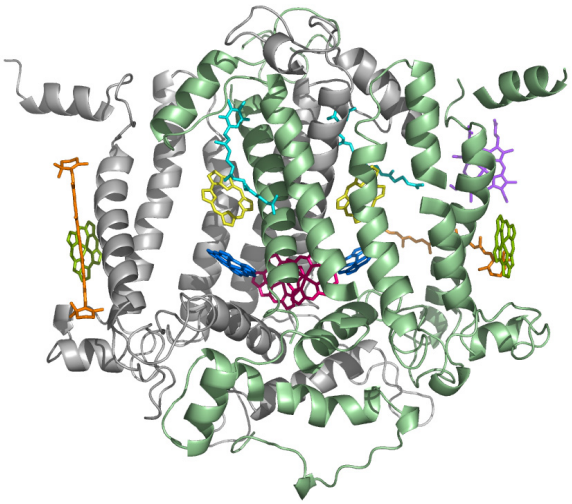

Fig. 1-6 PSII RC cofactors embedded in the protein matrix: D1 is shown as grey ribbon and D2 as green ribbon (side view). Color coding of the RC cofactors as in Fig. 1-5. For better clarity Chls and Pheos are presented without the phytol chains. The figure was prepared on the basis of the file 2AXT.pdb (*8*).

However, the biochemical isolation procedure of the RC polypeptides results in a so-called D1-D2-cyt *b-559* preparation, which lacks both the quinones and the water splitting complex (*15-17*).

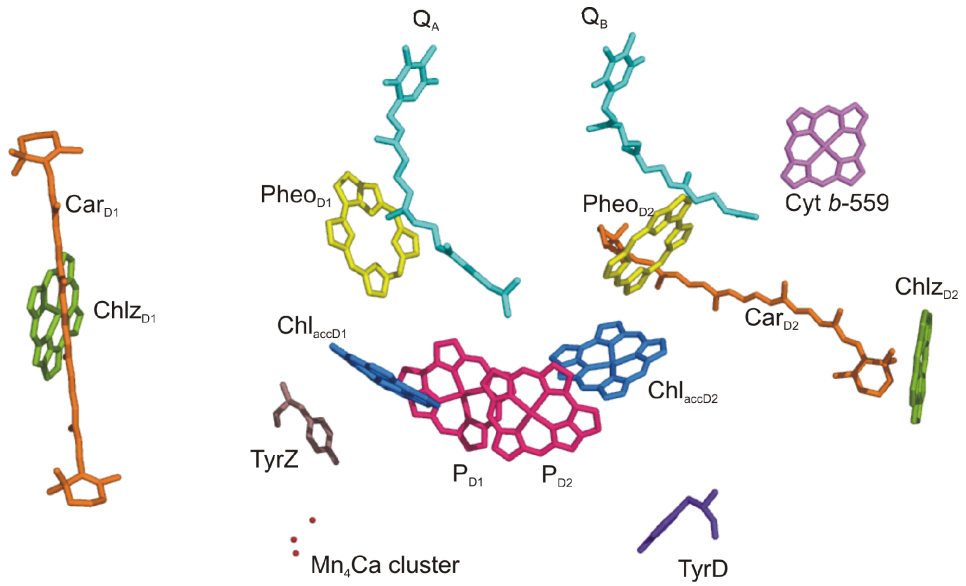

Fig. 1-7 Redox-active cofactors and electron transfer chain in PSII (side view). For better clarity Chls and Pheos are presented without the phytol chains. The figure was prepared on the basis of the following PDB entry: 2AXT.pdb (*8*).

CP43 and CP47, the core antenna subunits

PS II captures photons by a small core antenna, built up by two chlorophyll-binding, sequence-related proteins (CPs): CP43 and CP47. Each of them consists of six TMH and contains 13 and 16 Chl molecules and 4 and 5 Cars, respectively (Fig. 1-5). In both complexes, the Chl molecules are arranged in two layers in the membrane plane (Fig. 1-8), one closer to the stromal side, and the other one in the vicinity of the lumenal side of the membrane (*18*). CP43 has a more peripheral location in the PSII homodimer than CP47, and therefore it is more loosely bound to the RC (*19*). For that reason CP43 is supposed to be more easily disconnected from the PSII core.

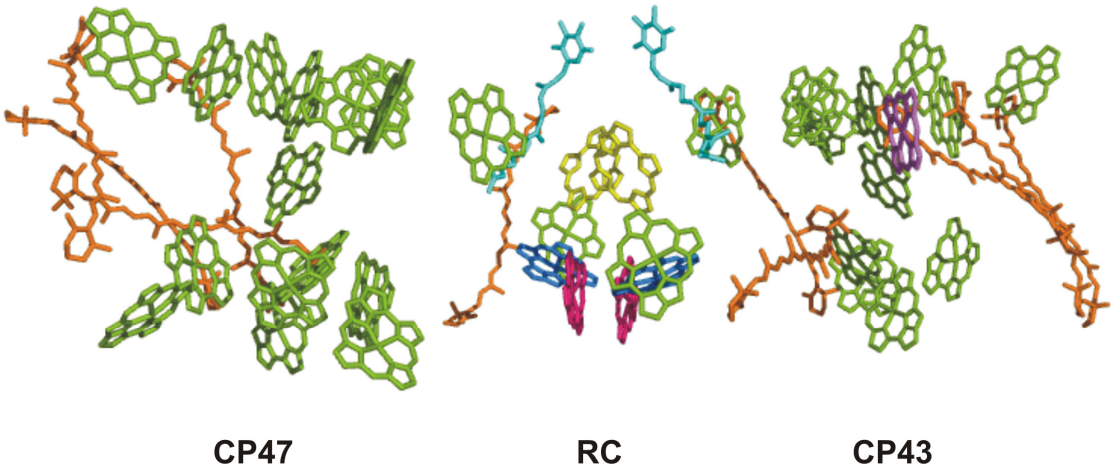

Fig. 1-8 PSII core monomer cofactors, shown without the protein matrix (side view). The antenna Chls are shown in green, Cars in orange, the RC Chls: P_{D1} and P_{D2} in magenta and Chl_{accD1} and Chl_{accD2} in blue, pheophytins $Pheo_{D1}$ and $Pheo_{D2}$ in yellow, quinones Q_A and Q_B in cyan, and cyt *b-559* in violet. Chls and Pheos are presented without the phytol chains. The figure was prepared on the basis of 2AXT.pdb (*8*).

Oxygen-evolving complex, the site of the water-splitting

The exact position of all the important cofactors constituting the oxygen-evolving complex (OEC) and their redox state is not completely clear due to the possible radiation damage when the PSII crystals are exposed to the X-ray experiments (*20;21*). However, the crystal structure (*22*) suggests two di-μ-oxo and two mono-μ-oxo bridges linking four Mn atoms to form a Y-shape structure. The Ca^{2+} seems to be positioned in between one of the Mn atoms and D1-Tyr161 residue, whilst both the presence and position of a chlorine atom is enigmatic.

Protein subunits

Besides the above-mentioned PSII elements, the crystal structures also revealed a number of membrane intrinsic subunits whose function is not yet known.

1.3.2 Processes in PSII

Light absorption

Light absorbed by a molecule creates an electronically excited state, which can relax back to the ground state in many different ways. In principle, the excitation energy can be transferred to another molecule, it can be used to form a triplet state, it can be released as fluorescence, it can be dissipated in the form of heat or it can be used in *e.g.* some chemical process (see Jablonski diagram in Fig. 1-9). PSII photochemical processes are characterized by very high efficiency, which means that under standard conditions most of the absorbed solar energy is utilized to drive water splitting, as well as ATP and NADPH production.

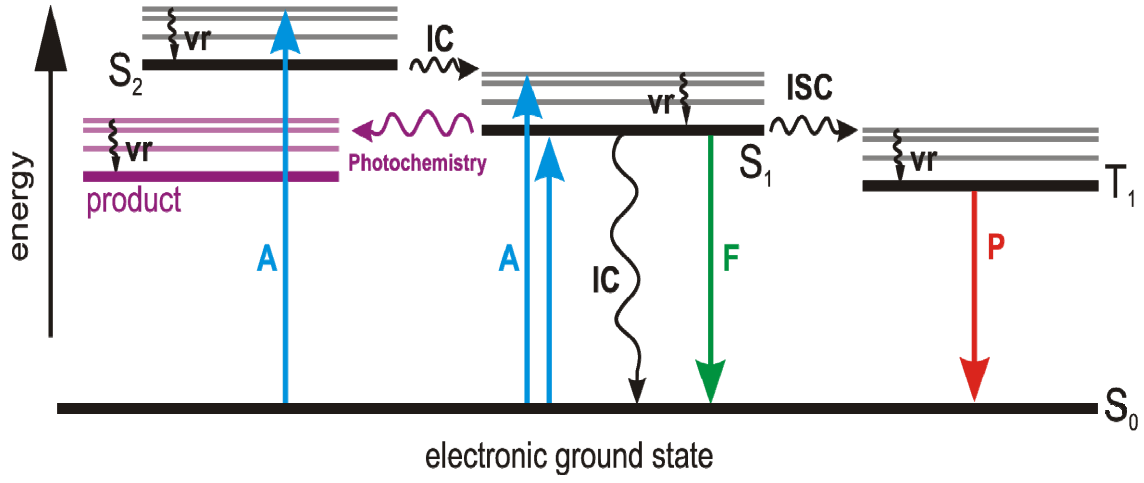

Fig. 1-9 Jablonski diagram illustrates the electronic states of a molecule and the possible transitions between them. S denotes a singlet electronic state (S_0 – ground state, S_1, and S_2,– excited states), T_1– triplet state, A – absorption of a photon, F – fluorescence, P – phosphorescence, IC – internal conversion, ISC – intersystem crossing, vr – vibrational relaxation. Photoproduct (as a result of a photochemical process, like *e.g.* charge separation in PSII) electronic and vibrational states are shown in purple. Thin lines above S_1, S_2, T_1 and "product" represent vibrational states (rotational states are omitted for clarity).

Energy and electron transfer in PSII with open RC

The absorbed light energy is transferred from the antenna to the RC pigments, where it triggers the primary charge separation process and the following secondary electron transfer steps (for recent reviews on the primary processes in PSII see (*23-25*)). In PSII particles with open RC, meaning oxidized Q_A, the "active" electron transfer branch consists of P_{D1}, Chl_{accD1}, $Pheo_{D1}$, Q_A and Q_B (see Fig. 1-7). The early investigations on the electron transfer kinetics assumed that P_{D1} is the primary electron donor and the accessory chlorophyll Chl_{accD1} the primary electron acceptor. Nevertheless, recent studies (*26-28*) provided evidence that actually at physiological temperatures the very first charge separation takes place between Chl_{accD1} and $Pheo_{D1}$. In the following step the $P_{D1}^{+}Pheo_{D1}^{-}$ radical pair (RP) is formed. Subsequently the electron is transferred to Q_A and finally to Q_B. The double reduction and successive protonation of Q_B leads to the release of Q_BH_2 to the membrane forming the plastoquinone (PQ) pool. Afterwards a new plastoquinone molecule enters the Q_B cavity. P_{D1}^{+}, due to its very high (above 1.1 V) oxidation potential, oxidizes TyrZ (D1-Y161), which is in turn reduced by a manganese cluster. Finally, manganese cluster oxidizes water to molecular oxygen.

Energy and electron transfer in PSII with closed RC

Despite the fact that PSII with open RC represents the physiological condition at which the enzyme typically operates, it is of great importance to understand the processes taking place in PSII with reduced Q_A. Such a state of PSII corresponds to the rather common situation, when plants or cyanobacterial cells are suddenly exposed to high intensity of light. Previous studies on PSII with reduced Q_A showed an increased yield of emitted fluorescence and a higher average lifetime of fluorescence in comparison with PSII with open RC (*29-31*). These changes provided evidence for the blockage of electron transport from Q_A to Q_B. In addition, the negative charge on Q_A raises the energy level of the first RP, and therefore the forward electron transfer rate becomes smaller with concomitant increase of the backward electron transfer rate (*29*). This in turn leads to a very dangerous situation for the enzyme, since the already longer-living singlet RPs can be transformed with a much higher yield into triplet RPs and finally cause formation of a triplet Chl (^{3}Chl). In the presence of oxygen the latter can produce the highly damaging species, singlet oxygen.

1.3.3 Energy trapping in PSII

In a fully functional PSII particle the absorbed light energy is trapped in the RC due to the charge separation process. Even though the early studies on the very first events in PSII triggered by the absorption of a photon were performed long time ago, there is still no agreement which step is the bottleneck in the overall energy trapping process. There are three main views in the literature on this issue: two extreme ones assuming that either the energy transfer from the antenna to the RC is very slow with much faster charge separation (diffusion-limited model) (*32*), or the charge separation and not the energy delivery to the RC

is the bottleck (trap-limited model) (*28;33;34*). The third option finds the kinetics in CP47-D1/D2 to be in between the two extremes, with the energy transfer taking place on the same time scale, as the charge separation (*35*).

1.3.4 Protein dynamics

In all the processes described above various pigments, *e.g.* Chls and Cars, are involved. However, the kinetics, energetics, and efficiency of the energy and electron transfer processes do not depend exclusively on the characteristics of these cofactors. All of these cofactors are embedded in the protein matrix (Fig. 1-10), and the latter is of great importance to the overall function of the enzyme. Thus, the interactions between the protein and the pigments can regulate the properties of the latter; modify their light absorption, their redox potentials, *etc.* MacMahon *et al.* (*36*) pointed out the structural difference between proteins before and after the electron transfer reaction in photosynthetic RC and underlined that the distribution among the conformational substates of the protein and the fluctuating relaxation between them are of great importance for the reaction kinetics. Such dependence of the energy and electron transfer rates on the protein conformation and dynamics has been already shown for bacterial RCs (*37-41*) and D1-D2-cyt *b-559* (*42;43*).

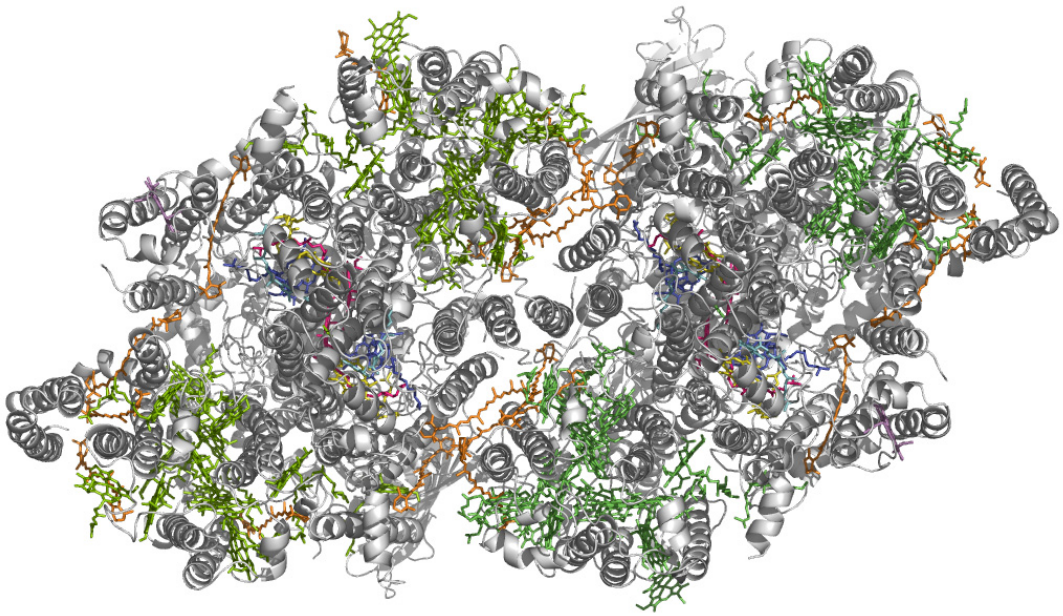

Fig. 1-10 PSII core dimer cofactors embedded in the protein matrix, marked in grey (top view). Color coding as in Fig. 1-5. Although the details of the PSII dimer structure are not completely visible in this figure, this presentation is intended to help realize that PSII is not composed exclusively from the energy and electron transfer cofactors, but also from the equally important protein matrix. The figure was prepared on the basis of 2AXT.pdb (*8*)

1.4 Goals of the work

The first aim of this work was to find evidence for protein dynamics in the photosynthetic pigment-protein complexes of PSII, since such protein relaxation was discovered already long time ago in bacterial RCs (see chapter 1.3.4). In the view of the fact that the excitation of PSII particles leads to the charge separation and electron transfer processes, the present work concentrates on the interactions between protein and charged species created due to the absorption of light. It is well-known that the dynamics of a protein can be described over many different time scales. Therefore, one of the interesting questions was if the electron transfer in PSII RC is slow enough to be "sensed" by the protein surrounding and at the same time if our experimental method is good (fast, sensitive, *etc.*) enough to resolve it. For this purpose the study involved PSII core particles with the RC prepared in two different redox states, with oxidized and reduced Q_A. While PSII with open RCs is supposed to reflect the "normal", physiological state of the enzyme, PSII with closed RCs is believed to mimic the conditions in which a photosynthetic organism (plant or cyanobacteria) is exposed to higher radiation than it can utilize. It was assumed that in the latter case the charge separation and the subsequent electron transfer steps should be much slower, due to the repulsive interactions between the electron ejected in the CS and the negative charge localized on Q_A. This feature should facilitate the investigation of the protein influence on the electron transfer and vice versa. Hence, we expected the protein to react in different ways in both redox conditions. This variation should be observed in the lifetimes as well as in the energetics associated with the processes that involve the conformational changes of the protein. Another approach used to confirm the importance of the protein matrix that surrounds the electron transfer chain in PSII concerned the single-point mutations. The question we asked was: What happens if we remove/exchange one important for the studied processes (but maybe not especially the most important) amino acid? Is the protein able to keep the "normal" efficiency of the crucial processes? To validate our hypothesis, we performed the experiments on the TyrD-less PSII core complexes, in which the tyrosine at position 160 in a D2 protein was replaced with phenylalanine.

The second, but equally important aim of the work emerged naturally from the intended study on the protein conformational response. It concerned the energy and electron transfer processes in PSII, with a careful plan to finally localize the bottleneck in the energy trapping process (see section 1.3.3) and to explore and assign the electron transfer steps. However, since the chlorophylls contributing to both processes are almost isoenergetic, they are spectrally almost indistinguishable. This, together with the comparable time scales of the energy and electron transfer steps, makes such studies very challenging. Hence, also this issue was approached with the help of the PSII particles with closed RCs, which are supposed to show much slower electron transfer steps than PSII with oxidized Q_A. This means that the charge transfer process should be more separated from the energy transfer process, and therefore easier to distinguish between the two. Additionally, on the basis of the reports

present in the literature that show the energy transfer characteristics of the isolated core antenna complexes, CP43 and CP47, we expected to resolve also the intra-antenna energy transfer steps in the description of the kinetics in PSII core particles.

Along with the trapping problem came the assignment of the radical pairs. It was previously shown that in PSII with open RC the primary electron donor is the accessory chlorophyll, and the primary electron acceptor is the pheophytin (see section 1.3.2). However, such experimentally proven assignment was still lacking for PSII with closed RCs, and the charge separation and transfer mechanisms were assumed to be identical as in PSII with open RC. To test this hypothesis we used once again the above-mentioned PSII particles with introduced single-point mutation.

2 Materials and methods

2.1 Experimental techniques

2.1.1 Time-correlated single photon counting (TCSPC)

Time-correlated single photon counting (TCSPC), called also single photon timing (SPT), is one of the time-resolved optical spectroscopy techniques for measuring fluorescence lifetimes. TCSPC is very sensitive since single photon events are detected. It is characterized by high time-resolving power, typically in the order of a few picoseconds (*44*). The basic idea of this method is to measure the correlation function between the exciting pulses and the emitted fluorescence photons. Therefore, the experiment concerns a large number of excitations of the investigated sample, each followed by the emission of a single photon. Ideally, each photon is timed and recorded, and the information about its time of arrival at the detector in respect to the excitation pulse is stored in a histogram (Fig. 2-1). The full histogram represents the decay curve of the fluorescence emitted by the sample.

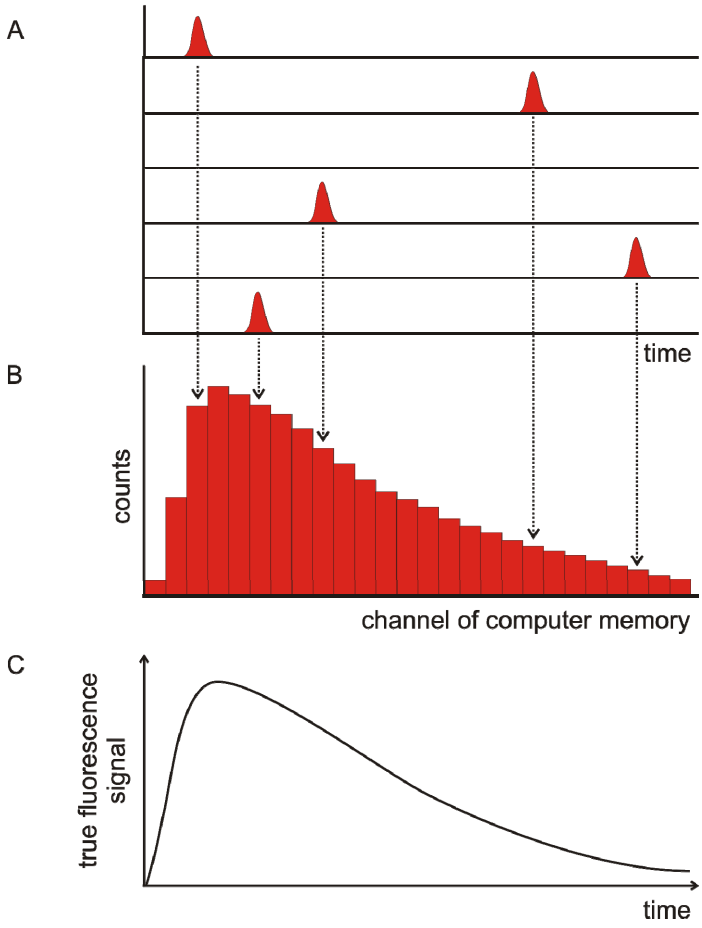

Fig. 2-1 General idea of the fluorescence lifetime measurement with TCSPC: A) emitted photons which are being detected as a response to a single excitation pulse; B) histogram of the photon counts in the data storage channels; and C) the original fluorescence decay curve (adapted from "The bh TCSPC Handbook" by Wolfgang Becker, 2005).

The general principle of TCSPC is presented in Fig. 2-1. In the scheme of the experimental setup used in the study (Fig. 2-2) an ultrashort laser pulse triggers the time-to-amplitude converter (TAC), which activates charging of a capacitor (START signal). This process is stopped with a signal created by a photon emitted by the sample (STOP signal). The charge in the capacitor is proportional to the time between the sample excitation and emission of a photon. The signal from the TAC is further transformed into a numerical value by an analog-to-digital converter (ADC), and the count in the corresponding channel of he data storage device, the multichannel analyzer (MCA), is incremented. Every time when the particular time between START and STOP pulses is recorded, the value in the corresponding channel of MCA is increased by one. Finally, after many repetitions, usually in the order of 10^6, the data can be presented in the form of a histogram, as shown in Fig. 2-1B. The whole process, from excitation, through emission to data recording, should be repeated as many times as it is necessary to achieve good signal-to-noise ratio.

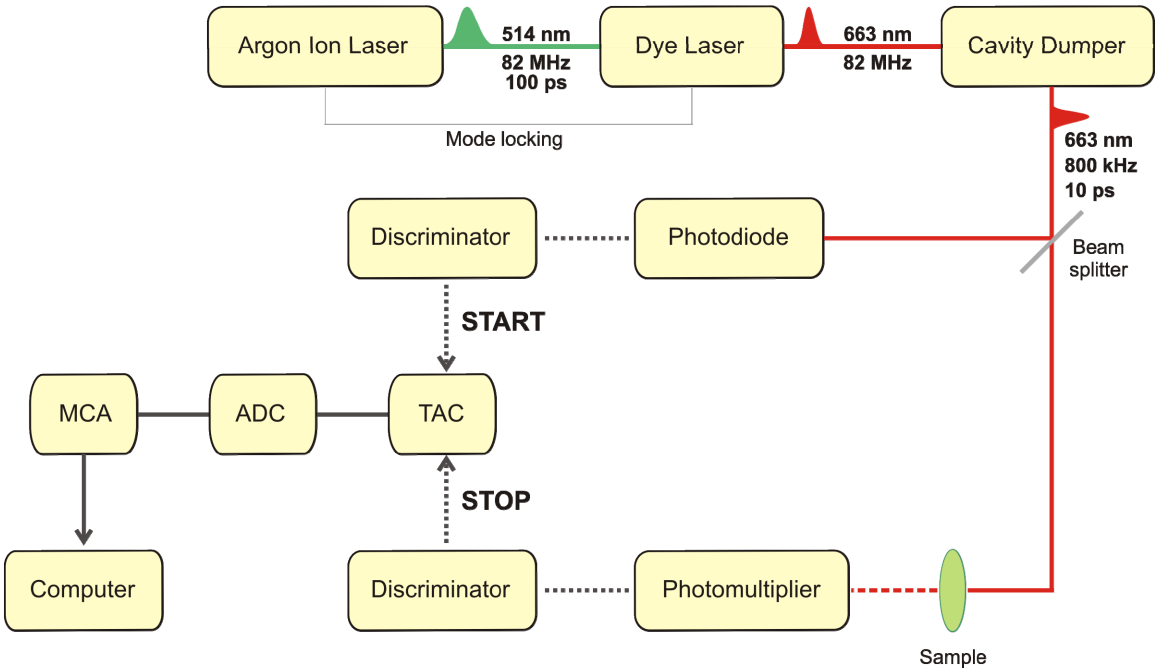

Fig. 2-2 The general scheme of the TCSPC experimental setup; TAC – time-to-amplitude converter; ADC – analog to digital converter; MCA – multichannel analyzer.

Our studies are focused on ultrafast reactions, however the experimental setup has some time limitations (*e.g.* the detection system is fast, but not infinitely fast, and also the exciting laser pulse is not a δ-pulse) and thus the acquired signal is not the true δ-response fluorescence signal. Therefore, to obtain the real fluorescence decay, the detected signal has to be deconvoluted with the instrument response function (IRF or PR, standing for prompt response). PR can be measured, using for example a scattering medium. However, one should be careful to perform the experiment under the same conditions as the fluorescence measurement. Usually one uses the same cuvette and the same volume as the sample of interest.

Experimental details

The experimental setup was previously described in (*45;46*). The TCSPC measurements were performed with the use of a synchronously pumped, mode-locked dye laser (Spectra Physics) at a repetition rate of 800 kHz, unless stated otherwise. 4-(dicyanomethylene)-2-methyl-6-(p-dimethylaminostyryl)-4H-pyran (DCM) ((*47*)) was used as a laser dye, which provided well-shaped and short laser pulses (usual pulse width of ~ 10 ps) at the desired excitation wavelength, namely in the range from 650 nm to 690 nm. The dye laser was pumped by an argon ion laser (Spectra Physics), which was operated at the 514 nm line.

For the fluorescence measurements a rotating cuvette was used. The cuvette had the diameter of 10 cm and the thickness of 1.5 mm (equal to the optical path length), and the active volume of the sample about 10.5 ml. The cuvette was in most cases rotated with 3500 rpm and moved aside 66 at rpm. The laser power at the sample cell, the rotation and the side movement of the cuvette, and the laser repetition rate were chosen such that multiple excitations of a particle were avoided (for detailed calculations see section 2.1.3). For example, when the PSII core dimer particles were excited at 663 nm with a laser pulse train of power ~ 100 μW, and a laser beam diameter of ~ 0.8 mm, less than 10% of the PSII particles were excited while they stayed in the laser beam, even though the number of the laser shots during this time was in the order of 100 (see section 2.1.3 for details of the calculation).

The PR was measured with the use of fresh milk (1.5 % fat) as a scattering solution. Milk solution in distilled H_2O with dilution ratio 1:1250 was the most suitable for the investigated samples.

The stop criteria used in the experiments were as following, unless stated otherwise:

– for the fluorescing sample: data at one particular emission wavelength was recorded until either the counts in the peak channel reached the value of 30000 or 50 minutes passed.
– for the PR: data was recorded until the counts in the peak channel reached the value of 50000.

Fluorescence signals were stored in 4096 channels of the computer memory, which together with the time-window used resulted in a time step of 2.61 ps per channel. After the specific deconvolution of the emission signal with the PR, which is implemented in the used in the present work home-built data analysis program, one is able to resolve a lifetime of about 1-2 ps, given the high relative amplitude of this shortest component. PR was usually characterized with full-width at half-maximum (FWHM) ~ 28 ps.

2.1.2 Synchroscan streak camera (SC)

Another optical time-resolved technique used in this study was a streak camera (SC) setup. The main advantage of the SC system over the above-described TCSPC is the higher time resolution. In addition, SC provides the simultaneous recording of the fluorescence photons across the whole accessible wavelength range.

The principle of SC operation is presented in Fig. 2-3. Photons emitted by the sample are characterized by different delay time and wavelength (shown as four photons separated in time and space; the wavelength separation can be achieved by using a spectrograph between the sample and the SC entrance slit). Photons are focused on the photocatode, causing ejection of electrons. The latter are accelerated by a mesh and swept by a pair of deflection plates, with the sweep amplitude depending on the arrival time to the plates, thus resulting in separation in two axes: one is wavelength and the other delay time. The electrons subsequently hit a multi-channel plate (MCP), where they are multiplied, and eventually they reach a phosphor screen. This leads to emission of many photons, which are subsequently recorded by *e.g.* a CCD camera.

The temporal sweep of the sychroscan SC unit is a sinusoidal wave in synchrony (phase-locked) to the high repetition laser pulse train.

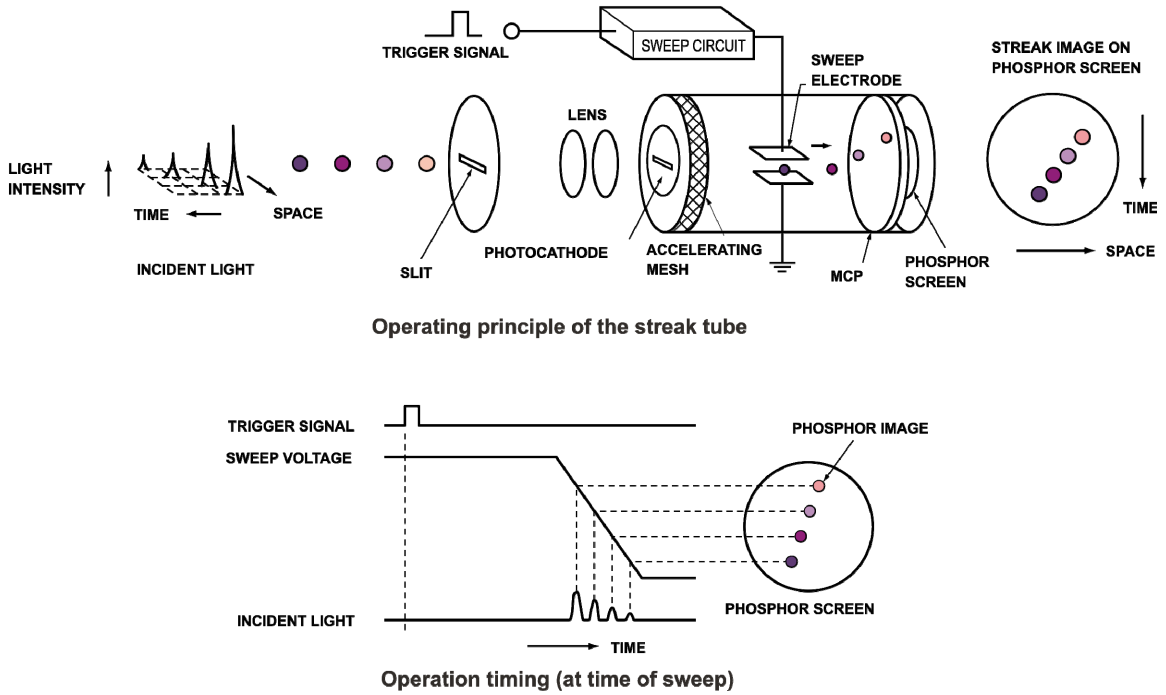

Fig. 2-3 Schematic illustration of the streak camera operation principle (adapted from Hamamatsu manual to the streak camera system used in the presented work).

Experimental details

The experimental setup is presented in a scheme in Fig. 2-3. It consists of:

– a solid state diode pumped frequency doubled cw laser (Verdi V10, Coherent), operated at 9W at 532 nm, that pumps

– a solid state mode-locked Ti:sapphire laser (Tsunami, Spectra-Physics), which output beam (tuned to 800 nm with a power of 1.8W, set to a frequency 81.468 MHz, 20-50 fs pulses) passes afterwards through

– an optical parametric oscillator with intracavity second harmonic generation of the IR-OPO signal to the VIS (Ring OPO, APE Berlin).

The OPO uses a nonlinear, periodically poled LBO (LiB_3O_5, lithium triborate) crystal for tuning the laser beam wavelength in a relatively broad range, from 550 to 750 nm. In the conducted experiments the excitation wavelength was usually set to 660 nm, unless stated otherwise. In this case the pulse width (full-width at half-maximum, FWHM) is typically ~ 9 nm, with the autocorrelation signal of ~ 450 fs, meaning a pulse width of ~ 300 fs. A pulse Picker 3980 (Spectra-Physics) is used to reduce the frequency of the laser beam from 81.5 MHz to 4 MHz. The diameter of the excitation beam on the cuvette is ~ 300 μm.

The emitted fluorescence is resolved in the wavelength space in an imaging spectrograph (Chromex 250 IS) to finally reach the synchroscan streak camera (C5680, Hamamatsu), where the time-resolution is achieved. A CCD camera records the optical signal emitted by the streak camera phosphor screen. Data was collected and stored with the software provided by Hamamatsu.

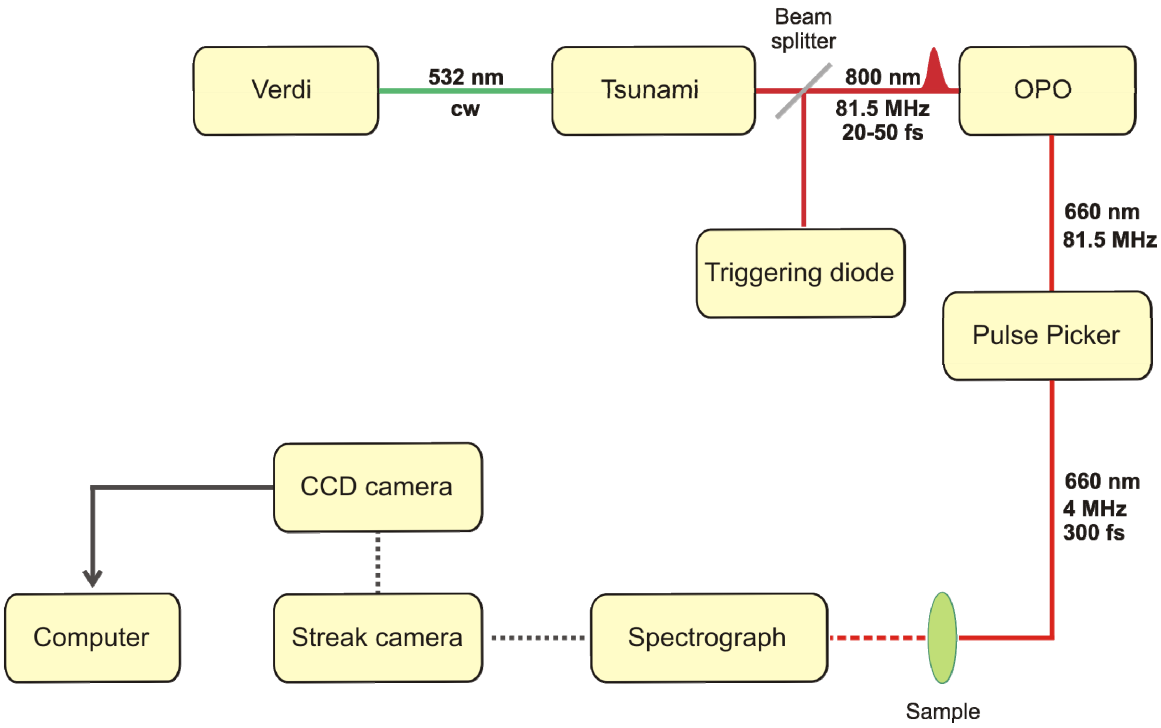

Fig. 2-4 The general scheme of the experimental streak camera setup; OPO – optical parametric oscillator.

For the fluorescence measurements a rotating cuvette was used. The diameter of the cuvette is 10 cm, 1 mm path length, and the active volume of the sample about 7.2 ml. The cuvette was in most cases rotated with 4000 rpm and moved aside with 32 rpm. As in the measurements performed with TCSPC apparatus, the laser power at the sample cell (in the order of 80-100 μW), the rotation and side movement of the cuvette, and the laser repetition rate were chosen such that the multiple excitations were avoided (see section 2.1.3). For all measurements the emission was set at magic angle (54.7°), which assures the nonselective detection of the fluorescence, otherwise the acquired signal might be polarized mostly in one particular plane.

Data was recorded in photon counting mode in two time ranges:

– time range 1: 0-116 ps (0.243 ps per channel);

– time range 2: 0-600 ps (1.25 ps per channel).

2.1.3 Excitation conditions for the time-resolved fluorescence measurements

To find the experimental conditions that will provide a single excitation of the PSII particles and at the same time relatively high fluorescence signal, the following calculations were performed. Firstly, one can calculate how many photons are absorbed by a single particle during one laser pulse. Additionally, due to the specific arrangement of the performed experiments (meaning the use of a rotation cuvette) the real number of excitations that a particle receives during the time it actually stays in the laser beam can be estimated.

Thus, the total number of photons absorbed by a particle during one laser shot is defined as:

$$N_{abs} = N \cdot S_a \cdot \sigma(\lambda) \tag{2.1}$$

where N is the number of photons in one laser pulse, S_a is the number of Chls in one PSII particle (the size of the antenna), and σ is the effective cross-section of a Chl molecule. N can be calculated given the power of the laser train P, the laser repetition frequency f, the excitation wavelength λ used, and the radius of the laser beam on the cuvette r_{lb}:

$$N = \frac{P}{f} \cdot \frac{\lambda}{\mathrm{hc}} \cdot \frac{1}{\pi r_{lb}^2} \tag{2.2}$$

(here h is Planck constant and c – velocity of light).

The absorption cross-section can be expressed as a function of the molar absorption coefficient ε(λ) at particular excitation wavelength λ (*48*):

$$\sigma(\lambda) = \ln 10 \cdot \varepsilon(\lambda) / \mathrm{N_A} \tag{2.3}$$

where $\mathrm{N_A}$ is Avogadro's constant.

Combining the equations (2.1)-(2.3) results in the final estimation of the number of photons absorbed per particle per laser pulse:

$$N_{abs} = \frac{\ln 10}{\mathrm{hc}\pi \mathrm{N_A}} \cdot \frac{P \lambda \varepsilon(\lambda) S_a}{f r_{lb}^2} \tag{2.4}$$

If now the sample is going to be exchanged during the measurement, so the laser beam hits always fresh "dark-adapted" particles, one can easily determine how many photons a particle absorbs during the time it stays in the laser spot. Such calculation for the rotating cuvette is presented below.

Eq. (2.5) describes how many photons are absorbed by a particle during the time it stays in the laser beam (N_{abslb}):

$$N_{abslb} = N_{abs} \cdot n \tag{2.5}$$

where n is the number of laser shots during the time a particle spends in the laser spot. n depends on the repetition frequency of the laser f and the frequency of the rotation f_r:

$$n = f \cdot \frac{2r_{lb}}{2\pi f_r R} \tag{2.6}$$

R is the distance from the center of the cuvette to the position of the laser beam on the cuvette. From eq. (2.5)-(2.6) one can easily find the desired number of photons.

The rotation cuvette used in the presented here experiments was additionally moved aside. Given the frequency of the cuvette rotation f_r, the diameter of the laser spot ($2r_{lb}$), and the amplitude of the side movement s one can furthermore estimate the minimal rate f_{side}, with which the cuvette should be moved in order to assure that with each rotation cycle laser beam hits fresh part of the sample:

$$f_{side} = \frac{2r_{lb} f_r}{s} \tag{2.7}$$

2.1.4 Chlorophyll *a* fluorescence induction

Chlorophyll *a* fluorescence transient measurement was primarily employed to study the oxygenic photosynthesis of whole plants. It proved to be capable of providing vast information about the investigated photosynthetic organisms (for a review see (*49*)), amongst which the most relevant to the current work is the estimation of the efficiency of PSII photochemistry.

Illumination of a previously dark-adapted leaf initiates the time-dependent emission of light. This induction of a fluorescence signal is called Kautsky effect, after its discoverer. Immediately after the illumination, the fluorescence rises to the F_0 level, and afterwards rapidly increases upon continuous illumination, until it reaches the level of maximum fluorescence, called F_m (or F_{max}). However, to reach F_m the leaf has to be illuminated with a saturating light intensity. The F_0 level is interpreted as a state in which all PSII have open RCs, while F_m represents the complete closure of the RCs. The transition from F_0 to F_m consists of various phases, and therefore is commonly called OJIP. Three major phases are interpreted (*50*) as follows:

- O-J is a photochemical phase that represents the full reduction of the primary electron acceptor, quinone Q_A, causing a fluorescence increase;
- J-I phase, according to (*51;52*), corresponds to the activity of the OEC complex, which reduces $P680^{\cdot+}$ and in this way releases the fluorescence, as $P680^{+}$ radical is a fluorescence quencher;
- I level is suggested to be correlated with the heterogeneity in filling up the PQ pool;
- I-P phase describes reduction of the PQ pool.

As all these phases in the whole leaf concern mostly the activity of PSII, it is also possible to record and study the fluorescence induction in isolated PSII particles.

Chlorophyll *a* fluorescence transient experiments were performed with a Handy-Pea-fluorimeter (Hansatech Instruments, UK). Samples were dark-adapted for 2 min before the measurements and then illuminated with continuous light (650 nm peak wavelength, photon flux 1250 μE/m^{2}s, unless stated otherwise) provided by the focused array of ultra-bright red LEDs. The fluorescence data were recorded for 15 seconds.

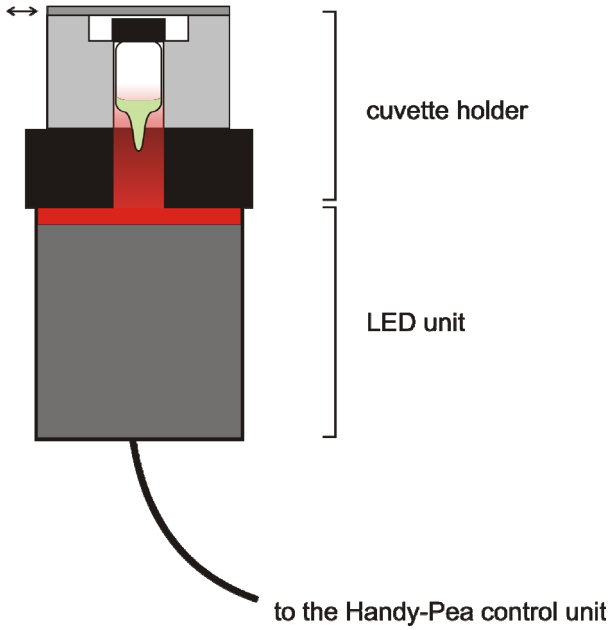

Fig. 2-5 Schematic representation of the home-built cuvette holder that can be attached to the LED unit of the Handy-Pea fluorimeter. The top part of the holder can be moved to the sides (marked with an arrow) in order to place the cuvette inside the holder. PSII sample is shown in green, while the red colour indicates the red light from the LED array.

In order to perform the measurements of the PSII solution in complete darkness, a special holder was built (Fig. 2-5). The HPLC cuvette (Boro 5.1 conical, thread 8-425, Scherf Präzision Europa, Meiningen, Germany) was filled with 150 μl of sample and placed in the cuvette holder, which was subsequently mounted on the LED unit of the Handy-Pea instrument.

2.2 Sample treatment

For the time-resolved fluorescence and the chlorophyll *a* fluorescence induction measurements the samples were diluted in the following buffer solutions to the desired Chl *a* concentration:

1) Photosystem II core dimer complexes from *T. elongatus*, with active OEC (Matthias Rögner preparation, (*53*)):
   - 20 mM MES (Serva, Heidelberg, Germany);
   - 10 mM $MgCl_2$ (Roth, Karlsruhe, Germany);
   - 10 mM $CaCl_2$ (Merck, Darmstadt, Germany);
   - 0.5 M Mannitol (Fluka Biochemika, Buchs, Switzerland);
   - 0.03% β-DM (Glycon, Luckenwalde, Germany), pH 6.5.

These PSII core particles showed the oxygen activity in the order of 3200 μmol O_2/(mg Chl*h), and about 70% of Q_B/Q_A ratio.

2) Photosystem II core dimer complexes from *T. elongatus*, with active OEC (Miwa Sugiura preparation, (*54*;*55*)):
   - 40 mM MES (Serva, Heidelberg, Germany);
   - 15 mM $MgCl_2$ (Roth, Karlsruhe, Germany);
   - 15 mM $CaCl_2$ (Merck, Darmstadt, Germany);
   - 1 M Betaine·HCl (Sigma, Taufkirchen, Germany);
   - 0.03% β-DM (Glycon, Luckenwalde, Germany), pH 6.5.

   These PSII core particles showed the oxygen activity in the order of 3600 μmol O_2/(mg Chl*h) and 4200 μmol O_2/(mg Chl*h) for WT' (WT with attached His-tag on C-terminus of CP43, knockout *psbD2* gene) and the D2-Y160F mutant (called TyrD-less, knockout *psbD2* gene) (*55*) WT with attached His-tag to CP47), respectively, and 100% Q_B/Q_A ratio in both preparations.

The following additives were used:

1) To assure open RCs 0.4 mM FeCN was applied to the PSII sample.
2) To block the electron transfer from Q_A to Q_B the herbicide DCMU was used at 20 μM concentration, unless stated otherwise. To assure low ethanol concentration in the final sample preparation, firstly DCMU was dissolved in ethanol (20 mM DCMU), afterwards in the proper buffer solution (1 part of DCMU in ethanol + 3 parts of a buffer – this gave 5mM DCMU stock solution), and only then added to the final sample solution.
3) To remove oxygen from the sample solution, an oxygen-scavenging system was employed, according to (*56*) with small modification: 65 μg/ml catalase (Sigma-Aldrich, Taufkirchen, Germany), 65 μg/ml glucose oxidase (Sigma, Taufkirchen, Germany), and 8 mM glucose (Sigma, Taufkirchen, Germany).

For all the aqueous solutions filtered water was used (Millipore, Schwalbach, Germany), while for the ethanol solutions the UVASOL ethanol for spectroscopy (Merck, Darmstadt, Germany) was used. All chemicals were of analytical grade. In addition all the buffers were passed through sterile filters (Millipore, 0.22 μm pore size) to avoid dust particles or other objects that could cause unnecessary scattering of light in the fluorescence lifetime measurements.

For the purpose of both, the TCSPC and chlorophyll *a* fluorescence induction measurements the concentrations of the PSII samples were adjusted to OD = 0.2–0.3/cm at the excitation wavelength (λ_{exc} = 663 nm, unless stated otherwise), which corresponds to a Chl concentration of about 7–8 μg Chl/ml. While for the SC measurements the concentration of the samples was adjusted to OD = 1.0/cm in the Q_Y absorption maximum.

The buffer solutions used for the sample preparation were bubbled with N_2 or Ar gases.

2.3 Data analysis

The time-resolved fluorescence data cannot be interpreted in a reliable manner without applying further analysis. Therefore the acquired fluorescence signals were analyzed by global and target kinetic modeling (*57;58*).

2.3.1 Global analysis

In simple words, global analysis is a simultaneous analysis of several kinetic traces, and in general can be applied to different types of time-resolved experiments (*e.g.*, transient absorption, fluorescence). If the investigated sample consists of *n* spectrally different components, whose concentrations can be described by a set of linear differential equations, then their kinetics (here the fluorescence kinetics) can be expressed as a sum of *n* exponential decays:

$$F(t,\lambda_{exc},\lambda_{em}) = \sum_{j=1}^{n} A_j(\lambda_{exc},\lambda_{em}) \cdot \exp\left(-t/\tau_j\right) \tag{2.8}$$

where $F(t, \lambda_{exc}, \lambda_{em})$ is the time-dependent signal, λ_{exc} is the wavelength of excitation, λ_{em} is the emission wavelength at which the signal was collected, and A_j is the amplitude associated with the j-th decay lifetime τ_j. The set of lifetimes and their associated amplitudes constitutes the so-called decay associated spectra (DAS), which can be plotted against the wavelengths. For the purpose of this work we assume that the positive values of amplitudes correspond to the losses of the fluorescence, while the negative amplitudes are interpreted as energy transfer components. The quality of the fit is judged on the basis of the value of χ^2 and the shape of the DAS. The time-resolved fluorescence kinetics data was analyzed with a home-built program for global analysis (*45*).

It is noteworthy that one can treat global analysis as the example of the simplest compartment target analysis, with a number of non-interacting compartments.

2.3.2 Target analysis

While global analysis can be used in the case when there is no *a priori* knowledge about the investigated system, the target compartment modeling is applied mainly when such knowledge is already available or – more importantly – to find suitable kinetic models. The main advantage of the target modeling (called also kinetic modeling or compartmental analysis) is the character of the parameters resulting from the fitting procedure. Whereas global analysis results in plain mathematical parameters that describe the experimental signals, the kinetic modeling yields additionally their physical or chemical interpretation (*57*).

The investigated system can be presented as a set of (excited state) compartments, representing different species or states, chosen on the basis of the *a priori* knowledge. Let us take PSII core complex as an example. In general, the precise description of the kinetics of

such a complex system should include all the kinetic rates of the interactions between all the 35 Chls and the associated with them lifetimes. However, the experimental data basically does not allow for a proper determination of such complex kinetic scheme. Therefore, one can group the Chls on the basis of the already available information *e.g.* structural data. The arrangement of the Chl molecules in PSII core particle shown in Fig. 1-8 suggests the grouping according to the position of the pigment. In fact, in our modeling of PSII we group all the Chls in three clusters: CP43, CP47, and RC. This way of clustering naturally assumes that after the excitation all pigments in particular group are energetically equilibrated, or in other words the energy equilibration between these Chls is much faster that the time-resolution of our experimental method. Therefore we can only distinguish the energy transfer between the cluster of CP43 pigments and the RC compartment *etc.*, but not the extremely fast intra-antenna processes. Compartmentalization is not limited utterly to the excited states, as in the above example. It is also convenient to treat newly created species as separate compartments, like *e.g.* radical pairs (as for example RP1 in our results is assigned to $Chl_{accD1}^{+}Phe_{oD1}^{-}$).

The interacting compartments can be linked with each other *via* the rate constants (k_{ij}); furthermore each compartment can decay to the ground state *via* radiative and nonradiative processes (k_{i0}). The experimental fluorescence decay can be now approximated as a sum of N exponential decays:

$$F(t,\lambda_{em}) = \sum_{m=1}^{N} \mathrm{DAS}_m(\lambda_{em}) \cdot \exp\left(-t/\tau_m\right) \tag{2.9}$$

DAS were already introduced as the set of amplitudes corresponding to a particular lifetime. However DAS itself is a purely mathematical parameter. It can be however represented as a linear combination of physically meaningful species associated (emission) spectra (SAES), if a specific kinetic model is applied. The latter is indeed a steady-state fluorescence emission spectrum of a particular compartment; it is also a fitting parameter during data analysis procedure. One can write:

$$\mathrm{DAS}_m(\lambda_{em}) = \sum_{n=1}^{N} c_{mn} \cdot \mathrm{SAES}_n \tag{2.10}$$

where c_{mn} for a given kinetic model is an array of coefficients, depending on the rate constants k_{ij}, excitation wavelength λ_{exc}, and the extinction coefficient of the investigated sample $\varepsilon_i(\lambda_{exc})$ at the excitation wavelength. Importantly, in the target modeling the estimated lifetimes are dependent only on the kinetic rate constants: $\tau_i = f(k_{ij})$.

The above equation (Eq. (2.10)) gives the relation between mathematical parameters (DAS and lifetimes) with physical parameters (SAES) and rate constants.

In general, the kinetics in the tested model can be represented as a set of homogeneous first-order differential equations:

$$\frac{d}{dt}\mathbf{X}(t) = \mathbf{T}\cdot\mathbf{X}(t) + \boldsymbol{\alpha}\cdot \mathrm{IRF}(t) \tag{2.11}$$

$\mathbf{X}(t)$ in the above equation corresponds to a vector of time-dependent population of species, $\mathbf{T}$ is the kinetic transfer matrix, $\boldsymbol{\alpha}$ is a vector of the initial absorbance of the species, and IRF stands for the instrument response function. The off-diagonal elements of the transfer matrix $\mathbf{T}$ represent the transition rates between the compartments, while the diagonal elements describe the decay rates of the compartments.

Eq. (2.9) can be now rewritten in the following manner:

$$F(t,\lambda_{em}) = \sum_{j=1}^{N} \exp(d_j t)\cdot \sum_{k=1}^{N} \mathrm{SAES}_k(\lambda_{em})(\mathbf{U}^{-1}\cdot\alpha(\lambda_{exc}))_j \cdot U_{jk} \tag{2.12}$$

d_j is a j-th eigenvalue of the transfer matrix $\mathbf{T}$ and therefore is related to the measured lifetime as following: $d_j = -1/\tau_j$; SAES_k is an emission spectrum of k-th species, and $\mathbf{U}$ is the matrix of the eigenvectors of $\mathbf{T}$. The eigenvector matrix carries important information on the origin of the lifetimes associated with the model and their assignment to particular physical processes. A negative value in this matrix represents the rise of the population of a compartment, while a positive value corresponds to the depopulation of a compartment.

In summary, target modeling results in the SAES, kinetic rates, and lifetimes as fitting parameters for a chosen model (*58*). The procedure of finding the model that sufficiently describes the experimental data is however tedious, since several requirements have to be fulfilled:

- The fitting quality is judged by both the χ^2 value, which should be as close to unity as possible, and also the residuals plots (for example of the differences in the residuals depending on the quality of the fit see chapter 3.6);
- The lifetimes and their amplitudes should not exhibit a compensation behavior in the DAS plots;
- The SAES should be smooth and reasonable (*e.g.* its values should be positive across the whole wavelength range);
- Rate constants and lifetimes should have realistic values.

(The first two requirements should be also met in the global analysis approach.) Therefore many different models have to be tested to satisfy the above conditions.

2.3.3 Average lifetime of fluorescence

Commonly used parameter in time-resolved fluorescence spectroscopy is the so-called average lifetime of the excited state (or shortly "average lifetime" of fluorescence). The average lifetime of fluorescence at a particular detection wavelength λ is defined in the following manner:

$$\tau_{av} = \frac{\sum_{i=1}^{k} A_i \cdot \tau_i}{\sum_{i=1}^{k} A_i} \tag{2.13}$$

where the summation is carried out over all lifetime components τ_i and their amplitudes A_i at this wavelength. Lifetimes and amplitudes are determined in the global analysis of the data. However, in the case of target modeling, the summation in Eq. (2.13) is done only over the lifetimes of the excited states.

2.3.4 Calculation of the standard free energy

Another important parameter used in this study is the standard free energy difference (ΔG) of the electron transfer steps. It represents the free energy difference between two energy states with degeneracy n_1 and n_2, respectively. It can be derived from the reaction rate and the Maxwell-Boltzmann distribution laws:

$$\Delta G = \mathrm{k_B} T \cdot \ln \frac{k_b n_2}{k_f n_1} \tag{2.14}$$

k_f and k_b represent the forward and backward reaction rates, respectively, $\mathrm{k_B}$ is the Boltzmann constant, and T is the temperature given in K. Typically ΔG values are given in the units of meV.

3 Charge Separation Kinetics in Intact Photosystem II Core Particles is Trap-Limited. A Picosecond Fluorescence Study

This chapter is based on the publication: Y. Milaslavina, M. Szczepaniak, M.G. Müller, J. Sander, M. Nowaczyk, M. Rögner, A.R. Holzwarth. Biochemistry 45 (2006), 2436-2442.

The fluorescence kinetics in intact photosystem II core particles from the cyanobacterium *Thermosynechococcus elongatus* have been measured with picosecond resolution at room temperature in open reaction centers. At least two new lifetime components of ~2 and 9 ps have been resolved in the kinetics by global analysis in addition to several known longer-lived components (from 42 ps to ~2 ns). Kinetic compartment modeling yields a kinetic description in full agreement with the one found recently by femtosecond transient absorption spectroscopy [Holzwarth *et al.* (2006) *Proc. Natl. Acad. Sci. U.S.A.* 103, 6895-6900]. We have for the first time resolved directly the fluorescence spectrum and the kinetics of the equilibrated excited reaction center in intact photosystem II and have found two early radical pairs before the electron is transferred to the quinone Q_A. The *apparent lifetime* for primary charge separation is 7 ps, that is, by a factor of 8-12 faster than assumed on the basis of earlier analyses. The main component of excited-state decay is 42 ps. The effective primary charge separation rate constant is 170 ns^{-1}, and the secondary electron-transfer rate constant is 112 ns^{-1}. Both electron-transfer steps are reversible. Electron transfer from pheophytin to Q_A occurs with an apparent overall lifetime of 350 ps. The energy equilibration between the CP43/CP47 antenna and the reaction center occurs with a main *apparent lifetime* of ~1.5 ps and a minor 10 ps lifetime component. Analysis of the overall trapping kinetics based on the theory of energy migration and trapping on lattices shows that the charge separation kinetics in photosystem II is extremely trap-limited and not diffusion-to-the-trap-limited as claimed in several recent papers. These findings support the validity of the assumptions made in deriving the earlier exciton radical pair equilibrium model [Schatz, G. H., Brock, H., and Holzwarth, A. R. (1988) *Biophys. J.* 54, 397-405].

3.1 Introduction

Photosystem (PS) II is responsible in oxygenic photosynthesis for water splitting and for providing reduction equivalents to reduce $P700^+$ of PS I. The structure of PS II from cyanobacteria has recently been determined by X-ray diffraction to a resolution of 3.2-3.5 Å (*7;59-62*). The PS II core consists of the antenna polypeptides CP43 and CP47, which carry 13

and 16 chlorophyll (Chl) *a* molecules, respectively, organized in two layers located near the cytoplasmic and the lumenal sides of the membrane. Furthermore, they contain the D1-D2-cyt *b-559* reaction center (RC) polypeptides, which carry the cofactors of the electron-transfer chain [four Chls, two pheophytins (Pheo), and two quinones] and two additional antenna Chls (the so-called peripheral Chl_{Z1} and Chl_{Z2} molecules), which are located ~25 Å apart from the pigments of the electron transfer chain. In the native state PS II cores occur as dimmers (*63*). The initial processes are light absorption in the antenna, followed by energy transfer to the RC in which ultrafast photon-induced charge separation across the membrane occurs. Eventually the oxygen-evolving complex is oxidized by the RC cofactors and water-splitting occurs at a tetra-nuclear manganese complex (see ref (*25*) for a recent review on electron-transfer processes in PS II).

The energy transfer and charge separation kinetics in intact PS II core particles were studied about two decades ago by time-resolved fluorescence and transient absorption with a resolution of ~10 ps (*29;64;65*). Dominant lifetime components with open RCs (*i.e.*, the F_0 state) were observed in the range from 35 ps (*64*) to 60-80 ps (*65*), depending on the method used, which was ascribed to antenna trapping by primary charge separation and ~300-500 ps, which was assigned to secondary electron transfer to the quinone acceptor Q_A (*29;64;65*). These data subsequently gave rise to the development of a kinetic model for the early energy- and electron-transfer processes in PS II cores, which became known as the "exciton/radical pair equilibrium model" (ERPE model) (*29*). The ERPE model has been used extensively in the field to analyze and explain a wide range of phenomena related to the kinetics of the early processes in PS II such as radical pair formation, its dependence on the redox states of the cofactors, and Chl quenching in the antenna and the RC.

The ERPE model made the hypothesis that internal energy equilibration within the PS II core antennae and from the antennae to the RC should occur on a time scale of a few picoseconds(*29*), that is, below the ~10 ps resolution of the time-resolved experiments at the time (actually an equilibration time of ≤3 ps was estimated). It was therefore assumed in the ERPE model that the charge separation would start from an equilibrated excitation state distributed over both the antenna and the RC pigments. Consequently, no details of the energy-transfer processes were considered in the model. This assumption gave rise to a relatively simple and straightforward description of the excited-state dynamics, which resulted in a biexponential decay and overall trap-limited charge separation kinetics (*29*).[1] The time scale of this energy equilibration process is, however, of central importance for recent discussions which, on the basis of the relatively large distance of 14-17 Å from the antenna Chls to the RC pigments (*60*), questioned the possibility of an energy equilibration on a time

[1] We note here in passing that recently in the literature the typical excited-state equilibration time that was assumed in the derivation of the "exciton/radical pair equilibrium model" has been misquoted to be in the range of a few hundreds of femtoseconds (*35*), *i.e.*, by an order of magnitude shorter than the ≤ 3 ps value that had actually been assumed (*29*).

scale faster than primary charge separation (*32;66*). In fact, it was concluded in these papers that energy transfer to the RC was slow as compared to primary charge separation. Consequently, it has been concluded by Vasil'ev *et al.* as well as other authors that the ERPE model is inadequate to describe the charge separation and trapping dynamics in PS II and that the kinetics is in fact "transfer-to-the-trap-limited" (*24;32*). The latter conclusion implies that the transfer from the antenna to the RC pigments is the rate-limiting step rather than charge separation. In view of this controversial situation a clarification of the rate of the energy-transfer processes in relation to the rates of the electron-transfer processes in intact PS II particles is required. Interestingly, recent time-resolved fluorescence data on intact core particles (*32;66*) did not reveal any components faster than the ~40-60 ps process reported much earlier (*29;64;65*). Yet, very recent transient absorption measurements on the intact PS II cores revealed much faster components (*28*). Similarly, time-resolved experiments on smaller systems, such as the CP47/D1-D2 complex, revealed also faster lifetime components on the time scale of a few picoseconds and 10-20 ps (*35*). However, the assignment of the various lifetime components to energy transfer and/or charge separation processes in these systems is also under debate.

Another controversial discussion that has come up recently concerns the question of whether the rates and the mechanism of the early electron-transfer processes in intact PS II cores and in isolated D1-D2-cyt *b-559* RCs are identical or not. Whereas we estimated very similar intrinsic rate constants for the primary charge separation in intact PS II cores (*29*) and in D1-D2-cyt *b-559* RCs (*67*), the identity of these processes in the two systems has also been questioned recently (*32;66*) (for recent reviews see refs (*25*) and (*68*). In view of this situation we aim in the present work to provide new fluorescence kinetic data on intact PS II cores that complement the recent transient absorption kinetics and are suitable for an improved kinetic modeling of the energy- and electron-transfer processes in PS II. We will in particular address the question of "transfer-to-the-trap-limited" (*i.e.*, diffusion-limited) versus "trap-limited" kinetics.

3.2 Materials and methods

Time-resolved fluorescence measurements have been performed at room temperature on dimeric PS II core particles from *Thermosynechococcus elongatus* (*T. elongatus*) with intact oxygen evolution isolated and purified according to ref (*53*). These particles showed an average oxygen evolution rate of 3200 (±10%) μmol of O_2/(mg of Chl)/h. Fluorescence measurements have been performed in a buffer of 20 mM MES (pH 6.5), containing 500 mM mannitol, and ferricyanide (0.4 mM) was added to keep the RC in an open (F_0) state. To ensure that no significant amount of closed RCs was present, the sample was kept in a rotating (4000 rpm) cuvette of 1.5 mm path length with a diameter of 10 cm, which was also oscillated sideways with 66 rpm. Stopping the movement (and thus allowing RCs to close) of the cuvette led to an increase by a factor of 11-12 in the fluorescence intensity. The laser excitation

intensity was low enough to ensure that during a single passage of the sample volume through the laser beam the excitation probability for a PS II particle was <~50%. Fluorescence kinetics was detected by a single-photon-counting apparatus, which allows measurements with a resolution of 1-2 ps, as described elsewhere (*46;69*). Initial kinetic analysis has been performed by global lifetime analysis (*57*). Subsequent global compartment modeling has been used to test and compare various kinetic models directly on the original data (not on the results of the global lifetime analysis). Advantages of the latter kind of analysis have been discussed previously (*46;57;70*).

3.3 Results

An excitation wavelength of 663 nm, located in the blue absorbing edge of the Q_y band of the Chl antenna, has been chosen. This excites preferentially the CP43 complex (*71;72*). Fluorescence kinetics has been measured with a high signal/noise ratio (30000 counts in the peak channel at all wavelengths) at 4 nm intervals in the range from 673 to 701 nm with very low excitation intensity ($<10^{-4}$ absorbed photons/particle/pulse). Extreme care has been taken to avoid re-excitation of the same particle before reopening of the RC. Thus, the measured kinetics reflects >99% open RCs (see Materials and Methods for details).

For a good description of the kinetics across the whole wavelength range 6 lifetimes were required in global analysis over a fitting range of 2 ns [*cf.* Fig. 3-1 for the decay-associated spectrum (DAS)]. The lifetimes with dominant amplitude were 2, 9, 42, 106, and 332 ps. An additional lifetime of 2 ns with very small amplitude was also required. The χ^2 value for this global fit was 1.07. Leaving out the shortest lifetime component from the fit worsened the χ^2 value drastically to 1.15 and led to large deviations in the residual plots (the data for six- and five-component analyses are given in the Supporting materials). Whereas the longer lifetimes, including the ~40 ps component, have been resolved earlier in the fluorescence kinetics of intact PS II cores (*29;32;65;66*), the two faster lifetimes of 2 and 9 ps have not been resolved before.

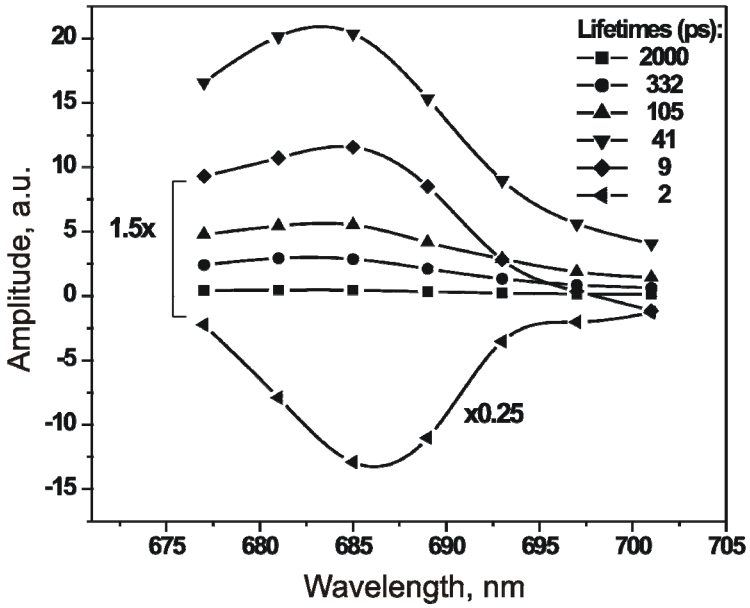

Fig. 3-1 Decay-associated emission spectra (DAS) of PS II core particles from *T. elongatus* excited at 663 nm as analyzed by global lifetime analysis.

The amplitude of the fastest lifetime component is negative across the whole wavelength range with a minimum around 685 nm and approaches zero near 675 nm. At slightly shorter detection wavelengths a positive amplitude has been observed for this component. However, we did not include these short wavelength data in the present fit because below 676 nm we cannot exclude a scattering contribution from the exciting pulse. The amplitudes of all other lifetime components are positive across the whole spectrum with peaks around 680-685 nm, except for the 9 ps component, which is also slightly negative at the longest detection wavelength. The fastest component (~2 ps) clearly shows the amplitude feature of an energy-transfer process, and we assign it to a mixture of both energy transfer within the antenna complexes CP43 and CP47 (*73*) and to energy transfer from the antenna complexes to the RC, in agreement with recent femtosecond transient absorption data on the same system (*28*) (*vide infra* for a detailed discussion). All longer lifetime components must be assigned to energy trapping by primary charge separation and to secondary electron-transfer processes, which can be observed in the Chl fluorescence decay due to the charge recombination processes active in PS II (*29;46*). The assignment of the ~330 ps process is likely electron transfer from $Pheo^-$ to Q_A (*29*). Strictly speaking, each of the lifetimes, which are the inverse eigenvalues of the kinetic matrix of the system, depends on all rate constants in the system and generally does not reflect the property of a particular excited state species or radical pair intermediate. For this reason an interpretation in terms of lifetime components can provide at best a qualitative interpretation, and a detailed kinetic modeling is required to get physical insight into the kinetics of the system.

3.4 Kinetic modeling

We have applied global compartment modeling to the kinetics by testing several different kinetic models on the data. The simplest kinetic scheme that allowed a good description of the experimental data is shown in Fig. 3-2 together with the optimal rate constants from a global target modeling. The system contains five compartments, that is, three excited-state compartments (CP43*, CP47*, and RC*) and two radical pair compartments (RP1 and RP2). RC* stands for the equilibrated excited state of the six pigments comprising the RC. The species-associated emission spectra (SAS) of the compartments are given in Fig. 3-4, and the time-dependence of the populations of the compartments is shown in Fig. 3-5. The SAS of radical pairs are zero by definition, because RPs are not fluorescent. Nevertheless, the kinetics of the RP states is observed in fluorescence indirectly by way of the charge recombination fluorescence because both early electron-transfer steps are reversible.

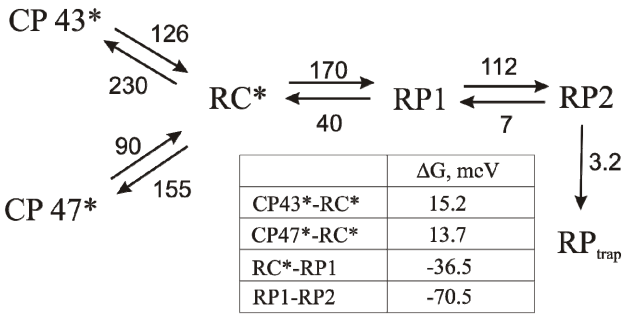

	ΔG, meV
CP43*-RC*	15.2
CP47*-RC*	13.7
RC*-RP1	-36.5
RP1-RP2	-70.5

Fig. 3-2 Kinetic model for dimeric PS II core particles resulted from target analyses. Rate constants are given in ns^{-1}. Errors of electron-transfer rates are ±10%, whereas errors in energy-transfer rates may be up to ±20% due to the lifetime of 1.5 ps being close to the resolution limit of the apparatus. Lifetimes resulting from the model are shown at the bottom. (*Inset*) Free energy differences Δ*G* between compartments as calculated from the forward and backward rates of energy or electron transfer.

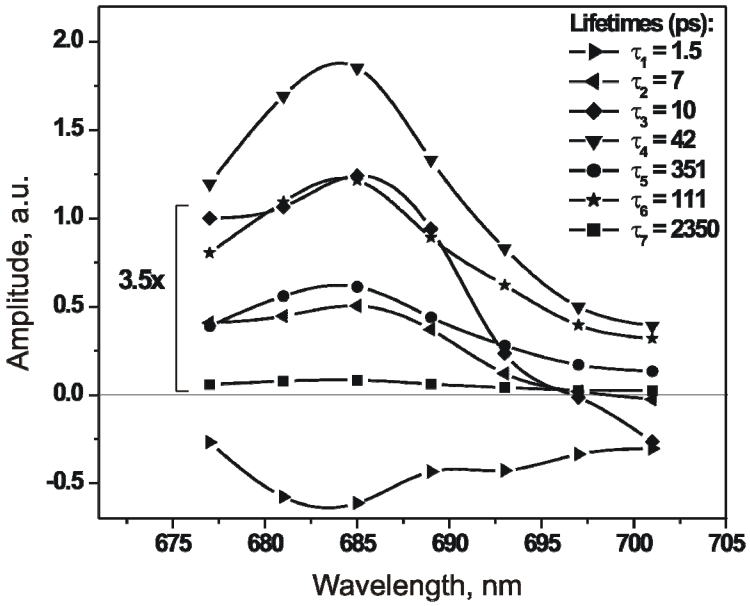

Fig. 3-3 DAS from target analysis leading to the kinetic scheme shown in Fig. 3-2. Lifetimes τ_1-τ_5 are those that result from the kinetic model. The 111 and 2350 ps lifetime components are additional free running components outside the kinetic scheme, which are required for a good fit.

This kinetic scheme results in lifetime components of 1.5, 7, 10, 42, and 351 ps. In the modeling two additional free running lifetime components of 111 ps and 2.3 ns of small amplitude were required for a good fit (see Fig. 3-3 for the corresponding DAS). Thus, all lifetime components from the global analysis are present in this model. However, the 9 ps lifetime from global analysis is now split into two components of 7 and 10 ps, which would be too close-lying to be resolved in global analysis. The small 2.3 ns component is clearly due to a very small amount of closed RCs in the sample, whereas the origin of the 111 ps component, which is outside the kinetic scheme shown in Fig. 3-2, is unclear at present. Thus, there is possibly room for a slightly extended or more complex model (*vide infra*). Other and/or simpler kinetic schemes than the one shown in Fig. 3-2 either did not result in a good fit to the data or did not provide any reasonable SAS or both.

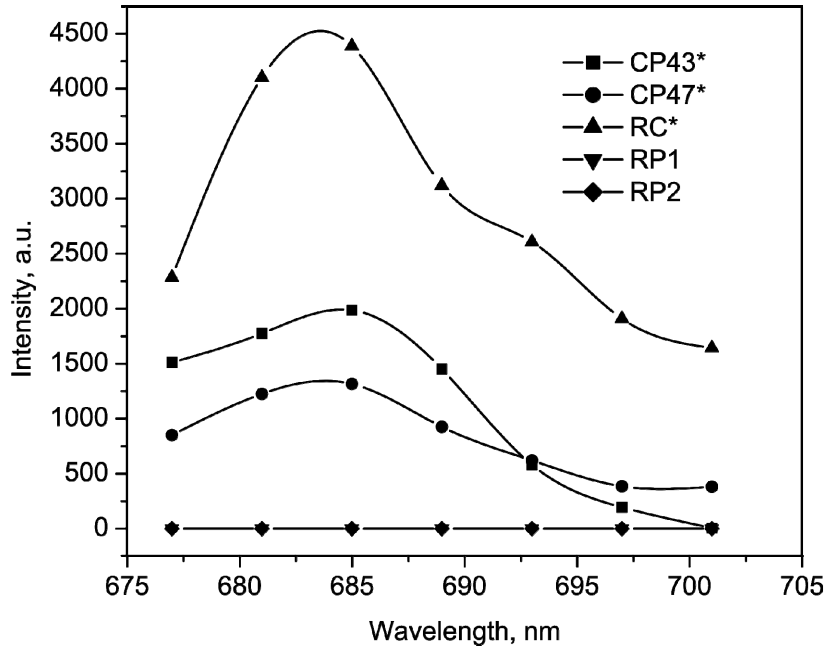

Fig. 3-4 Species-associated emission spectra (SAS) resulting from the fit of the kinetic model present in Fig. 3-2 to the data.

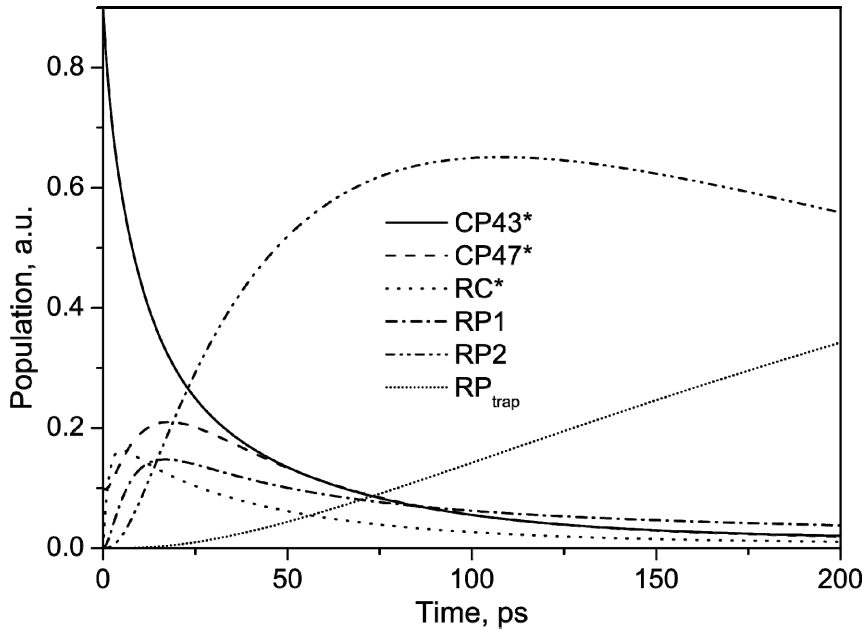

Fig. 3-5 Calculated time dependence of populations of the compartments as shown in Fig. 3-2.

3.5 Discussion

The kinetic scheme giving a good fit to the data is analogous to the one found earlier explaining the femtosecond transient absorption data (*28*). The rate constants for the electron-transfer processes are in fact the same within the error limits as found for transient absorption. Also, the rate constants of energy transfer are very similar, except for a slight difference in the rate constant of forward energy transfer from CP43 to the RC, which is somewhat higher in transient absorption than in the fluorescence model.

We believe, however, that the 111 ps component (contributing ~10% to the relative amplitude) is outside of our present kinetic model and that it most likely derives from the intact PS II core system, unless we assume some heterogeneity. If one wants to include such a

111 ps component, the kinetic scheme has to be extended beyond the one shown in this paper. From the expected rate constant of a process giving rise to a 111 ps component (somewhere in the range of 6-9 ns^{-1}) one can conclude that this should be a process that happens after formation of the second radical pair but before the electron transfer to Q_A. We have tested various such extended models on our fluorescence data but could not come to a clear conclusion as to the origin of the 111 ps component. One likely possibility would be that this component reflects a protein relaxation step after formation of RP2 and before the electron transfer to Q_A. Protein relaxation steps have been described for PS II cores and RCs by various authors, including ourselves (see, *e.g.*, refs (*66*) and (*67*). The upshot is that the model presented here should be considered as a minimal model that provides a very good description for the mechanism and rates of the electron-transfer steps (note that any potential further electron transfer step should have shown up in the transient absorption data), but might have to be extended later to include some protein relaxation as well.

The important conclusion for the present paper – and that is the result from all our modeling of more extended kinetic scheme – is, however, that whatever extension in the kinetic scheme is made, it does not change to any significant extent the rate constants of the energy-transfer processes between antenna and RC or the rate constants of the early electron transfer step(s). Because the focus of the present paper is primarily on the clarification of the trap- versus diffusion-limited model and of the rate constant [and *apparent lifetime* (for clarification of the kinetic terms, see ref (*46*)] of the primary charge separation, any further extension of the kinetic scheme would not affect in any way our conclusions drawn in this paper (or the rate constants in Fig. 3-2 for the processes up to and including the rate constants for the formation of RP2).

The weighted eigenvectors corresponding to the kinetic scheme in Fig. 3-2 are given in Table 3-1. This eigenvector matrix allows one to assign the origin of the various lifetimes in the model to the physical processes and the compartment kinetics. A negative value indicates a rise of a compartment population, and a positive value indicates a decay. Generally, the lifetimes are functions of all rate constants in the model. Thus, there is essentially some contribution of all lifetimes to each of the compartment populations. However, we are looking here only for the amplitudes that make the dominant contributions to the various compartment populations. It can be clearly seen from Table 3-1 that the 1.5 ps lifetime represents primarily the rise of the RC* population; that is, it is the dominant component describing the energy-transfer kinetics from the antennae to the RC besides a very small contribution to the RC* rise by the 7 ps lifetime. Thus, the overall equilibration time between antenna and RC should be in the range of a few picoseconds. The 7 ps component represents primarily the rise of the RP1 population. It thus reflects the *apparent lifetime* for primary charge separation, which is at least a factor of 5 faster than believed previously (*65*). The 10 ps component is a mixed component that cannot be assigned exclusively to one process. The energy transfer between the not directly connected CP43 and CP47 antennae makes a strong

contribution, as does the rise of RP1. The 42 ps component is the dominant excited-state decay component (all three excited-state compartments contribute with decay terms to this component), and it also reflects the main rise of the RP2 population. RP1 and RP2 have been identified as representing the radical pair states $Chl_{accD1}^{+}Pheo_{D1}^{-}$ and $P_{D1}^{+}Pheo_{D1}^{-}$, respectively (*28*). The 351 ps component reflects the rise of the RP trap state, which in analogy with previous data (*28;29*) represents the state $Pheo_{D1}^{+}Q_{A}^{-}$.

Table 3-1 Weighted eigenvectors (amplitudes) of the compartments for the kinetic model shown in Fig. 3-2 (excitation vector is given in parentheses)

lifetime, ps	**CP43*** (0.9)	**CP47*** (0.1)	**RC*** (0)	**RP1** (0)	**RP2** (0)	**RP_{trap}** (0)
1.5	0.087	0.055	-0.198	0.068	-0.012	$5.9 \cdot 10^{-5}$
7	0.076	0.022	-0.009	-0.38	0.297	-0.006
10	0.354	-0.372	0.034	0.102	-0.122	0.004
42	0.352	0.366	0.156	0.144	-1.168	0.158
351	0.031	0.030	0.017	0.065	1.005	-1.143

The time dependence of populations $C_j(t)$ for each intermediate compartment j (top row) follows the equation $c(t) = \sum_{i=1}^{n} A_{ij} \exp(-t/\tau_i)$, where A_{ij} represents the elements of the eigenvector matrix and τ_i are the lifetimes given in the left column. Inspection of this matrix allows one to easily deduce the *apparent lifetimes* and their amplitudes that contribute to the rise (negative amplitude) and decay (positive amplitude) of population of each of the intermediates (compartments). For further details of this presentation see M.G. Müller, J. Niklas, W. Lubitz, and A. R. Holzwarth, *Biophys.J.* 85:3899-3922, 2003.

The SAS of the excited states of the antenna complexes CP43 and CP47 have their emission peaks around 685 nm. The emission spectrum (SAS) of the excited RC state in an intact PS II core is resolved here for the first time. It peaks between 683 and 685 nm and has more than twice the amplitude of the SAS of the antenna complexes. The area under an SAS being proportional to the radiative transition probability of the corresponding state implies that the radiative rate of the RC* state is by a factor of 2-3 higher than that of the antenna excited states. This higher rate reflects, and is consistent with, the well-known increase of transition probability due to exciton coupling of the lower exciton states of the RC complex (*74;75*). It is interesting to compare the SAS of the RC* state to the one obtained earlier for the isolated D1-D2-cyt *b-559* complex, which is very similar in shape and also substantially higher in amplitude than the SAS of the peripheral monomeric Chl_Z molecules in the D1-D2 RC (*67*). Thus, in both the intact PS II cores and the isolated D1-D2 RC the transition probability of the emitting exciton states of the RC is by a factor of 2-3 higher than for a monomeric Chl. However, the maximum of the RC emission in intact PS II cores seems to be red-shifted by ~2 nm as compared to isolated D1-D2 RCs (*67*). It is also worth mentioning that the SAS of the RC shows a pronounced shoulder on the long-wavelength tail around 693 nm, and the spectrum shows substantial amplitude well above 700 nm. It is possible that the long-wavelength tail is caused by emission from low-lying emitting states, either exciton states or

even charge-transfer states with significant optical transition probability. The presence of the latter states has recently been proposed for the isolated D1-D2 RC on the basis of exciton calculations (*76*).

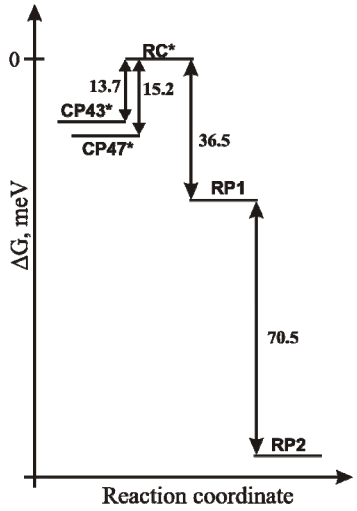

Fig. 3-6 Scheme of free energy differences Δ*G* between the model compartments. The free energy of the RC excited state is used as thermodynamic reference.

From the rate constants of forward and reverse electron transfer in Fig. 3-2 one can calculate the free energy differences between the excited RC* state and the radical pairs shown in Fig. 3-6. The drop in Δ*G* for RP1 is -37 meV and between RP1 and RP2 is -71 meV, resulting in a total free energy drop of slightly less than -110 meV for the state RP2. Thus, the main energy drop occurs in the second electron-transfer process.

Trap versus transfer-to-the-trap limit

The main energy transfer lifetime between antenna and RC is 1.5 ps, with some small contribution of the 7 ps component to the rise of the RC* population (*vide supra*). In addition, the 10 ps component contributes with a small amplitude to energy equilibration between CP43 and CP47. The overall very fast energy transfer between antenna and RC is reflected in the fact that after antenna excitation the population of RC* reaches its maximal value at ~4-5 ps, whereas the RP1 state reaches its maximal population after ~15 ps and the RP2 state after ~100 ps. According to these data the energy transfer between antenna and RC (the transfer to the trap) is not rate-limiting for the overall charge separation process. Our results, which resolve for the first time the kinetics of energy transfer between the antenna and the RC directly, are in excellent agreement with the assumptions made previously in the derivation of the ERPE model (*29*).

The most transparent way of deciding upon the individual contributions of energy transfer (diffusion) and charge separation to the overall trapping process is the average lifetime of the decay of all excited states and their dependence on the rates of energy transfer and charge separation. The total average trapping time $\tau_{tot\ trap}$ as derived from theoretical work on energy transfer and trapping (*77*;*78*) is given by a sum of the individual contributions of diffusion within the antenna τ_{diff}, the transfer-to-the-trap (RC) time $\tau_{transfer\text{-}to\text{-}trap}$, and the charge

separation time τ_{CS}, respectively. Because in our simple compartment model (Fig. 3-2) we are not distinguishing between internal antenna diffusion and transfer to the trap processes, the relationship can be simplified to two terms as follows:

$$\tau_{tot\ trap} = \tau_{diff} + \tau_{transfer-to-trap} + \tau_{CS} = \tau_{et} + \tau_{CS} \tag{3.1}$$

Thus, τ_{et} represents the sum of the intra-antenna diffusion and transfer-to-the-trap times. The contributions of the charge separation time τ_{CS}, on the one hand, and the total energy transfer time τ_{et} to the total average trapping time, on the other hand, can be calculated easily within the kinetic model of Fig. 3-2 by scaling up either the energy-transfer rates or the electron-transfer rates by a factor of >100, respectively. In this way the contributions of either τ_{et} or τ_{CS}, respectively, to the total trapping time are negligible and the value of the other term can be obtained. An alternative and equivalent way of obtaining τ_{CS} consists of solving the system of differential equations for the kinetic scheme with all of the initial excitation starting on the RC.

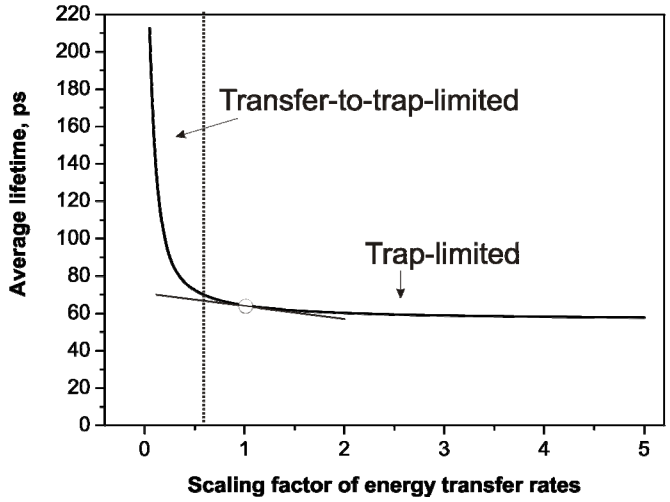

Fig. 3-7 Dependence of the excited-state average lifetime $\tau_{tot\ trap}$ on the scaling of the energy-transfer rates given in the kinetic model (see Fig. 3-2).

In a transfer-to-the-trap-limited kinetics the contribution of τ_{et} to the total trapping time is the dominant term, whereas in a trap-limited kinetics the τ_{CS} is the dominant term. Thus, in trap-limited kinetics the total trapping time depends only very weakly on the up-scaling of the energy-transfer rates. The dependence of the total trapping time (equivalent to the average excited-state decay lifetime) on the scaling of the energy-transfer rates in our model is shown in Fig. 3-7. The scaling factor 1 corresponds to the experimental situation. As expected, the total trapping time depends only very weakly on the up-scaling of the energy-transfer rates, thus indicating a trap-limited overall kinetics for PS II cores. The calculation yields $\tau_{tot\ trap}$ = 65 ps, τ_{et} = 9 ps, and τ_{CS} = 56 ps. With a ratio of τ_{CS} /$\tau_{et} \geq 6$ the kinetics in PS II cores is on the extreme trap-limited side. This result is in vast disagreement with recent conclusions for the overall trapping kinetics in PS II cores to be transfer-to-the-trap-limited (*24;32*). The conclusions of Vasil'ev *et al.* claiming a transfer-to-the-trap-limited model result from a huge overestimation of the primary charge separation rate in PS II [rate constants for

the primary charge separation process from P680 ranging from a minimum of 1400 ns^{-1} (*32*) to 7000 ns^{-1} (*66*) were reported] and a pronounced underestimation of the antenna to RC energy-transfer rates (*32;66*). Some of the likely reasons for the inadequacy of their estimated energy- and electron-transfer rates are revealed by their sequential radical pair relaxation model (*66*). In that analysis the assumed intermediates RP1 to RP3 as well as the rate constants connecting P680* and these radical pairs are pure fitting artifacts that have no experimental foundation. This is clearly borne out by the fact that the fastest experimentally resolved lifetime component in the Vasil'ev data for PS II cores with open RC was 60 ps. This fastest lifetime can be obtained in their data by completely leaving out RP1-RP3 from the modeling. On the basis of the same arguments their conclusion of a significant radical pair relaxation contribution to the kinetics of PS II cores with open RCs lacks experimental support. We also note that there exists a severe discrepancy between the average lifetime of antenna decay of PS II cores with open RCs (F_0) in the measurements of Vasil'ev (*66*), which is 174 ps, and our average fluorescence decay lifetime with open centers of 65 ps (*vide supra*). The discrepancy is primarily caused by the significant contributions of 0.97 and 5 ns components in the fluorescence decay reported by Vasil'ev. These lifetime components according to our analysis are not related to PS II cores with intact open RCs but originate most likely from a contribution of closed RCs and/or damaged PS II particles. A non-negligible contribution of an 1.8 ns component to the fluorescence decay of PS II cores at F_0 – also likely resulting from a contribution of PS II cores with closed RCs – was also found earlier by Schatz *et al.* (*65*). It requires very high sample purity and extreme care in avoiding multiple excitation of RCs closed by previous laser pulses in order to be able to achieve an experimental fluorescence decay that is essentially free of long-lived components in the range of 1 ns or longer.

Conclusions

The analysis of recent femtosecond transient absorption data of PS II cores with open RCs (*28*) and the analysis of the present fluorescence kinetic data show that both kinds of data can be described by the same kinetic model. The results presented here confirm the validity of the assumptions regarding energy equilibration made in deriving the earlier ERPE model for the trapping and charge separation kinetics in PS II cores (*29;65*). However, both the recent transient absorption data and the refined fluorescence kinetics reported here require an extension of the early ERPE model to include one additional electron-transfer step leading to an additional early radical pair. This first radical pair is the $Chl_{accD1}^{+}Pheo_{D1}^{-}$ state (*28*). Formation of this intermediate reflects itself in the fluorescence kinetics by an additional 7 ps component, which was not contained in the ERPE model. It is particularly gratifying that the same mechanism and also the same rates of the two early electron transfer steps have been found for isolated PS II cores (this work and ref (*28*)) and for isolated D1-D2-cyt *b-559* RC (*28*). This finding is in vast contrast to the claim of a ~100-fold difference in the primary

charge separation rate constants for isolated PS II RCs, on the one hand, and intact PS II cores, on the other (*66*).

3.6 Supporting materials

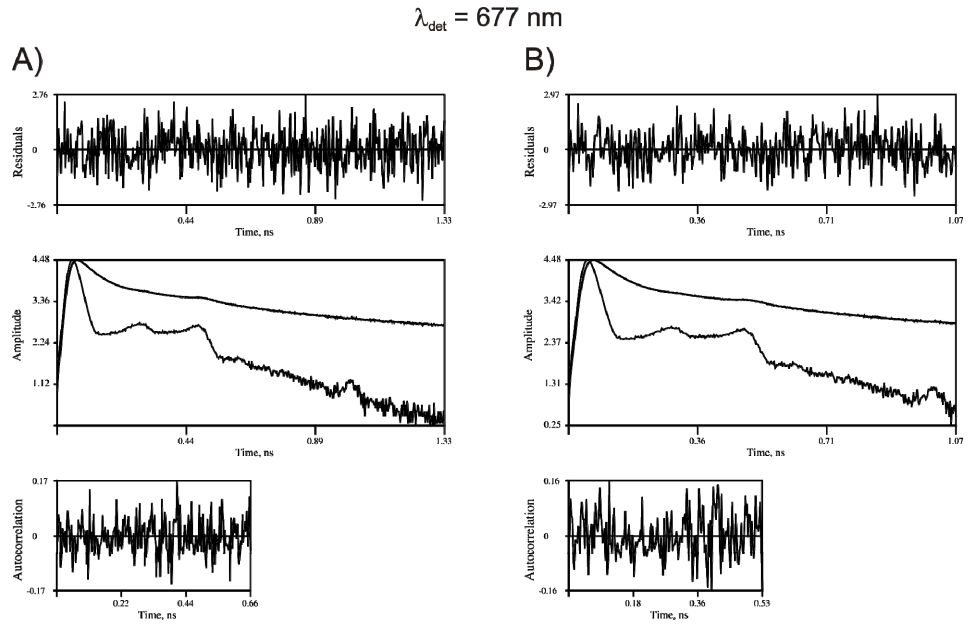

Fig. S3-1 *(top)* Residuals plot; *(middle)* Original decay at 677 nm overlaid with fit (thin line) and laser pulse (all on logarithmic scale) for the decays at the indicated wavelengths; *(bottom)* Autocorrelation function of the residuals. A) 6-component fit (2 ps, 9 ps, 41 ps, 105 ps, 332 ps and 2 ns); B) 5-component fit (6 ps, 8.2 ps, 49 ps, 245 ps and 2ns).

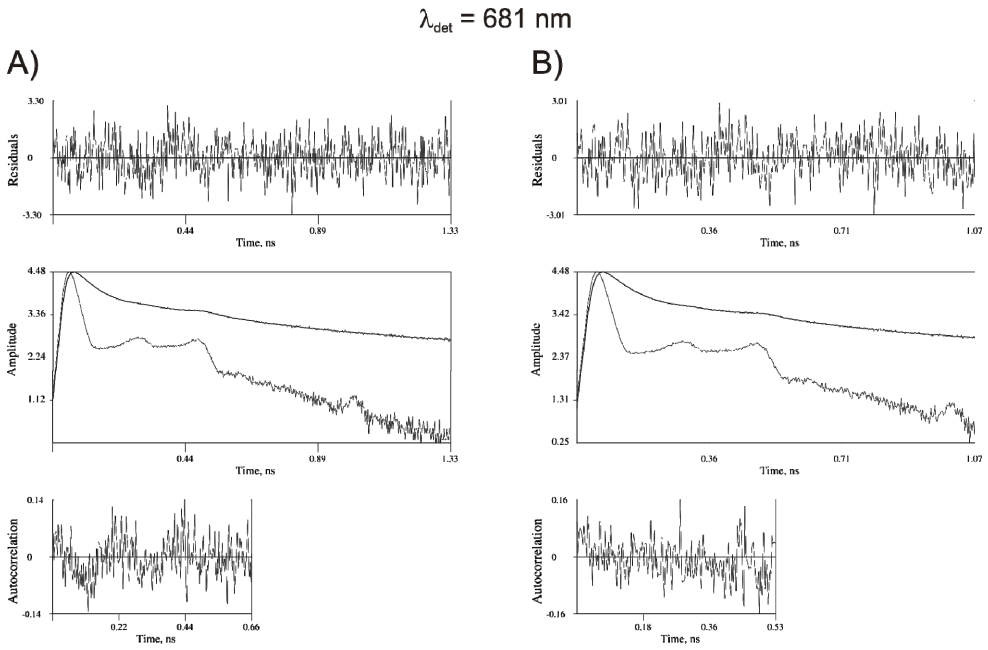

Fig. S3-2 *(top)* Residuals plot; *(middle)* Original decay at 681 nm overlaid with fit (thin line) and laser pulse (all on logarithmic scale) for the decays at the indicated wavelengths; *(bottom)* Autocorrelation function of the residuals. A) 6-component fit (2 ps, 9 ps, 41 ps, 105 ps, 332 ps and 2 ns); B) 5-component fit (6 ps, 8.2 ps, 49 ps, 245 ps and 2ns).

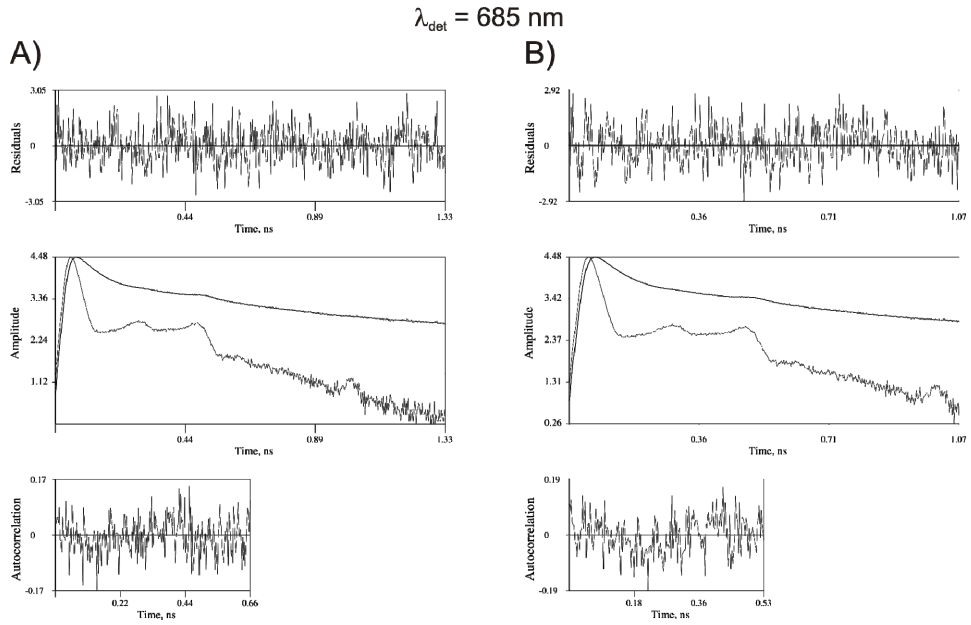

Fig. S3-3 *(top)* Residuals plot; *(middle)* Original decay at 685 nm overlaid with fit (thin line) and laser pulse (all on logarithmic scale) for the decays at the indicated wavelengths; *(bottom)* Autocorrelation function of the residuals. A) 6-component fit (2 ps, 9 ps, 41 ps, 105 ps, 332 ps and 2 ns); B) 5-component fit (6 ps, 8.2 ps, 49 ps, 245 ps and 2ns).

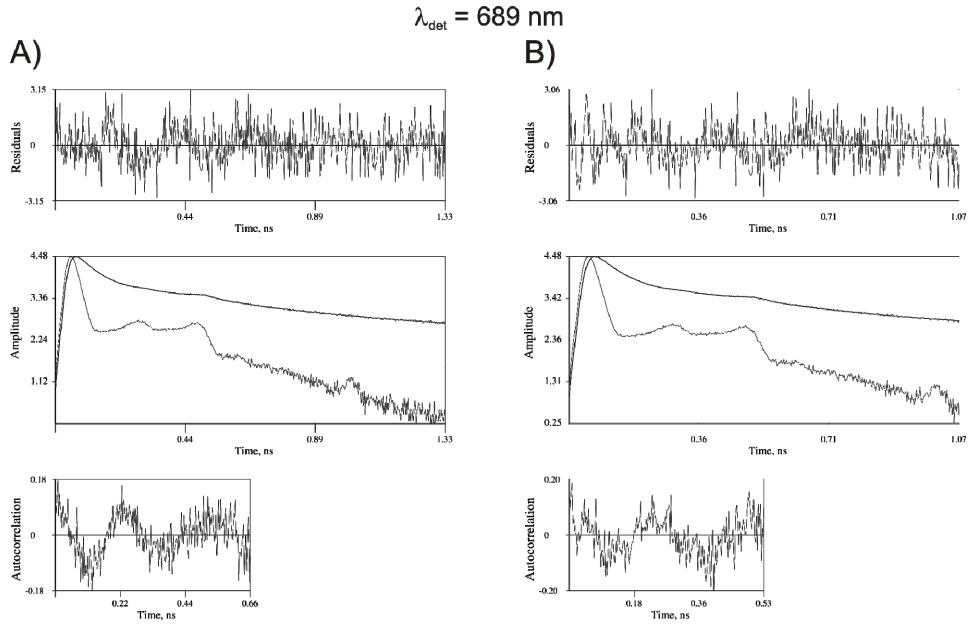

Fig. S3-4 *(top)* Residuals plot; *(middle)* Original decay at 689 nm overlaid with fit (thin line) and laser pulse (all on logarithmic scale) for the decays at the indicated wavelengths; *(bottom)* Autocorrelation function of the residuals. A) 6-component fit (2 ps, 9 ps, 41 ps, 105 ps, 332 ps and 2 ns); B) 5-component fit (6 ps, 8.2 ps, 49 ps, 245 ps and 2ns).

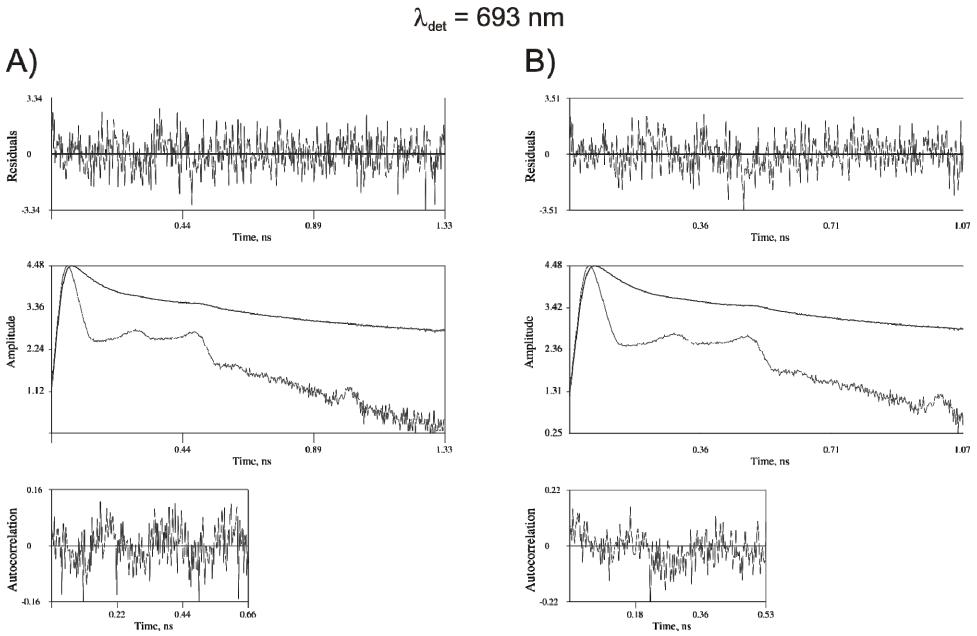

Fig. S3-5 *(top)* Residuals plot; *(middle)* Original decay at 693 nm overlaid with fit (thin line) and laser pulse (all on logarithmic scale) for the decays at the indicated wavelengths; *(bottom)* Autocorrelation function of the residuals. A) 6-component fit (2 ps, 9 ps, 41 ps, 105 ps, 332 ps and 2 ns); B) 5-component fit (6 ps, 8.2 ps, 49 ps, 245 ps and 2ns).

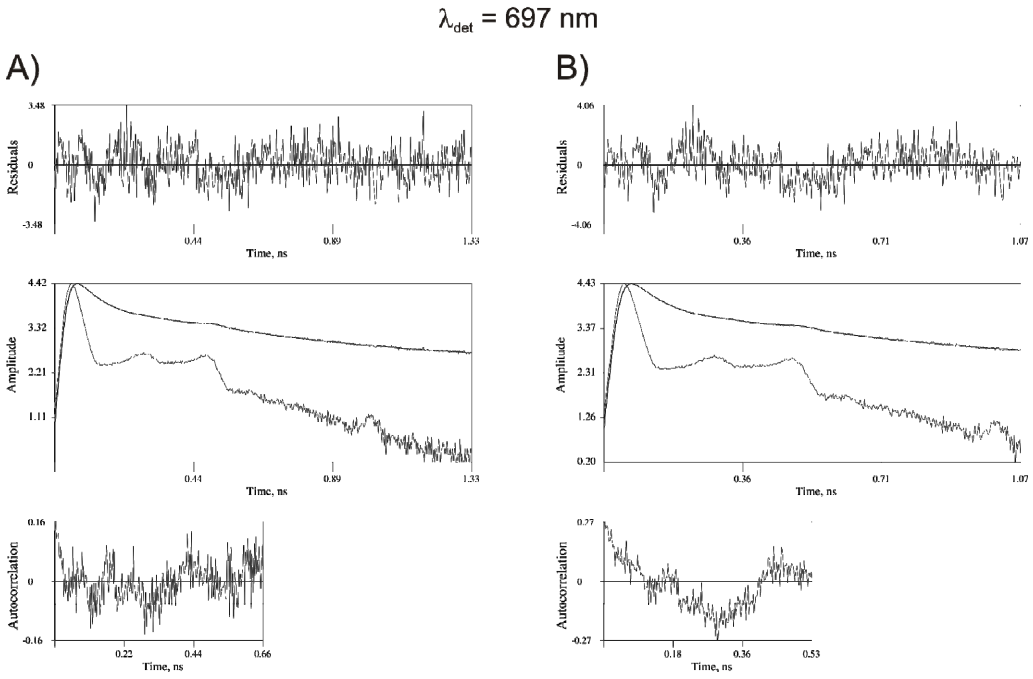

Fig. S3-6 *(top)* Residuals plot; *(middle)* Original decay at 697 nm overlaid with fit (thin line) and laser pulse (all on logarithmic scale) for the decays at the indicated wavelengths; *(bottom)* Autocorrelation function of the residuals. A) 6-component fit (2 ps, 9 ps, 41 ps, 105 ps, 332 ps and 2 ns); B) 5-component fit (6 ps, 8.2 ps, 49 ps, 245 ps and 2ns).

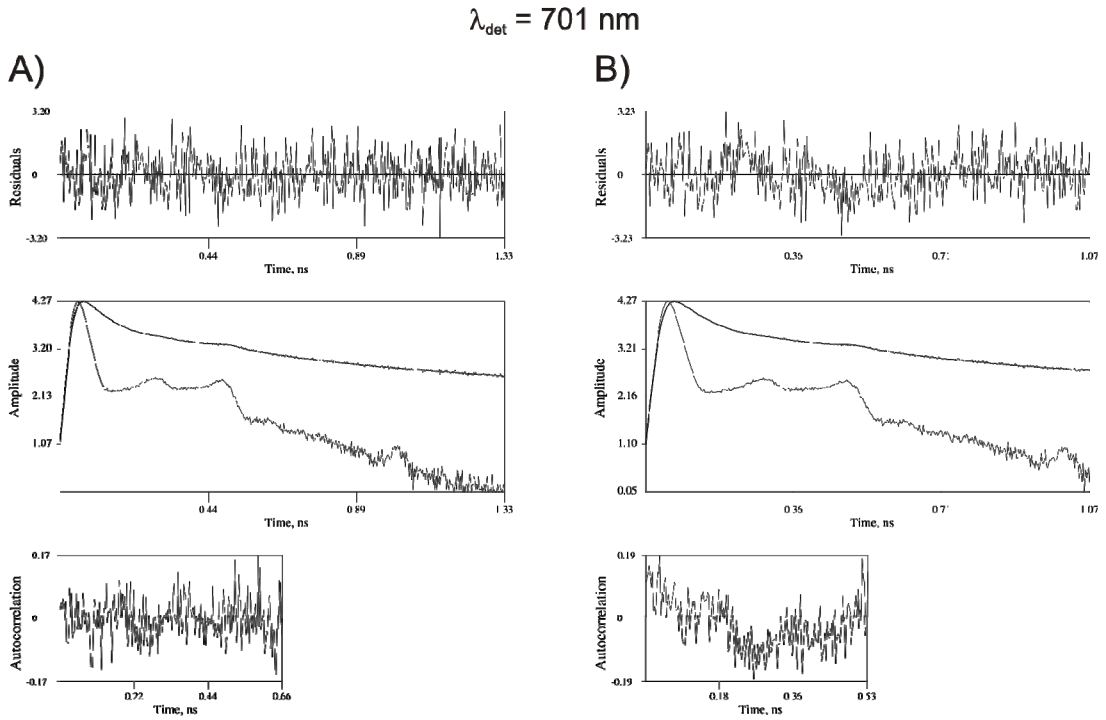

Fig. S3-7 *(top)* Residuals plot; *(middle)* Original decay at 701 nm overlaid with fit (thin line) and laser pulse (all on logarithmic scale) for the decays at the indicated wavelengths; *(bottom)* Autocorrelation function of the residuals. A) 6-component fit (2 ps, 9 ps, 41 ps, 105 ps, 332 ps and 2 ns); B) 5-component fit (6 ps, 8.2 ps, 49 ps, 245 ps and 2ns).

4 Charge separation, stabilization, and protein relaxation in photosystem II particles with closed reaction center

This chapter is based on the publication: M. Szczepaniak, J. Sander, M. Nowaczyk, M.G. Müller, M. Rögner, A.R. Holzwarth. Biophysical Journal 96 (2009), 621-631.

The fluorescence kinetics of cyanobacterial Photosystem II core particles with closed reaction centers have been studied with picosecond resolution. The data are modeled in terms of electron transfer and associated protein conformational relaxation processes, resolving four different radical pair states. The target analyses reveal the importance of protein relaxation steps in the electron transfer chain for the functioning of PS II. We also tested previously published data on cyanobacterial PSII with open RC using models that involved protein relaxation steps as suggested by our data on closed RCs. The rationale for this reanalysis is that at least one short-lived component could not be described within the previous simpler models (Miloslavina,Y., M. Szczepaniak, M. G. Müller, J. Sander, M. Nowaczyk, M. Rögner, and A. R. Holzwarth. 2006. Biochemistry. 45: 2436-2442). This new analysis supports the involvement of a protein relaxation step also for open RCs. In this model the rate of electron transfer from reduced pheophytin to the primary quinone Q_A is determined to be 4.1 ns^{-1}. The rate of initial charge separation is slowed down substantially from about 170 ns^{-1} in PS II with open reaction centers to 56 ns^{-1} upon reduction of Q_A. However the free energy drop of the first RP is not changed substantially between the two RC redox states. The currently assumed mechanistic model, assuming the same early radical pair intermediates in both states of RC is inconsistent with the presented energetics of the RPs. Additionally, comparison between PS II with closed RCs in isolated cores and in intact cells reveals slightly different relaxation kinetics, with a ca. 3.7 ns component present only in isolated cores.

4.1 Introduction

Photosystem II (PS II) is one of the photosystems of oxygenic photosynthetic organisms that is responsible for oxygen evolution (*79;80*). Its structure has been recently determined to relatively high resolution, down to 3 Å (*7;8*). In cyanobacteria PS II captures light energy by a small core antenna, consisting of the CP43 and CP47 antenna subunits, which is consequently transferred to the reaction center (RC) pigments, where it triggers the charge separation process and secondary electron transfer steps. The electron transfer chain consists of chlorophyll P_{D1}, accessory chlorophyll (Chl_{accD1}), pheophytin ($Pheo_{D1}$), plastoquinones A (Q_A) and B (Q_B). After double reduction and succeeding protonation of Q_B, quinone B is released to the plastoquinole pool and new plastoquinone enters the Q_B cavity. On the donor side water is

oxidized to molecular oxygen by the manganese cluster (Mn_4Ca) driven by highly oxidizing P_{D1}^+ *via* tyrosine (TyrZ) – for recent reviews see (*23-25*).

In contrast to earlier mechanistic models that assumed P_{D1} as the primary electron donor and $Pheo_{D1}$ as the primary acceptor, it has been shown recently that for intact PSII cores with open RC (Q_A oxidized) (*28*) and also for isolated D1-D2-cyt *b-559* RCs that do not contain Q_A (*27;28*) the primary electron donor is Chl_{accD1} and the primary acceptor is $Pheo_{D1}$ at physiological temperatures. Only in the second electron transfer (ET) step is P_{D1}^+ formed by oxidation from Chl_{accD1}. It had already been shown earlier by Prokhorenko and Holzwarth (*26*) that at low temperature for isolated RCs the primary electron donor is Chl_{accD1}, which was recently also confirmed by the transient absorption spectroscopy on the PSII RC mutants (*81*). The same rate constants for the primary electron transfer steps were found for isolated RCs and for open PSII cores (*28*). Despite the fact that Groot *et al.* (*27*) and Holzwarth *et al.* (*28*) proposed the same ET mechanism for RCs the rate constants for primary charge separation differed by a factor of more than 5 in their models.

The kinetics of PSII with closed RCs (Q_A reduced) in isolated cores, BBY particles, and intact organisms like green algae has been studied by a number of authors (for reviews see (*30;34;82*)). One of the most pronounced effects of closing the RC in PSII is an increase in the yield of fluorescence by a factor of 4-6, and a corresponding lengthening of the average fluorescence lifetime (*31;34*). This effect has been explained in the "exciton-radical pair equilibrium" (ERPE) model (*65*) by electrostatic repulsion of the charge on Q_A and the corresponding negative charge on $Pheo_{D1}$. As a consequence the energy of the primary RP (at that time assumed to be P^+Pheo^-) would be raised above the energy of the equilibrated excited state [Ant-P680]*, resulting in a decrease of the primary charge separation rate and a concomitant increase of the charge recombination rate (*29*). Gibasiewicz *et al.* (*83*), performing time-resolved photovoltage measurements on destacked PSII membranes came to similar conclusions. They found however a larger influence of Q_A^- on the charge recombination rate than on the primary charge separation rate, in contrast to Schatz *et al.* (*29*). The long lifetimes for PSII with closed RCs found in a large variety of studies varied from 1 to 7 ns (*29;31;64;66;84*). Even longer lifetimes (≥10 ns with large amplitudes) are found when the primary quinone Q_A is double-reduced (*84;85*).

Although studies on the primary events in PSII were initiated over 20 years ago, there still exists no agreement on the character of the energy and electron transfer kinetics (for a more detailed state of the current knowledge on this topic see the following review articles (*23;25*)). Schatz *et al.* (*65*) developed the ERPE model representing exciton trapping, charge separation, charge recombination and charge stabilization processes. The key point of this model is a trap-limited kinetics, implying rapid energy equilibration between antenna and RC chlorophylls and a much slower charge separation (CS) step. The main idea of the ERPE model was confirmed by a number of experiments (*28;33;34*), which resulted in the common value of the intrinsic charge separation rate of about $(5\text{-}6\ ps)^{-1}$. Interestingly Andrizhiyevskaya

et al. (*35*) for a CP47-D1/D2 preparation reported an intermediate kinetics just between the trap- and the diffusion-limited cases, while other authors proposed a diffusion-limited kinetics for intact PS II cores (*32;56*).

All photosystems consist of pigments and other cofactors embedded in a protein matrix. As a consequence the rates of the energy and electron transfer reactions depend critically on the pigment-protein interactions. Time-dependent radical pair (RP) relaxation has been studied in detail for bacterial RCs (*37-40*) (see also (*25*) for a review). For bacterial RCs the rates of charge recombination from $P^+Q_B^-$ and $P^+Q_A^-$ are strongly dependent on multiple turnover processes and/or dark/light adaptation (*36;86-90*) proving the involvement of protein conformational changes. These processes have been discussed in terms of non-equilibrium self-organization of proteins in electron transfer reactions (*87*). For PS II a dynamical RP relaxation has been demonstrated already for isolated D1-D2-cyt *b-559* RCs (*28;42;43;91*) and may thus be expected also for intact PSII cores.

The current work reports a picosecond fluorescence study on cyanobacterial intact PSII core complexes with closed RCs. We address the following questions: i) what are the rates of the electron transfer steps[2], ii) what is the nature of the RPs in PSII with reduced Q_A, and iii) and most importantly, which role does protein relaxation play in charge separation and stabilization of the RPs. Thus, in the present work we are focusing exclusively on the electron transfer steps and therefore the experimental data are analyzed in terms of models with 3 or 4 RPs that reflect both electron transfer processes as well as protein relaxation steps.

4.2 Materials and methods

Sample preparation

Time-resolved fluorescence measurements were conducted on PS II core complexes from *T. elongatus* with an active oxygen evolving complex as described earlier (*33*). Samples with closed RCs were measured under oxygen-free conditions by adding an oxygen-scavenging system (65 µg/ml glucoseoxidase, 65 µg/ml catalase and 8mM glucose). Buffer components were as following: 20 mM MES (pH 6.5) containing 10 mM $MgCl_2$, 10 mM $CaCl_2$, 0.5 M mannitol and 0.03% β-DM. Since 60-70% of the particles contain a Q_B molecule, DCMU plus weak light irradiation was used to assure complete removal of Q_B from its binding pocket (*92;93*) and to reliably reduce Q_A but at the same time avoid double reduction of Q_A (*85*). Two different concentrations of DCMU were tested: 20 µM and 100 µM but no influence

[2] Note that recently published theoretical calculations by Raszewski *et al.* (*128*) propose that the bottleneck for the decay of PSII excited states decay is energy transfer from the antennae system to the RC. Experimental data (*28*) are in conflict with the slow energy transfer hypothesis. If energy transfer were indeed slow this would have some influence on the primary charge separation rate determined in our model for open RCs. For closed RCs the influence would be negligible anyway due to the slowing down of electron transfer. Overall the issue of the exact energy transfer rate is thus of minor importance at best for the presented work. We will deal with this issue in a separate work.

on the kinetics was observed under these conditions. Results presented in this work used 20μM DCMU unless mentioned otherwise. During measurements Q_A was kept in the reduced state by illumination of the rotation cuvette with an orange LED (λ = 630 nm, intensity of 3 μE/m^{2}s), just before entering the measuring laser beam. This LED intensity corresponds to less than 4 photons absorbed per PSII particle per second. In order to clarify the origin of the long lifetime component, pH-dependent measurements were carried out in the pH range from 5.5 to 8.5. For that purpose different buffers were used: MES (pH 5.5, 6.0, 6.5), HEPES (pH 7.0, 7.5, 8.0) and Tricine (pH 8.5).

Additional measurements were performed on intact cells of *T. elongatus* for clarifying the origin of the longer ns lifetime(s). The cultures were grown in a rotary shaker in BG-11 medium, bubbled with CO_2-enriched air (5%) and illuminated with white light (40 μE/m^{2}s intensity). For time-resolved fluorescence experiments the cells were centrifuged for 4 minutes at room temperature (4000g) and afterwards resuspended in fresh medium BG-11 to a concentration corresponding to OD = 0.26 at 675nm. The sample was slowly pumped through a flow cuvette with 1mm path length. To achieve prereduction of Q_A 20μM DCMU was used together with additional background light (LED, λ = 630 nm, 500 μE/m^2 s) for a short time (1-2 sec) just before the sample entered the cuvette.

Experimental technique

Measurements were performed using the single photon timing technique, as described (*33;69*). For PSII particles a particularly important part of the experimental setup is the rotating cuvette (~10 cm diameter), which moved sideways with 66 Hz and was rotated at 4000 rpm. This assures, together with low excitation intensity, that multiple excitations of the PSII particles both by the same laser pulse and by subsequent laser pulses are avoided. The estimated probability of a PS II particle being excited during the passage through the laser beam is $\leq 10^{-2}$. All measurements were carried out at room temperature.

To check the stability of the sample steady-state fluorescence spectra were collected before and after each lifetime experiment.

Time-resolved fluorescence kinetics data analyses

The time-resolved fluorescence data were first analyzed by global lifetime analysis. Advanced kinetic modeling was subsequently performed by global target analysis (*57;58*). Several alternative compartmental models were tested on the data and the results were judged by the χ^2 values, the residuals plots and the shape of the species-associated (emission) spectra (SAES). The excitation vectors used in this paper were determined from calculations based on the absorption spectra of isolated CP43, CP47 and PSII D1-D2-cyt *b-559* RCs (*94*).

4.3 Results

PSII core complexes with closed RC

PS II cores were excited at the blue side of the Q_y absorption band of the antenna Chls (at 663 nm) and fluorescence was detected in the range 677 nm to 697 nm, with a step size of 4 nm. Global analysis resulted in decay-associated spectra (DAS), representing a set of lifetimes and their associated amplitudes (Fig. 4-1). The fluorescence decays required five exponentials for a good fit, with lifetimes: 4 ps, 52 ps, 232 ps, 1.25 ns and ~3.75 ns. The shortest lifetime shows large negative amplitude over the whole detection range. It represents an energy transfer process, *i.e.* energy transfer between the two core antennae subunits CP43 and CP47 and the RC. The largest positive amplitude is associated with a 52 ps lifetime component, while the longer lifetimes have about half that amplitude.

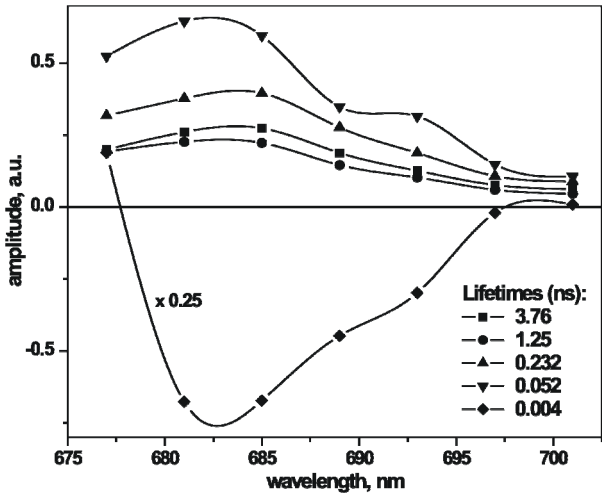

Fig. 4-1 Decay-associated emission spectra (DAS) of cyanobacterial PSII with closed RC (upon 100 μM DCMU treatment) resulting from global analysis calculations.

Target modeling. In order to explore various kinetic models and to determine the rates of processes compartment modeling was applied to the data. A number of different models were tested. All of them incorporated three excited states (corresponding to CP43*, CP47* and RC*) (*33*). Some models included only two RPs and no/one/ or two additional lifetime components, not connected to the kinetic scheme. Other models comprised three or four RPs with one or no additional components required for a good fit. It was the aim of the modeling to arrive at a consistent model capable of describing all major lifetime components found in global lifetime analysis (Fig. 4-1). Different starting values for rate constants were applied and the final models were subjected to an extensive error search of the parameters. The acceptance or rejection of a model was based on the fit parameters (χ^2 value and residuals) and also on the spectral shape of the SAES. This time consuming but necessary procedure of probing the solution space resulted in the two final models shown in Fig. 4-2 and Fig. 4-3. The simplest kinetic scheme that fulfils the above-mentioned conditions involves six compartments (Fig. 4-2A): three excited states (antennae CP43*, CP47*, and RC*), three RPs (RP1, RP2, RP3), and one additional component. The three SAES (Fig. 4-2B) describe the excited-states

compartments, while the SAES of RPs are zero by definition, since RPs do not emit fluorescence. The figure also shows the compartment population dynamics (Fig. 4-2C). The best solution found in the target modeling procedure results in a set of six lifetimes: 1.8 ps, 8.1 ps, 31.9 ps, 145 ps, 575 ps and 3.6 ns. The additional component of 1.3 ns shows a contribution to the fluorescence signal with a relative amplitude of ~20%, ~13% relative yield and a very similar spectrum as the long-lived component of the model. Thus, in a further model (Fig. 4-3) it was tested whether the remaining additional component could also be incorporated into a consistent model in a sequential scheme because there was *a priori* no reason to assume a large heterogeneity of the sample to which this additional component (20% amplitude) should be ascribed. This incorporation was indeed possible with an equally good fit quality. The enlarged model results in the following lifetimes: 1.8 ps, 8.1 ps, 19.3 ps, 67 ps, 206 ps, 953 ps, and 3.5 ns. These lifetimes differ slightly from the lifetimes obtained from global analysis (Fig. 4-1). The differences result from the experimental errors and additionally from much more severe constraints used in the target modeling that in the global analysis.

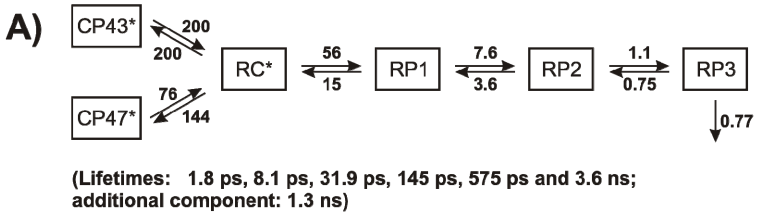

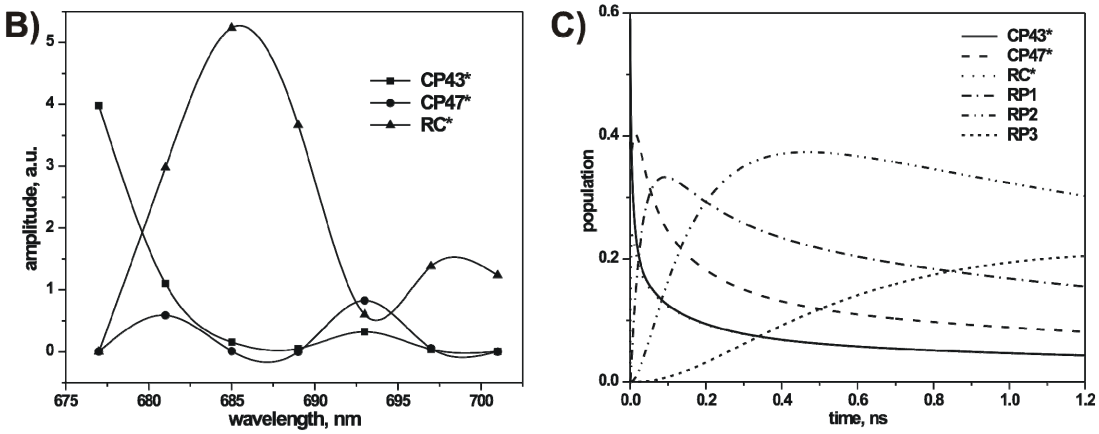

D)

τ (ps)	CP43*	CP47*	RC*	RP1	RP2	RP3
1.8	0.159	0.084	-0.271	0.029	0	0
8.1	0.188	-0.223	0.073	-0.040	0.003	0
31.9	0.070	0.191	0.059	-0.441	0.126	-0.005
145	0.090	0.182	0.087	0.163	-0.631	0.134
575	0.027	0.052	0.027	0.088	0.098	-0.501
~3600	0.055	0.105	0.055	0.201	0.405	0.372

Fig. 4-2 Results of target analyses of the fluorescence decay of dimeric PSII core particles in the closed form upon excitation at 663 nm – kinetic model with three RPs. A) Kinetic scheme (all rates are given in ns^{-1}); rates corresponding to energy transfer processes are characterized with the errors of 15%, while electron transfer rates of about 10%. B) Species-associated emission spectra (SAES) associated with the kinetic model presented in A. C) Population dynamics of the kinetic model compartments. D) Weighted eigenvectors representing amplitudes of compartments of the kinetic model shown in A; excitation vector used in the analyses: 0.59 (CP43*), 0.39 (CP47*) and 0.03 (RC*).

Influence of pH. The long lifetime components were tested on their dependence on the pH of the medium. However, global and target modeling performed on these data did not reveal any correlation between buffer pH and the average lifetime of fluorescence (ca. 850 ps) or the relative yield of the long lifetime components.

(Lifetimes: 1.8 ps, 8.1 ps, 19.3 ps, 67 ps, 206 ps, 953 ps and 3.5 ns)

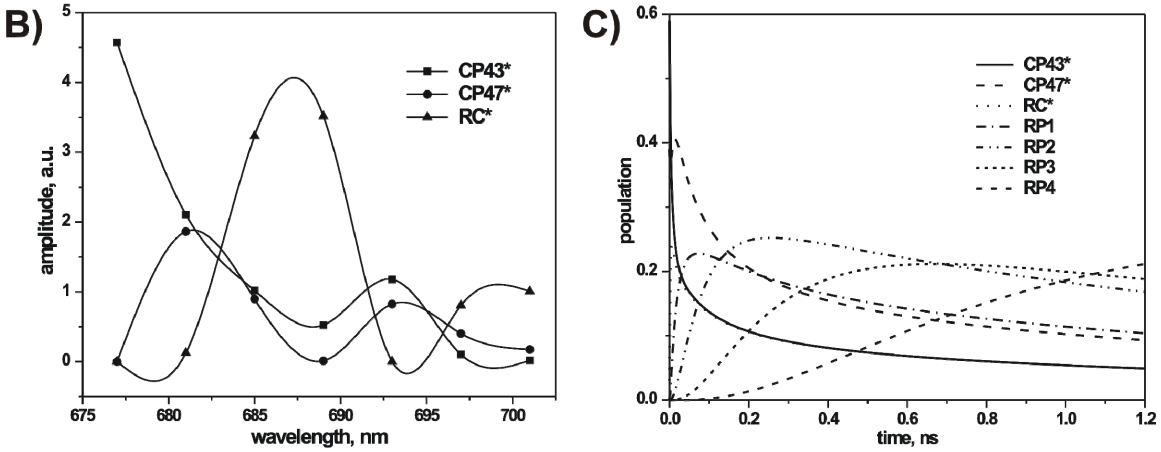

D)

τ (ps)	CP43*	CP47*	RC*	RP1	RP2	RP3	RP4
1.8	0.158	0.083	-0.270	0.030	0	0	0
8.1	0.194	-0.223	0.074	-0.052	0.008	0	0
19.3	0.021	0.094	0.016	-0.228	0.107	-0.001	0
67	0.067	0.146	0.062	-0.024	-0.041	0.182	-0.021
206	0.059	0.117	0.058	0.083	-0.006	-0.472	0.194
953	0.037	0.070	0.037	0.075	0.108	0.056	-0.786
~3500	0.054	0.103	0.054	0.116	0.194	0.245	0.613

Fig. 4-3 Results of target analyses of the fluorescence decay of dimeric PSII core particles in the closed form upon excitation at 663 nm – kinetic model with four RPs. A) Kinetic scheme (all rates are given in ns^{-1}); rates corresponding to energy transfer processes are characterized with the errors of 15%, while electron transfer rates of about 10%. B) Species-associated emission spectra (SAES) associated with the kinetic model presented in A. C) Population dynamics of the kinetic model compartments. D) Weighted eigenvectors representing amplitudes of compartments of the kinetic model shown in A; excitation vector used in the analyses: 0.59 (CP43*), 0.39 (CP47*) and 0.03 (RC*).

PSII core complexes with open RC – target modeling

Time-resolved fluorescence decay data on PSII core complexes with open RCs (Q_A oxidized) were already analyzed in terms of target modeling and were published previously (*33*). The model presented in that work represents the minimal scheme that described the charge separation and energy transfer processes and their corresponding rates. One lifetime component could not be incorporated into the model and remained unassigned. The authors speculated about the possibility of a protein relaxation step to explain that additional component. Therefore, we have now reanalyzed the same data in the framework of an

extended model comprising an additional RP, which would represent a protein relaxation step. The current kinetic model (Fig. 4-4A) thus involves three excited states (CP43*, CP47* and RC*) and three RPs (RP1, RP2 and $RP2_{relax}$). In addition a very small amplitude component of a 3.6 ns lifetime is present, reflecting PSII with closed centers (*33*).

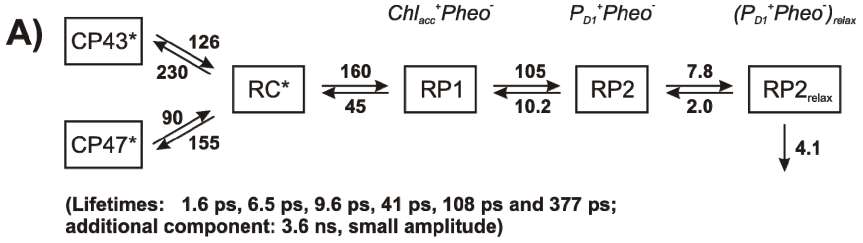

B)

τ (ps)	CP43*	CP47*	RC*	RP1	RP2	$RP2_{relax}$
1.6	0.086	0.054	-0.193	0.063	-0.011	0
6.5	0.073	0.021	0.008	-0.325	0.252	-0.013
9.6	0.255	-0.271	0.024	0.067	-0.082	-0.006
41	0.297	0.310	0.131	0.067	-1.234	0.521
108	0.062	0.061	0.032	0.081	0.627	-1.540
377	0.026	0.025	0.014	0.046	0.448	1.025

Fig. 4-4 A) Extended kinetic model for cyanobacterial PSII in open state – assignment of RPs is shown. B) Weighted eigenvectors representing amplitudes of compartments of the kinetic model for open PSII particles; excitation vector: 0.9 (CP43*), 0.1 (CP47*).

Intact cells – global and target modeling

Intact cells of *T. elongatus* were excited at 675 nm in order to avoid the excitation of the allophycocyanin antenna present in the cyanobacterial light-harvesting complexes. The fluorescence was detected in the range 685 – 697 nm. Global analysis resulted in the set of 5 lifetimes and corresponding DAS, shown in Fig. 4-5. The shortest lifetime component (1 ps), with characteristic negative/positive features indicates an energy transfer process. The second shortest lifetime (39 ps) does not exhibit the spectral shape typical for PSII since it shows high amplitude in the red tail of the spectrum. It is thus assigned mainly to PSI. Three longer lifetimes ranging between 200 ps and 1.4 ns can be attributed to PSII, again because of their spectral shape. It is noteworthy that no component with a lifetime > 1.4 ns could be detected. However, we cannot exclude that due to the intact cells forming much bigger system, the energy transfer from PSII to other complexes present in the cells might shorten the observed lifetimes.

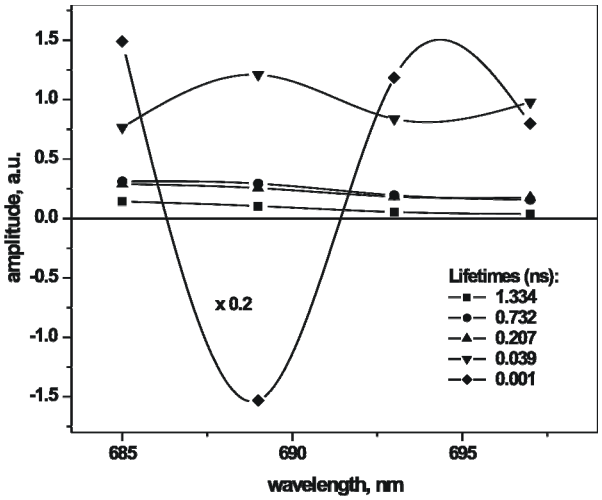

Fig. 4-5 Decay-associated emission spectra (DAS) resulting from global analysis of the fluorescence decay of intact cyanobacterial cells in the closed form; the amplitude of the shortest lifetime was divided five times for better understanding and presentation of other components.

4.4 Discussion

Closed RC – target modeling

Fig. 4-2 illustrates the results of the target modeling on our data in the form of the kinetic scheme and rates (Fig. 4-2A), SAES (Fig. 4-2B), the population dynamics (Fig. 4-2C) and the eigenvector matrix (Fig. 4-2D). The charge separation process is described with the 56 ns^{-1} rate constant, which is about four times larger than the charge recombination rate. The ratio of forward and backward rates (k_{for} and k_{back}, respectively) between RP1 and RP2 is about two times smaller (7.6 ns^{-1}/3.6 ns^{-1} = 2.1), while the k_{for}/k_{back} ratio of the last resolved step reaches only ca. 1.5. The kinetic scheme allows constructing the matrix of the so-called weighted eigenvectors. This matrix allows the association of a particular lifetime with a particular reaction step. A negative value of the matrix element describes the rise of the population of a particular compartment, whereas a positive value describes its decay (for details see (*95*)). Thus, the two shortest lifetimes in Fig. 4-2A are attributed to the energy transfer and equilibration between excited states of antennae and RC, with 1.8 ps representing the main contribution to the rise of the RC* state population. The apparent charge separation and consequently first RP formation is characterized by the 31.9 ps lifetime and to a very small extent also by the 8 ps lifetime. The first charge stabilization occurs with 145 ps lifetime, whilst RP3 is formed with 575 ps lifetime and decays with more than 3.5 ns. The ca. 1.3 ns lifetime component is not included in the model. Target analysis resulted in the SAES presented in Fig. 4-2B and the plot in Fig. 4-2C, which shows the time course of the relative populations.

Since there exists no *a priori* reason to not assign the relatively large amplitude of the ca. 1.3 ns lifetime to intact PS II particles, we have tested additionally an extended model, which contains one additional RP. The results of these fits are given in Fig. 4-3. Comparison of the SAES in Fig. 4-2B and Fig. 4-3B shows no major differences of the excited state emission spectra between both models, with RC* peaking around 686-687 nm. The early processes have

the same meaning and very similar lifetimes as in the simpler model are obtained. However, the extended model associates the CS step with the 19.3 ps lifetime, and the first charge stabilization with the 67 ps lifetime, while the formation of RP3 and RP4 is almost exclusively related to the 205 ps and 953 ps lifetimes, respectively. The last RP decays with 3.6 ns lifetime, *i.e.* quite similar to the simpler kinetic scheme. In essence, the 31.9 ps component is resolved into two components in the extended model.

PS II with open RC – target modeling revisited

The kinetic modeling for open PS II cores presented previously by Miloslavina *et al.* (*33*) included two RPs and two unconnected components of 111 ps and 2.3 ns. The latter is due to a small amount of closed RCs. Two possible explanations for the 111 ps lifetime were made. The first one considers the possibility of a heterogeneous nature of the electron transfer from pheophytin to quinone A, while an alternative explanation assumed a protein conformational response to the charges flowing through the reaction center (RC), *i.e.* a RP relaxation process. The latter case is well documented for bacterial RCs and also for isolated PS II RCs (*28;37-40;42;43;91*). The transient absorption measurements on the same particles (*28*) did not show any changes in the transient spectra on the 100 ps time scale. Such changes would be expected if at least one of the chromophores involved in the RP states would change its redox state. The data (*28*) show however a rather wide range of a lifetime distribution ranging from about 100 ps to nearly 300 ps. Thus the most reasonable assignment of the ca. 110 ps component is a protein relaxation step not involving a change in the redox state of any of the cofactors. Thus the RPs in Fig. 4-4A are assigned, in analogy with (*28*), as follows: RP1 = $Chl_{accD1}^{+}Pheo_{D1}^{-}$, RP2 = $P_{D1}^{+}Pheo_{D1}^{-}$, $RP2_{relax}$ = $(P_{D1}^{+}Pheo_{D1}^{-})_{relax}$. The two latter RPs reflect the same redox state, but differ in their energy and in the conformation of the surrounding protein.

The eigenvector matrix corresponding to the kinetic scheme presented in Fig. 4-4A can be found in Fig. 4-4B. In this model the energy transfer between antennae and the RC is described by the lifetimes of 1.6 ps and 9.6 ps, while the main part of the apparent charge separation process occurs with the 6.5 ps lifetime. This is essentially the same as for the previously published simpler model. The RP2 redox state is populated with the 41 ps lifetime. RP2 then relaxes to $RP2_{relax}$ by protein relaxation with the 108 ps lifetime component as a response to the charges moving along the cofactor chain. The state $RP2_{relax}$ is depopulated with 380 ps lifetime, reflecting the apparent electron transfer from $Pheo_{D1}^{-}$ to Q_A. Its rate constant is 4.1 ns^{-1}, resulting in an effective transfer lifetime of ~245 ps. As suggested in our previous paper (*33*) extension of the model does not affect the kinetics of the Q_A reduction.

In the current model the total trapping time $\tau_{tot\ trap}$ = 72 ps, while in the simpler scheme the trapping was $\tau_{tot\ trap}$ = 65 ps, with 9 ps energy transfer and 56 ps charge separation times. Therefore, the contribution of the charge separation process to the overall trapping kinetics remains dominant, whereas the energy delivery to the RC is extremely fast and hardly

contributes to $\tau_{tot\ trap}$. Thus the model remains trap-limited, as assigned already on the basis of the simpler model (*28;33*). Closure of the RCs slows down charge separation and thus also does not change the type of kinetics. Somewhat different energy transfer rates were found for particles with open RC (*33*) and with closed RC (this work). These differences, which however do not change to any significant extent the excited state equilibration between antenna and RC, are explained by two factors. Measurements on open RCs were made without a polarizer in the emission beam and thus the early kinetics may be somewhat distorted. The reason was that in order to keep RCs open the strong reduction of fluorescence intensity by the polarizer was not acceptable. This problem does not arise with closed RCs, where the fluorescence intensity is much higher and thus it was possible to use the polarizer. Secondly for the modeling of the closed RCs (*vide supra*) we used an excitation vector that reflects correctly the relative absorptions of CP43, CP47 and the RC. This was not the case for the previous modeling of the open RCs, and was a matter of concern.

Energetics and CS mechanism in closed RC

From the rate constants of forward and backward transfer one can calculate the free energy differences ΔG between the excited RC* state and the RPs (Fig. 4-6 shows the results for both open (*left*) and closed (*middle* and *right*) RCs). Both graphs corresponding to the models with three RPs illustrate a similar drop in the free energy, *i.e.* 32 - 33 meV, for the first electron transfer step, regardless of the redox state of Q_A. The overall drop in free energy is smaller for closed RCs than for open RCs, in agreement with earlier findings (*29;83*). However, great care must be taken when comparing the free energy drops found here for the individual steps with previous data. It had been argued that the electrostatic interaction between reduced Q_A in closed RCs and the formed $Pheo_{D1}^-$ would greatly increase the free energy of the first RP (*29;83*). Furthermore the free energy data derived from photovoltage measurements of Gibasiewicz *et al.* (*83*) combine the free energies of the actual redox processes on the one hand and the protein relaxation steps on the other hand, unlike the fluorescence kinetics data. Since the earlier measurements (*29*) an additional RP has been resolved for PS II cores with open RCs (*28*). However this RP also involves a reduced $Pheo_{D1}$ and thus would be also expected to show a substantial rise in the free energy vs. the same state with open RC. This is however not the case in our data (Fig. 4-6). For the simpler model (Fig. 4-2) the free energy drop of the first RP is about the same as for open RCs, while for the extended model (Fig. 4-3) that drop is only slightly smaller. Ishikita *et al.* (*96*) have predicted from theoretical calculations an increase in the free energy of about 90 meV in closed RCs due to the electrostatic repulsions between reduced Q_A and $Pheo_{D1}^-$. Our data for the free energy of the first RP in closed RCs do not at all reflect such a drastic effect. The only possible way to reconcile these data is the hypothesis that $Pheo_{D1}$ is not reduced in the RPs in closed RCs and a different redox state is formed. We cannot get any direct information on the redox nature of an RP from fluorescence measurements. However, recent experimental data on RC triplet

formation and quenching in PS II with closed RCs strongly suggest that different early RPs are formed in PS II with closed RCs (*97*). If $Pheo_{D1}$ is indeed not reduced and a different RP not involving $Pheo_{D1}$ is formed in closed RCs, then we also do not expect a large increase in the free energy of the first RP in closed RCs. This could also explain the large decrease in the charge separation rate of about 3 times in closed RCs vs. open RCs in our data. If the first electron transfer step were to form the same RP in open and closed RCs, then the drop in the charge separation rate would also have to be associated with a decrease in the free energy difference for this step. Thus we tentatively conclude that the RP(s) formed in open and closed RCs involve different redox cofactors. Vassiliev *et al.* (*66*) also found, based on a model which included protein dynamics, the decrease in the free energy for the CS step in PSII with both, open and closed RC. However, in contrast to our findings the ΔG values reported in their work differ for both preparations. Additionally, the authors show the overall free energy drop in PSII with reduced Q_A to be in the order of 160 meV, a factor of 2 bigger than reported here. This however may be explained with the differences in the method used to close RCs. The authors used hydroxylamine treatment, which inhibits the oxygen-evolving complex, while in our experiments the oxygen-evolving complex was fully functional. Gibasiewicz *et al.* (*83*) had concluded that the closing of the RC mainly causes an increase in the charge recombination rate but only very little change in the charge separation rate. This is not in agreement with our data. However, the discrepancy is easily explained, since Gibasiewicz *et al.* did not resolve the first electron transfer step in their measurements.

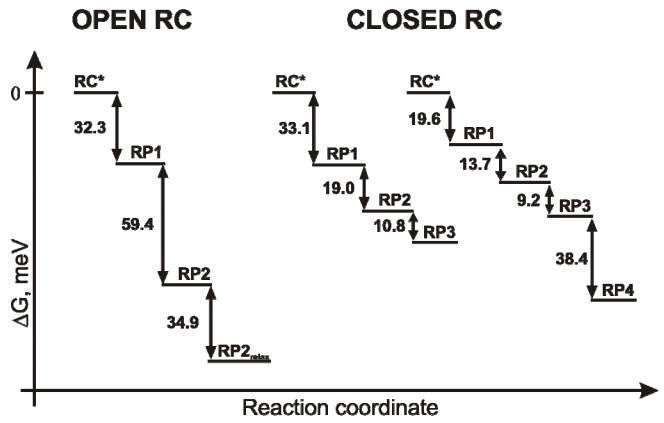

Fig. 4-6 Schematic representation of the free energy differences G between different compartments of kinetic models found for dimeric PSII core particles in both, open (*left*) and closed state. For the latter preparation both presented in the text models are shown (model with 3 RPs, *middle*; model wit 4 RPs, *right*). RC* stands for RC excited state and constitutes reference state for the free energy calculations.

Protein dynamics

All kinetic models presented above of the kinetics in PSII particles with open and closed RCs required more than two RP states for a satisfactory fit. For PS II with open RCs two different redox states of the RC were resolved that occur before the reduction of Q_A (*28*). We cannot by fluorescence characterize the redox nature of a RP even if it gives rise to charge

recombination fluorescence. However, it is quite unlikely that for PS II with closed RC there should be more than two RP reflecting different redox states. This implies that one or more of the RPs resolved in the fluorescence kinetics should be interpreted as RPs formed by protein relaxation steps but reflecting the same redox state. Protein relaxation steps lower the free energy of the RPs. Also the rates of fast electron transfer steps can be very sensitive to protein dynamics and conformation (*40;41;98*). Such protein relaxation is well-known for bacterial RCs (*38;39;41;99;100*) and also for isolated PS II RCs (*42;43;67;91;101;102*). Protein dynamic processes span a huge time range, from ps to hours (*87;103-105*). It is generally not easy to measure the free energy of the states involved in protein relaxation. However, photosynthetic reaction centers in general and PS II in particular provide a specially favorable case, since they show charge recombination fluorescence from the relaxing RP states (*29;39;66;99*). Importantly, in such measurements the excited state of the RC, from which all the observed fluorescence derives, functions as an energetic reference state, whose energy is essentially independent of protein relaxation.

In the light of the above considerations we will tentatively assume for the following discussion that for closed RCs the first two resolved RPs (RP1 and RP2) reflect different redox states formed by electron transfer, while the following two RPs (RP3 and RP4 in Fig. 4-3) reflect protein-relaxed RPs without involving an electron transfer process, *i.e.* the same redox states of the cofactors are involved. For open RCs (Fig. 4-4) the comparison with the transient absorption data (*28*) also indicates that the third RP resolved in the present fluorescence analysis (designated as $RP2_{relax}$) must reflect a protein-relaxed RP. It is clear that the actual electron transfer processes leading to RP formation also involve protein relaxation. However, the two processes occur concomitantly on the same time scale and cannot be separated in that case.

For PS II with open RCs the first resolved protein relaxation step occurs with a lifetime of 108 ps and involves a free energy relaxation of -35 meV (Fig. 4-6). Presumably further protein relaxation steps would follow. However for open RCs the electron transfer to Q_A prevents that process. For closed RCs two protein relaxation steps are resolved. They occur with ca. 200 ps and 950 ps lifetimes, and involve free energy relaxation of ca. -9 meV and of ca. -38 meV, respectively. The relationship is clear: Given more time, the free energy can relax more. In comparison to closed RCs the -35 meV drop with the short lifetime of 108 ps in open RCs is quite interesting. Presumably the very fast initial electron transfer steps in that case occur with relatively little protein relaxation. Thus a larger drop in free energy by protein relaxation occurs after charge separation. It follows from these data that charge separation in PS II would be overall much less efficient if protein relaxation did not occur as discussed in a recent review (*25*).

Origin of the long lifetime component

While it is well-known that the fluorescence yield and average lifetime of PS II increase upon closing of the RC (*30;31*),(*65*), a phenomenon which forms the basis of all fluorescence induction measurements (*49;106-110*), we detected an unusually large, up to 10-fold, increase in the fluorescence yield upon closure of the RCs (Fig. 4-7). This is also reflected in the increase of the average fluorescence lifetime τ_{av}, which changes from 0.09 ns to 0.87 ns for PSII with open and closed RCs, respectively. Fluorescence yield and lifetime increases of a factor of 5-7 are more common, in particular for PS II in intact thylakoids or BBY particles. This large increase in fluorescence yield is associated with the long-lived (~3.7 ns) component in our data. Interestingly we found no lifetime of about 11 ns, as was reported by (*30*) or ~7 ns as found by Vasiliev *et al.* (*66*). Such long-lived components are believed to arise from double reduction of Q_A due to the use of dithionite or hydroxylamine and strong light irradiation (*84;85*). We thus intentionally avoided such methods for closing the RCs and applied the milder and more clearly defined method of using DCMU to block Q_A to Q_B electron transfer. The longest lifetime under our conditions is 3 to 4 ns, found in both global and target analyses. We thus performed various experiments in order to better identify the origin of this long-lived component. We studied for example the possible dependence of the electron transfer processes on pH in the range from 5.5 to 8.5. However, we did not find any significant dependence of the electron transfer rates or lifetimes on pH. In addition the relative amplitude and relative yields of the long-lived components did not change. For all pH conditions applied in the experiment, the long lifetime is characterized with the relative yield of about 70 – 80% and relative amplitude varying from 17% to 21%. We have to conclude that the 3.6 ns lifetime cannot be associated with the changes in the protonation state of the protein. Other experimental conditions, like *e.g.* different DCMU concentrations or different intensity of the background light, also did not give rise to any substantial changes in the amplitudes or lifetimes of the long-lived (ca. 3.4 ns) component. Interestingly no substantial 3-4 ns component was detected in the fluorescence of intact leaves from higher plant either (unpublished). We thus performed measurements on intact cells of *T. elongatus* with closed RC. Quite interestingly, global analysis of these fluorescence decays did not reveal any lifetime longer than 1.5 ns. The shortest lifetime (1-2 ps) exhibits an energy transfer behavior (positive/negative amplitude), while the remaining ones display only positive amplitudes. The three longest lifetimes (1.3 ns, 732 ps and 207 ps) clearly describe the PSII part of the system, whereas the 39 ps component must be attributed to a large part to PSI, based on the strongly red-shifted spectrum.

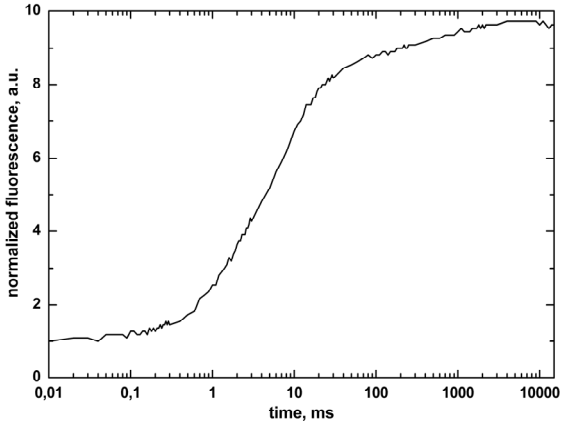

Fig. 4-7 Chlorophyll *a* fluorescence induction signal from PSII with RC in open state, normalized to the F_0 level. The measurement was carried out with a Handy Pea instrument (Hansatech Instruments, UK). Sample was dark-adapted for 2 min before the measurement and then illuminated with continuous light (650 nm peak wavelength, 1250 μE/m2s) provided by the focused array of ultra-bright red LED's. The fluorescence data was recorded for 15 seconds.

It is known (*12;14*) that $P680^+$ can be reduced at low temperature by the carotenoid present in the RC or at higher temperatures by Chl_Z (peripheral Chl). The oxidation of Car by $P680^+$ in isolated D1-D2-cyt *b-559* RCs takes place with a low rate of ~1/ ms. The electron donation to $P680^+$ and subsequent oxidation of Car^+ by cyt *b-559* or Chl_Z constitutes the so-called cyclic electron flow. However, these processes were proposed on the basis of experiments on Mn-depleted PSII particles or D1-D2-cyt *b-559* preparations, whereas our PSII core particles are highly active in oxygen evolution. We thus believe that such effects can be ruled out. A more likely explanation of the presence of the ~3.5 ns fluorescence lifetime component may be related to an alteration of the electron donation from tyrosine (TyrD) to $P680^+$ under our experimental conditions. Under normal physiological conditions reduced TyrD will be oxidized upon the onset of light. The tyrosyl radical ($TyrD^\bullet$) is stable for hours and – although not taking part directly in the redox activity of PSII - has been proposed to facilitate the reduction of P680+ by TyrZ (*11*). It has also been proposed that the $TyrD^\bullet$ radical is involved in the recombination reaction of $P^+Q_A^-$ under certain conditions (*111*). A different charge on a cofactor of the RC not involved in primary electron transfer could well provide a possible explanation for the differences between isolated PS II particles and the *in vivo* system. A likely candidate would be TyrD whose different redox states could easily influence the lifetimes of RP relaxation of PS II with closed RC. Such an influence could be exerted for example by a modification of the energetics of the RPs due to an electrostatic interaction of the primary or secondary RP with a charge on another cofactor not directly involved in the electron transfer reaction(s). An alternative possibility that cannot be excluded however consists in an influence of the surrounding of the PS II particle, *i.e.* native membrane vs. detergent, on the protein relaxation dynamics of the RC in the closed state. These points deserve further investigation.

4.5 Conclusions

Time-resolved fluorescence experiments reveal the interplay between fast photosynthetic charge separation processes and the relaxation of the protein environment. We have shown in this work that such process can be successfully incorporated into the description of the kinetics of PSII with open RC. PSII particles with reduced Q_A show similar behavior, with up to two resolved relaxed RPs. Interestingly the free energy drop for the first RP is similar to that for open RCs. This is inconsistent with the expected substantial drop of the redox potential of $Pheo_{D1}$, predicted to be -90meV in theoretical calculations, upon reduction of Q_A. We thus hypothesize that reduced $Pheo_{D1}$ is not formed in the RC with reduced Q_A. Instead, some other redox state must be present. We showed that the long lifetime component found in the PSII cores with closed RC does not depend on the pH of the medium, the concentration of herbicide inhibitor used, nor on the background light intensity. On the other hand it is not present in the fluorescence signal from intact cells with closed PS II RCs. The reason for this is unclear. It might suggest changes in the protein state (oxidation/reduction) or protonation of a component near the electron transfer cofactors but not participating directly in the RP formation. Such changes might cause modifications in the free energy landscape of the RPs.

5 The role of TyrD in the electron transfer kinetics in Photosystem II

This chapter is based on the publication: M. Szczepaniak, M. Sugiura, A.R. Holzwarth. Biochimica et Biophysica Acta 1777 (2008), 1510-1517.

Redox-active tyrosine (Tyr) D is indirectly involved in controlling the primary electron transfer in PSII. The presence of the oxidized TyrD renders $P680^+$ more oxidizing by localizing the charge more on P_{D1} and thus facilitates trapping of the excitation energy in PSII. We also conclude that the mechanism of the primary charge separation and stabilization is altered upon Q_A reduction.

5.1 Introduction

Photosystem II (PSII) functions as light-driven water-oxidizing enzyme in the thylakoid membranes of cyanobacteria and higher plants (*80*). The structure of PSII was recently determined at high 3Å resolution (*8*). The X-ray structure provided the basis for a model of the water-splitting site, the Mn_4Ca cluster (*21*). In the cyanobacterial PSII photons are absorbed by the chlorophyll (Chl) pigments in one of the core antennae, CP43 and CP47 (here CP stands for chlorophyll protein), and delivered to the reaction center (RC) for subsequent charge separation (CS) and transport of an electron across the membrane. The electron moves along the active cofactor branch, consisting of chlorophyll P_{D1}, accessory chlorophyll Chl_{accD1}, pheophytin $Pheo_{D1}$, and two quinone molecules, Q_A and Q_B (Fig. 5-1). The "inactive", quasi-symmetric branch is composed of chlorophylls P_{D2}, Chl_{accD2}, and $Pheo_{D2}$. The pseudo-C2 symmetry organization of the cofactors in the RC comprises also two peripheral chlorophylls, Chl_{ZD1} and Chl_{ZD2}, the two redox-active tyrosines, TyrZ and TyrD, and the Mn_4Ca cluster. PSII is characterized by an extraordinary high oxidative power, the highest found in nature, which is large enough to drive the water oxidation. Splitting of water is achieved in an oxidation-reduction chain that involves P_{D1}/TyrZ, TyrZ/(Mn_4Ca cluster), and finally (Mn_4Ca cluster)/H_2O redox reactions. Four such light-driven cycles are necessary to split water and release oxygen to the lumenal side of the membrane (review article on the light-driven reactions in PSII (*25*), and others in the same volume).

The redox-active TyrZ is the intermediate compound in the electron transfer from the Mn_4Ca cluster to $P680^+$. Its counterpart TyrD is not directly involved in the water oxidation, even though it shares with TyrZ similar spectroscopic features. The TyrD radical is much more stable, and its actual role(s) in PSII structure is still not completely clear (for a review on tyrosine D see (*11*)). Due to the strong analogy between the active and inactive branches in

PSII RC, it was postulated that the PSII ancestor was a homodimer enzyme, using both branches for charge separation and perhaps even oxidation of water (*112*).

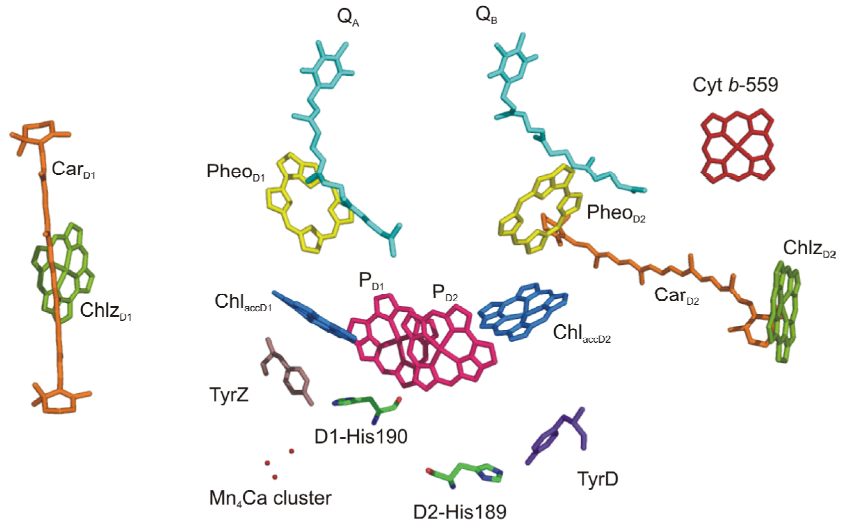

Fig. 5-1 PSII RC cofactors based on the 2AXT.pdb entry (*8*). The protein matrix is not shown for clear view. The cofactors form two branches in a pseudo-C2 symmetrical order: P_{D1} and P_{D2} (*magenta*), accessory chlorophylls Chl_{accD1} and Chl_{accD2} (*blue*), pheophytins $Pheo_{D1}$ and $Pheo_{D2}$ (*yellow*), quinones Q_A and Q_B (*cyan*), peripheral chlorophylls $Chlz_{D1}$ and $Chlz_{D2}$ (*green*), β-carotenes Car_{D1} and Car_{D2} (orange), tyrosines TyrZ (*grey*) and TyrD (*violet*), histidine residuals D1-His190 and D2-His189, Mn_4Ca cluster (*red dots*) and cytochrome Cyt *b*-559 (*dark red*).

It seems to be well established that PSII functions at physiological conditions with TyrD in its oxidized state, given that upon the onset of illumination TyrD gets oxidized by the charge equivalents accumulated in S_2/S_3 states of the manganese cluster. Concomitant with the oxidation of the Tyr molecule a proton transfer step between the Tyr radical and the neutral neighboring histidine D2-His189 occurs (*113*). As a consequence, TyrD, as well as TyrZ, are neutral radicals in their oxidized states (*114*). This is confirmed by FTIR experiments on the Mn-depleted PSII cores (*115*) which show that TyrD in the reduced state is likely to be protonated and to form a H-bond to the imidazole ring of a histidine, whereas other measurements suggested that TyrD in the oxidized form is deprotonated (*116-118*). This is the general idea of a proton rocking motion model proposed by Babcock in the late 1980s (*114*). Since the protein environment in the vicinity of TyrD has hydrophobic character and the Tyr site is not easily accessible to the lumen, the proton released upon TyrD oxidation stays in its proximity, interacting *via* the hydrogen bond with D2-His189. The TyrD radical is stable for a long time, for minutes to hours, when compared with its more "glamorous sister", TyrZ (*11*). However, the recent study of Hienerwadel *et al.* (*119*) introduces doubts as to the role of the histidine residue in the hydrogen-bonding interactions with TyrD. Nevertheless, TyrD is characterized by lower redox potential than TyrZ (0.75 V *vs.* 0.95-1.1 V) and much slower electron donation to $P680^+$ (*120*). However, in PSII lacking TyrZ it is able to donate the electrons to $P680^+$ as fast as TyrZ under physiological conditions (*121*).

At present the purpose of TyrD in the PSII reaction center is not entirely clear. The following redox and electrostatic functions of TyrD have been postulated: 1) it stabilizes higher valence states of the manganese cluster, which might be important during the

photoassembly of the manganese cluster (*122*); 2) TyrD radical increases the potential energy of $P680^+$; 3) $TyrD^{\cdot}(H^+)$ affects the donor side redox activity (*123*), possibly *via* the influence on the hydrogen-bond network in the vicinity of TyrZ (*124*); 4) after the first turnover it affects the distribution of the positive charge on the Chl pair $(P_{D1}P_{D2})^+$ and thus both accelerates the TyrZ oxidation (*i.e.* shifts the charge towards P_{D1}) and directs the photochemical reactions to the D1 protein side (*125*).

Despite being designed to study specifically the features of TyrZ, the TyrD-less mutant provides an excellent opportunity to investigate the puzzling functions of TyrD and the possible influence on the early electron transfer steps. The point mutation was introduced in the D2 protein of *Chlamydomonas* (*124*), *Synechocystis* (*126*), and finally *T. elongatus* (*55*). In view of the fact that the structural data are available for the cyanobacterial system, it is very suitable to study the latter system. In the generated mutant TyrD is substituted with redox-inactive phenylalanine (for details see (*55*)).

In this work we have studied the influence of TyrD on the early electron transfer in the intact, oxygen-evolving cyanobacterial PSII core complexes. Fast time resolved-fluorescence experiments were designed to investigate the effect of the tyrosine radical on the $P680^+$ redox potential and the charge distribution on the $(P_{D1}P_{D2})^+$ pair, and consequently the charge separation and electron transfer kinetics in the RC and in particular the effects on the energetics of the intermediates.

The electron transfer kinetics has been studied in detail in PSII WT preparations with open and closed RCs (*28;33;127*) (for review on the energy/electron transfer processes see (*25*)). If the assumption of the influence of $TyrD^{\cdot}(H^+)$ on the charge distribution on $(P_{D1}P_{D2})^+$ and the redox potential of $P680^+$ is correct, then we should be able to: 1) observe differences in the electron transfer reactions (rate constants and/or lifetimes and free energy differences of intermediates) between the WT and the TyrD-less preparation; and 2) possibly validate also further our previous findings on the switch in the CS and electron transfer mechanism in PSII with reduced Q_A (*127*).

5.2 Materials and methods

Samples

Time-resolved fluorescence measurements were performed on PSII core complexes (dimeric form) prepared from *Thermosynechococcus elongatus* WT' (attached His-tag on C-terminus of CP43, knockout psbD2) and the D2-Y160F mutant (called TyrD-less, knockout psbD2) (*55*). *T. elongatus* cells were cultivated in DTN medium under continuous light (~80 μmol photons/m^2/s), and PSII core complexes were purified as described in (*54*). The D2-Y160F mutation was introduced into *psbD1* after *psbD2* was deleted. Both preparations exhibited high activity, with the oxygen evolution ranging from 3600 μmol O_2/(mg Chl*h) to 4200 μmol O_2/(mg Chl*h). For the fluorescence kinetics experiment, isolated PSII complexes

were diluted in 40 mM MES buffer, pH 6.5 (Serva, Heidelberg, Germany) containing 15 mM $MgCl_2$ (Roth, Karlsruhe, Germany), 15 mM $CaCl_2$ (Merck, Darmstadt, Germany), 1 M Betaine (Sigma, Taufkirchen, Germany), 0.03% β–DM (Glycon, Luckenwalde, Germany). The final concentration was adjusted to be below OD = 0.3 at 663 nm. To keep the RCs in the open state (F_0, oxidized Q_A), 0.4mM ferricyanide was added, while the closure of the RCs (F_m state, meaning the single reduction of Q_A) was achieved by treatment with the electron transfer inhibitor DCMU (20 μM) and weak background irradiation during the measurement, provided by an LED (λ = 630 nm; intensity of 8 μE/m²s). Additionally an oxygen trap (65 μg/ml glucoseoxidase, 65 μg/ml catalase and 8 mM glucose) was used in the PSII samples with reduced Q_A.

Experimental technique

The fluorescence decays were recorded using the single-photon timing technique, with the experimental setup as described in (*33*) and conditions given in (*127*). The decays were recorded in the spectral range 673 nm – 701 nm, with the 4 nm step. All measurements were performed at room temperature. Taking the steady-state fluorescence spectra before and after each lifetime experiment allowed controlling the stability of the sample.

Furthermore, the chlorophyll *a* fluorescence induction measurements were carried out on each sample with a Handy Pea instrument (Hansatech Instruments, UK). Samples were dark-adapted for 2 min before the measurements and then illuminated with continuous light (650 nm peak wavelength, 1250 μE/m²s) provided by the focused array of ultra-bright red LED's. The fluorescence data were recorded for 15 seconds.

Data analysis

The time-resolved fluorescence signals were analyzed by global and target kinetic modeling (*57*). The quality of each fit was estimated by the χ^2-value and the residuals plot, together with the shape of the species-associated emission spectra (SAES) in the latter type of data analysis. Various kinetic models were tested, differing in the number of the radical pairs (RP) and/or additional components.

5.3 Results

Fluorescence induction

Chlorophyll *a* fluorescence induction signals are presented in Fig. 5-2 (for a review see (*49*)). The original curves (panel A) indicate an elevated F_0 level in PSII with closed RC, while the mutant preparation with oxidized Q_A has only slightly higher F_0 value when compared with the WT' PSII. However, normalization to the F_m level (panel B) results in similar curves in the FeCN-treated samples. The fluorescence induction curves of all PSII samples with open RC demonstrate comparable, very high F_m/F_0 ratios of about 9-10. The double normalization (to both F_0 and F_m, levels) reveals almost identical shapes of these curves (panel C).

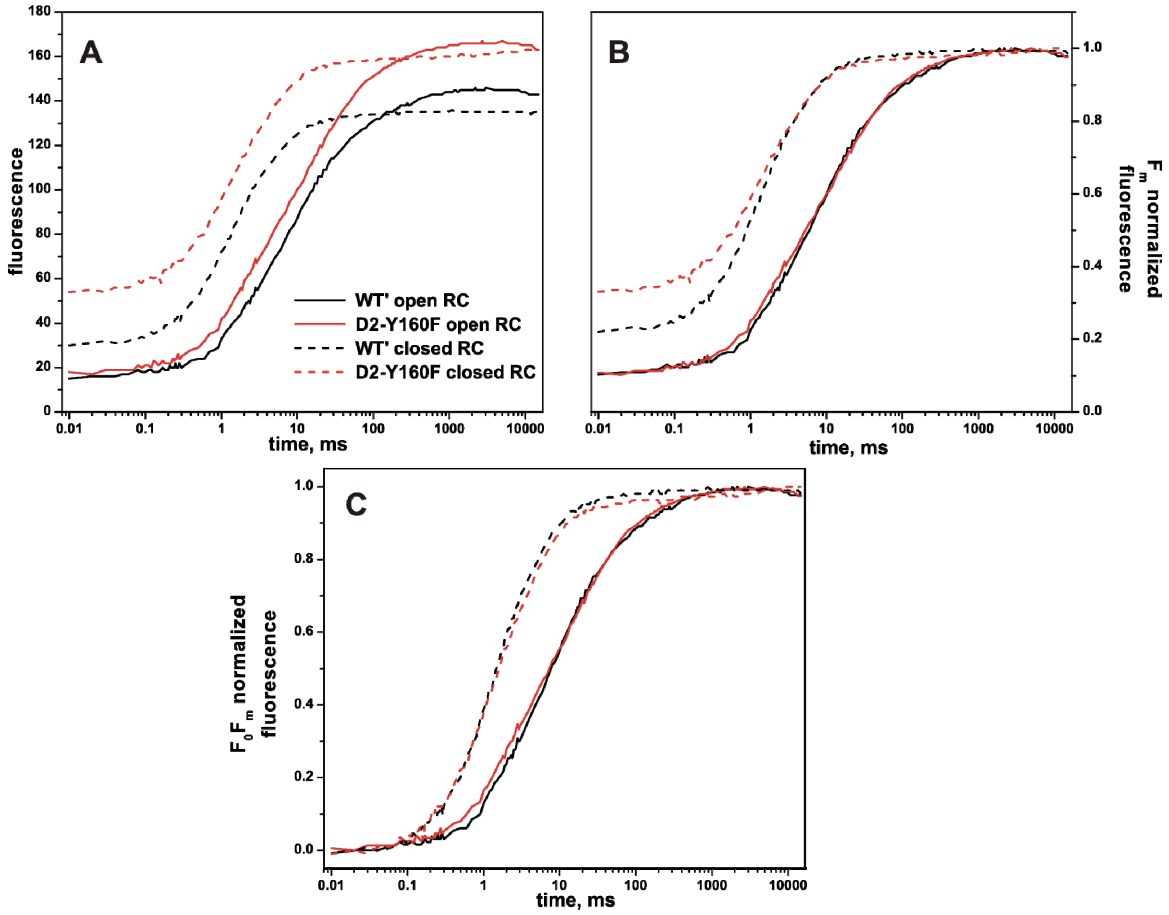

Fig. 5-2 Chlorophyll *a* fluorescence curves from PSII WT' and D2-Y160F mutant with RC in open and closed state (please, note different *y*-axis scales): A) original signals; B) all signals from A) normalized to the F_m level; and C) all signals from A) were doubly normalized to the F_0 and F_m levels for better comparison of the wild type and the mutant preparation.

Time-resolved fluorescence

Original data and global analysis. Fluorescence decay signals of PSII WT' and D2-Y160F mutant recorded at 681 nm are compared in Fig. 5-3, with Q_A oxidized and reduced, respectively. Clear differences exist in the fluorescence decays between the WT' and the TyrD-less mutant. In the case of PSII particles with RC in the open state both signals overlap in the first 60-80 ps, while on the longer time-scale the mutant fluorescence is characterized by a slower decay. However above 6 ns the signals are nearly identical. A similar trend is observed in the PSII preparations with reduced Q_A – the fluorescence signals overlap in the first 100 ps, but above 5 ns the signals show the longer decay time of the WT'. Both observations are explained by the longer-lived long component in the WT' PSII found in global analysis (Table 5-1). Table 5-1 summarizes the fluorescence lifetimes, their relative amplitudes and relative yields obtained in the global fitting of the data. In all investigated samples the shortest lifetime, in the order of 2-3 ps, is characterized by negative amplitudes over almost the whole spectral range. Typically this feature is associated with the energy transfer processes between the antennae units, CP43 and CP47, and the RC (*33*). Moreover, except for short lifetimes up to 500 ps, the samples with open RCs (oxidized Q_A) all contain small amplitude of a long-lived component. In PSII with reduced Q_A the long-lived components have large amplitudes as

observed previously (*127*). These long lifetimes contribute most to the total fluorescence signal (see Table 5-1, relative yield of fluorescence). The average lifetimes of fluorescence calculated on the basis of all the components found in the global analysis for each sample correlate well with the high fluorescence yield of the long-lived components. Moreover, the differences in the τ_{av}^{tot} between WT' and D2-Y160F indicate the importance of the tyrosine D in the photosynthetic activity of the enzyme. The average lifetime in PSII with oxidized Q_A is almost 35% longer in the TyrD-less preparation than in WT'. The relative effect is however smaller in PSII with closed RC, reaching only 15% increase.

Table 5-1 Lifetime components of the fluorescence signals resulting from the global modeling

	open RC		**closed RC**	
	WT'	**D2-Y160F**	**WT'**	**D2-Y160F**
Fluorescence lifetime components (ps)	2370 (3% / 45%)	1210 (8% / 50%)	4230 (21% / 73%)	3010 (39% / 81%)
	433 (7% / 19%)	229 (30% / 36%)	1550 (16% / 20%)	1270 (17% / 14%)
	149 (15% / 15%)	59 (29% / 9%)	303 (20% / 5%)	272 (24% / 5%)
	42 (75% / 21%)	27 (34%/ 4%)	58 (43% / 2%)	44 (20% / <1%)
	2 (neg.)	2 (neg.)	2 (neg.)	3 (neg.)
τ_{av}^{tot} (ps)	131	177	1215	1397
χ^2	1.016	1.040	1.033	1.018

Lifetimes (± 10 %) are given in ps, while in parentheses are given the average relative amplitude / the average relative yield of a fluorescence lifetime; the shortest lifetimes are characterized with large negative amplitude, and thus are excluded from the calculation of the average amplitudes or yields. τ_{av}^{tot} (ps) is the average lifetime of fluorescence calculated on the basis of all lifetimes present in the global analysis, while χ^2 is a measure of the quality of the fit.

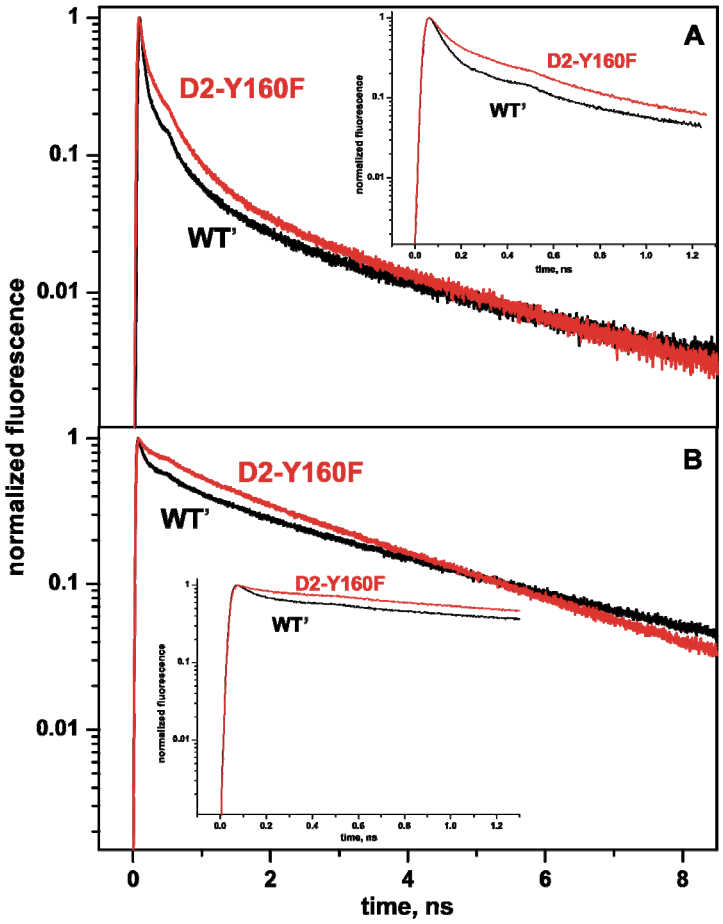

Fig. 5-3 Original time-resolved fluorescence signals detected at 681nm upon 663 nm excitation of the WT' and D2-Y160F PSII. The insets show the fluorescence decay on short time range, up to 1.2 ns, while the main plots on the longer time-scale, to 8.5 ns (the signals were normalized to the maximum of the fluorescence): A) WT' and mutant with oxidized Q_A; B) WT' and mutant with reduced Q_A.

Target modeling. Compartment modeling applied to the experimental data yielded a set of rate constants and species-associated spectra (SAES) describing the fluorescence kinetics. The final models were chosen on the basis of the quality of the fit and the plot of the residuals, together with the shape of SAES. For all described preparations the minimal models consist of three excited states (CP43*, CP47*, and RC*), three radical pairs (RP1, RP2, and RP3) and one or two additional not connected to the model components with small amplitude. The models follow our previous extensive analysis of the kinetics for WT PSII with open and closed RCs (*28;33;127*). The data sets were subjected to extensive error analysis, using varying starting conditions. The final models are presented in Fig. 5-4 (and Fig. S5-1 to Fig. S5-4 in Supporting materials). Only for the PSII WT' preparation with open RC two additional components were required, in other preparations one additional compartment was sufficient to obtain a good fit. Therefore, all kinetic schemes yielded a set of six lifetimes in the range from a few ps up to above 4 ns. The degree of participation of each lifetime in the energy and electron transfer processes is shown in the matrix of weighted eigenvectors (Fig. S5-1 to Fig. S5-4). For the interpretation of the matrices see (*33*). In all models the same rates for energy transfer processes between antennae and RC compartments were assumed, as determined in our previous work (*28*).

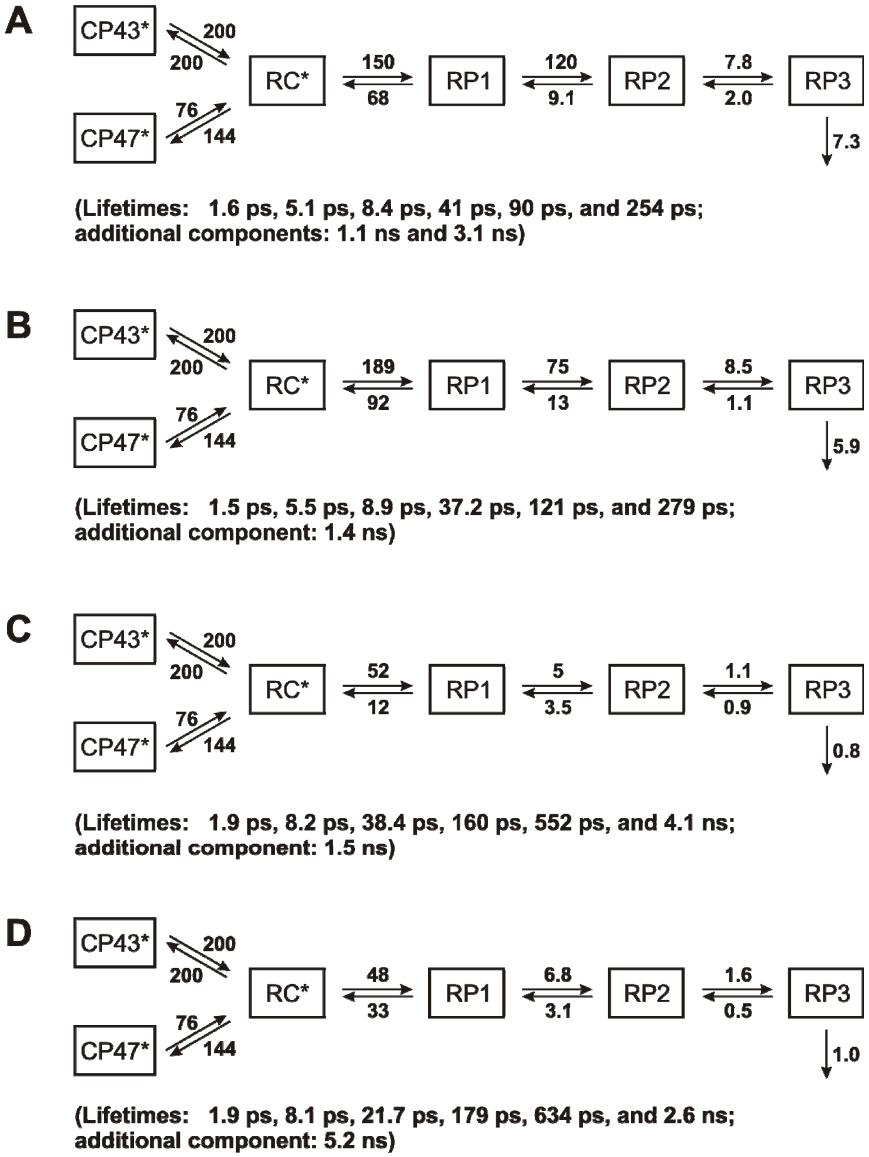

Fig. 5-4 Results of target analysis of the fluorescence signals from A) WT' with oxidized Q_A; B) D2-Y160F mutant with oxidized Q_A; C) WT' with reduced Q_A; and D) D2-Y160F mutant with reduced Q_A. Each kinetic model consists of six states: three excited states (CP43*, CP47*, and RC*) and three radical pairs (RP1, RP2, and RP3) plus 1 or 2 additional compartments. The rates are given in ns^{-1}.

5.4 Discussion

PSII with open RC WT' vs. D2-Y160F

Chlorophyll *a* fluorescence measurements on PSII with open RCs show no substantial differences between the WT' and the mutant (Fig. 5-2C). The F_m/F_0 value (between 9 and 10) is twice larger than reported before in the literature (*30*). However, it is fully compatible with the corresponding increase of the average fluorescence lifetime obtained upon the closure of RCs in the time-resolved fluorescence experiments (see Table 5-1). We assume that previous preparations of PSII core did have some amount of inefficiently connected antennae (which would increase F_0) and/or not a full equivalent of Q_A, which would have the same effect.

Comparison of the results of the global analysis (Table 5-1) reveals a large relative amplitude of the ~ 40 ps lifetime in WT' (75%), which is much higher than the amplitude of

other lifetimes, while in the mutant a 27 ps component has only 34% of the total amplitude, comparable to the amplitudes of the two longer lifetimes (59 ps and 229 ps). The same trend can be found in the relative fluorescence yield. In the D2-Y160F the longer lifetimes have much higher yields, whereas in the WT' the relative yield of the longest lifetime is only twice larger than the yield of the shortest one. The same conclusions can be made on the basis of the target modeling, where DAS plots show a rather large relative amplitude of the 41 ps lifetime in WT', while the corresponding component in D2-Y160F has still the largest amplitude, however much smaller in relation to the amplitudes of the other lifetimes.

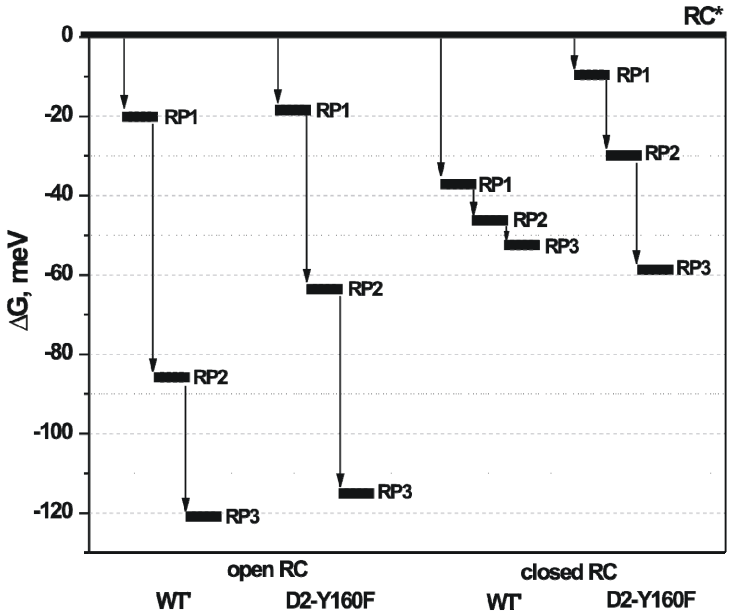

Fig. 5-5 Schematic illustration of the free energy differences Δ*G* between different compartments of the kinetic models presented in Fig. 5-4. RC* denotes RC excited state and represents the reference state for the free energy calculations.

The results of the kinetic target modeling of the WT' and the mutant data are shown in Fig. 5-4 and Fig. S5-1, Fig. S5-2, Fig. S5-3, and Fig. S5-4. The emission spectra of the excited RC compartment peak at about 683 nm in both preparations, whereas the antennae spectra are blue-shifted and of smaller amplitude. The target analysis indicates higher rates of charge separation and charge recombination processes in the TyrD-less PSII. However, the weighted eigenvector matrices show similar lifetimes (5.1 – 5.5 ps) associated with the formation of the first RP. (Note that the rise of the population of a kinetic compartment is indicated by a negative sign, while its decay by a positive sign). The resulting actual fluorescence lifetime, ~8.5 ps, cannot be exclusively assigned to one particular process; both energy and electron transfer steps contribute to it. The charge stabilization (formation of the second radical pair) is described with 37 – 41 ps lifetimes in WT' and D2-Y160F PSII, respectively. The rise of the RP3 population is 30 ps faster in the WT' than in the mutant. Nevertheless, the final resolved process, the decay of the third RP, is characterized by 260-280 ps lifetimes in both preparations. According to the previous findings ((*28;33*) *etc.*) the third radical pair decays to the $P_{D1}^{+}Q_{A}^{-}$ state. As shown in earlier experiments, the primary charge separation takes place between the accessory chlorophyll Chl_{accD1} and the pheophytin $Pheo_{D1}$ in the active branch of

RC (*27;28*). Thus, RP1 = $Chl_{accD1}^{+}Pheo_{D1}^{-}$; RP2 = $P_{D1}^{+}Pheo_{D1}^{-}$; and in line with the proposed protein relaxation arising in the RC we assign RP3 to the radical pair $P_{D1}^{+}Pheo_{D1}^{-}$ surrounded by a protein which has already undergone a conformational change. For better understanding of the TyrD influence on the primary events in PSII the free energy difference (ΔG) of the formation of the intermediate radical pairs can be calculated on the basis of the forward and backward rate constants of the discussed processes. Fig. 5-5 (*left side*) shows almost no difference in ΔG for the primary CS between WT' and mutant. This is not surprising since both chromophores involved in RP1 are rather distant to TyrD. However, the formation of RP2 is influenced by the lack of TyrD. This process is less favored in the mutant than in the WT'. The most likely explanation is the electrostatic influence of the H^{+} localized in the vicinity of the $TyrD^{\cdot}$ radical on the distribution of the positive charge on the $(P_{D1}P_{D2})^{+}$ chlorophyll pair. Therefore, a smaller loss of free energy in this step in the mutant could be caused by a mutation-triggered alteration in the hydrogen bond network around P_{D2} and thus its redox potential and/or distribution of the partial charge on $P_{D1}P_{D2}$ pair (*55;125*). However, the $P680^{+}$ reduction kinetics experiments on PSII core particles isolated from *C. reinhardtii* (*124*) did not show an influence of TyrD presence/absence on the P680/$P680^{+}$ redox potential. However, our data clearly show such an effect. As the most important consequence, the presence of $TyrD^{\cdot}(H^{+})$ increases the oxidative power of P_{D1}^{+}, improving in this way the rate of TyrZ oxidation and thus of the water-splitting process. This can be also visualized by the time course of the average loss of the free energy difference of all radical pairs during the reaction (Fig. S5-5 in Supporting materials). The drop in total ΔG is much faster in the WT' than in the TyrD-less mutant, indicating the influence of $TyrD^{\cdot}(H^{+})$ on the rate of the TyrZ oxidation. In spite of the lack of TyrD in the mutant PSII particles, the conformational change of the protein surroundings stabilizes the separated charges leading to the formation of the final state RP3, identical in both samples (see also Szczepaniak *et al.* (*127*)). It is clear from Fig. 5-5 that the total loss of free energy for WT' and D2-Y160F after protein relaxation is comparable in the experimental error limits. This shows again that it is primarily the forward rate, and thus the driving force for TyrZ oxidation, which is increased by the TyrD radical. The last resolved step in our experiment describes the formation of $P_{D1}^{+}Q_{A}^{-}$ pair. This process is characterized by the same lifetimes for both, WT' and D2-Y160F PSII particles, of 250-280 ps, which is not surprising since Q_A is located far from TyrD.

PSII with closed RCs

In PSII particles treated with DCMU the chlorophyll *a* fluorescence exhibits similar trends in both preparations. The global analysis of both preparations resulted in a set of five lifetimes, once again with the shortest one (a few ps) exhibiting the features of an energy transfer process. The other two components below 1 ns contribute very little to the yield of the total fluorescence signal (≤ 5%). The largest contribution to the fluorescence signal comes from the two longest lifetimes, 1.6 ns and 4.2 ns in WT' and 1.3 ns and 3.0 ns in D2-Y160F

PSII: 20% and 73% for WT' and 14% and 80% for the mutant, respectively. It is noteworthy to point out here that the amplitude of the ~50 ps lifetime is almost twice larger than the amplitude of the longest component in the WT' preparation, whereas the mutant shows the opposite effect. In consequence the average lifetime of fluorescence of the mutant is about 15% larger.

The compartmental modeling shows that in the PSII with closed RC the mutation does not seem to affect the primary charge separation rate, however the charge recombination step is almost 3 times faster in D2-Y160F. In addition the rate of the charge stabilization is almost 40% increased when compared with the corresponding rate in the WT' PSII, whereas the back reaction is characterized with comparable rates. The RP2 to RP3 electron transfer rate is also larger, by about 46%, in the mutant. In the lifetime domain the major difference between both samples can be observed in the charge separation process: it is characterized by a 38 ps component in the WT', while in the mutant it is faster (22 ps). The subsequent lifetimes, ~170 ps and ~590 ps, are comparable in the experimental error limits, although the longest lifetime (few ns) differs more than 40%.

As in the PSII with open RC, also here the rearranged hydrogen bond network around P_{D2} may cause modifications in the free energy differences for particular electron transfer steps (*55*). In accordance with Fig. 5-5, the effect of TyrD is obvious, especially in the first electron transfer step, where the free energy difference of the charge separation in WT' PSII is almost four times larger than in D2-Y160F. Additionally, in PSII with reduced Q_A the formation of RP2 is less favored in the TyrD-lacking mutant in same manner as in PSII with open RC – the magnitude of this effect is comparable, since $\Delta G(\mathrm{RP2})_{\mathrm{WT'}}$-$\Delta G(\mathrm{RP2})_{\mathrm{mutant}}$ is about –22 meV and –17 meV for open and closed RC, respectively. All of these effects of mutation and differences upon closing RCs suggest strongly that the D2 side of the protein, with charged radical species appearing close to the TyrD radical, is involved in the charge separation process in PSII with reduced Q_A.

In PSII with oxidized Q_A, the early processes are well understood (*27;28*). In contrast the mechanism of charge separation and electron transfer in PSII with closed RC seems to be different and still unclear (*127*). The prevailing hypothesis in the literature is that the mechanisms of charge separation and also the radical pairs involved are identical in PSII with open and closed RC. However, our data analysis on DCMU-treated PSII particles strongly suggests a switch in mechanism and the involvement of the D2 side in electron transfer of closed RCs (*127*). Fig. 5-5 (*right side*) clearly indicates the influence of the TyrD presence/absence on the formation of the first RP. The free energy difference of the charge separation in WT' PSII is almost four times bigger than in D2-Y160F. Therefore, we propose that one (or both) of the chromophores constituting RP1 has to be localized in the relative vicinity of TyrD, which leads to the idea of different chromophores involved in the radical pairs when compared to PSII with open RC. The requirement of a relatively short distance to

TyrD allows us to exclude $Pheo_{D1}$, as well as $Pheo_{D2}$, as a potential partner in RP1. Thus, the most likely molecules contributing to the first radical pair are: P_{D1}, P_{D2}, Chl_{accD1} and Chl_{accD2}.

The opposite trend can be found in the formation of the two subsequent radical pairs – the corresponding ΔGs are much smaller in the WT' than in the mutant. Nevertheless, the total ΔG change is comparable in both preparations (-53 and -59 meV for WT' and D2-Y160F, respectively). For this reason and on the basis of our previous findings (*127*) we can speculate here also about the involvement of the protein conformational changes in the stabilization of the charges in the energetically favored state. Consequently RP3 might be regarded again as a relaxed RP2.

Time-resolved transient absorption difference spectroscopy will be required to arrive at a correct mechanism and description of the involved RP intermediates for PSII with closed RCs.

5.5 Conclusions

The present work reveals the importance of TyrD for the primary reactions in PSII. Even though our data show that the enzyme can work efficiently without TyrD under physiological conditions (PSII with Q_A in oxidized state), the influence of its presence is very pronounced in the second electron transfer step. This however can be overcome with the help of the surrounding protein. The comparable total losses of free energy in both, WT' and D2-Y160F underline the often neglected input of the protein dynamics to the electron transfer processes in PSII.

Our data is interpreted in the framework of the trap-limited kinetics model that implies fast energy equilibration between antennae complexes and the RC compared with a slower charge separation process. This model is based on a vast experimental base, comprising both femtosecond transient absorption data as well as ultrafast fluorescence kinetics data (*28;33*). This is the only model that has been able to consistently describe both types of ultrafast experiments. There are some conflicting reports in the literature suggesting a diffusion-limited kinetics from the antenna to the RC, based either on experimental data (*32*) or theoretical modeling (*128*). The experimental study of (*32*) lacked the necessary time-resolution to actually resolve the fast energy transfer, and the theoretical study of (*128*) used only a very limited set of experimental data to fit their theoretical model. If we would in fact assume these alternative diffusion-limited models as the basis of our interpretation the consequences are clear: We would in this case have to interpret most of the rate constants that are changing in the mutant relative to the wild type as energy transfer rate constants. Thus the implication would be that upon mutating the TyrD the energy transfer between antenna and RC would change. This would be a totally illogical consequence of applying a diffusion-limited model. Clearly mutation at TyrD site cannot change the energy transfer rates in any substantial way, but it is completely logical that it changes some of the early electron transfer rates. Thus, quite in contrast to the implications of the above-mentioned diffusion-limited

models, we have to conclude that our present findings do require a trap-limited model, as applied by us in the present work. Any other interpretation would lead to severe inconsistencies. Without having to go into the intricate details of the analysis of the type of kinetics in PS II – which is amply discussed in the literature already – the present experimental findings thus demonstrate by themselves the necessity of a trap-limited kinetics and exclude a diffusion-limited kinetics.

Moreover, the different changes in kinetics of the WT' and the mutant preparations observed upon closing RCs not only show the effect of the presence/absence of TyrD, but in addition confirm our previous suggestion (*127*) of the alteration in the CS and electron transfer mechanism in PSII upon closing the RCs by reduction of Q_A.

5.6 Supporting materials

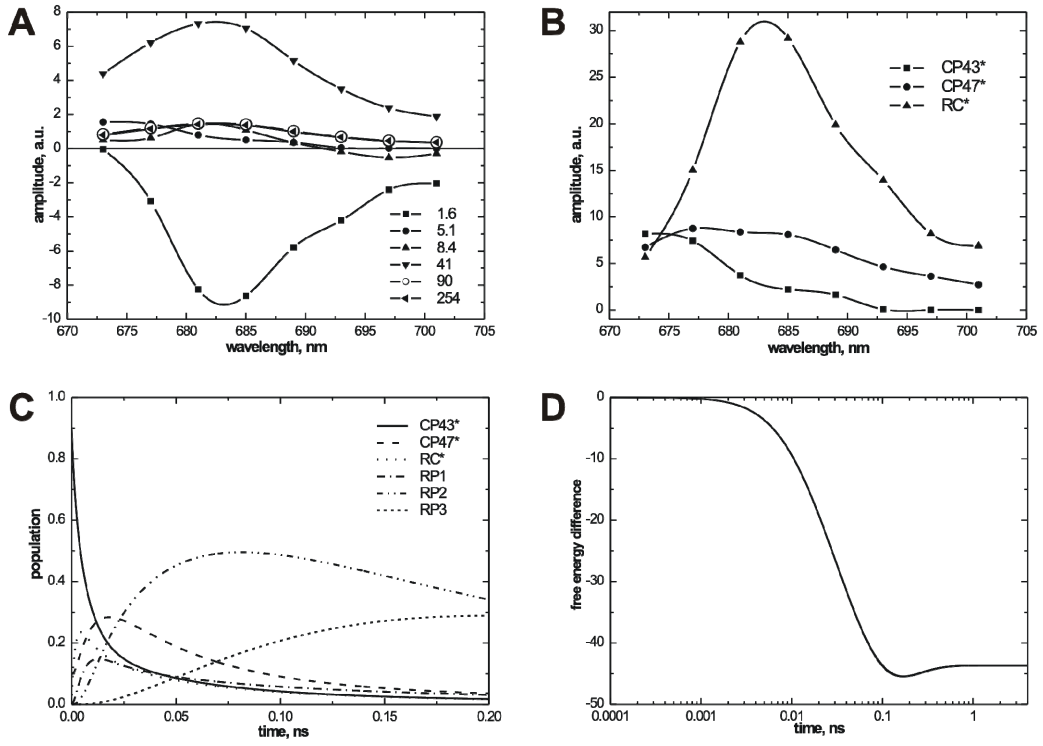

E

τ (ps)	CP43*	CP47*	RC*	RP1	RP2	RP3
1.6	0.15	0.09	-0.33	0.11	-0.02	0
5.1	0.19	0	0	-0.54	0.36	-0.02
8.4	0.35	-0.46	0.14	0.27	-0.31	0.02
41	0.15	0.36	0.13	0.06	-1.08	0.55
90	0.03	0.06	0.03	0.04	0.38	-1.56
254	0.03	0.06	0.03	0.06	0.68	1.00

Fig. S5-1 Results of target analysis of the fluorescence signals from WT' with open RC. With each kinetic model are associated: A) decay-associated spectra (DAS) with the related lifetimes (in ps); B) species-associated emission spectra (SAES); C) time course of the population of different states; D) time-dependence of the free energy difference of the radical pairs; E) and the matrix of weighted eigenvectors, representing the amplitudes of the compartments shown in the kinetic scheme (Fig. 5-4A).

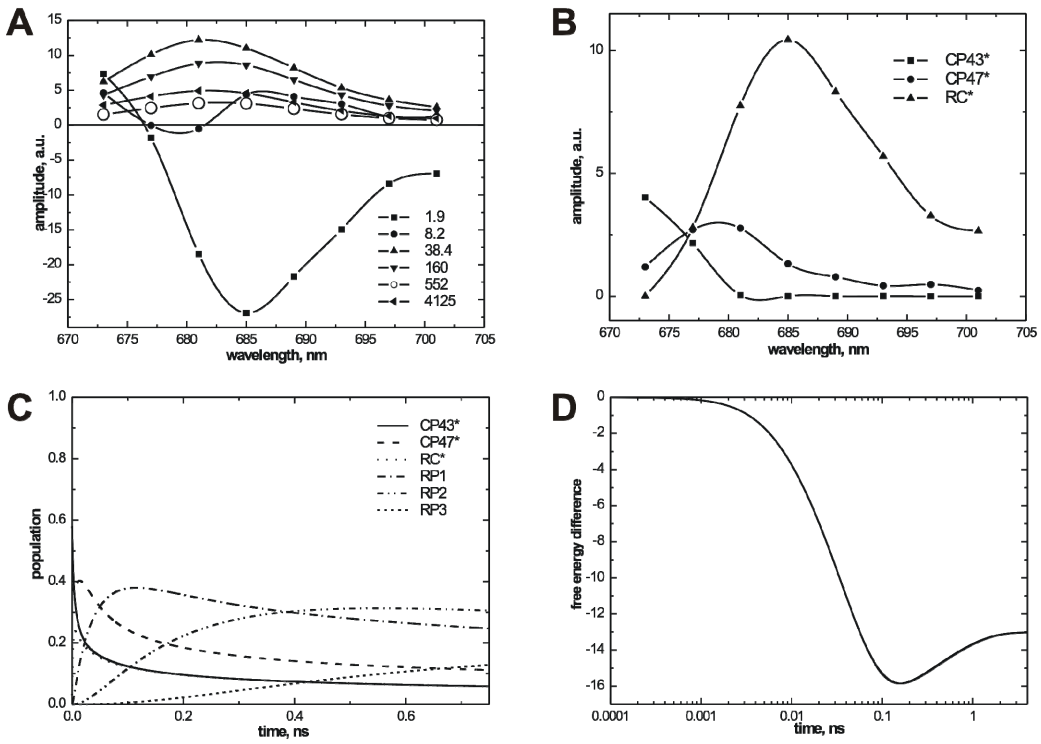

E

τ (ps)	CP43*	CP47*	RC*	RP1	RP2	RP3
1.9	0.16	0.08	-0.27	0.03	0	0
8.2	0.18	-0.22	0.07	-0.03	0	0
38.4	0.09	0.22	0.08	-0.50	0.12	0
160	0.07	0.14	0.07	0.15	-0.52	0.13
552	0.02	0.05	0.02	0.09	0.04	-0.39
4125	0.06	0.12	0.06	0.27	0.36	0.27

Fig. S5-2 Results of target analysis of the fluorescence signals from D2-Y160F mutant with open RC. With each kinetic model are associated: A) decay-associated spectra (DAS) with the related lifetimes (in ps); B) species-associated emission spectra (SAES); C) time course of the population of different states; D) time-dependence of the free energy difference of the radical pairs; E) and the matrix of weighted eigenvectors, representing the amplitudes of the compartments shown in the kinetic scheme (Fig. 5-4B).

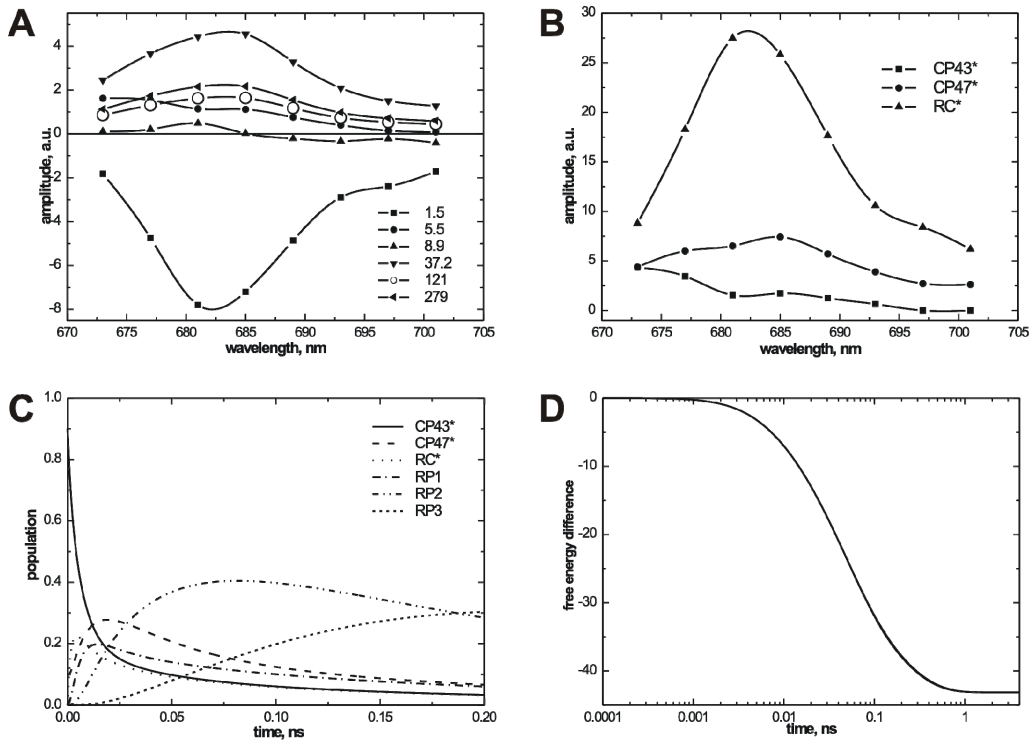

E

τ (ps)	CP43*	CP47*	RC*	RP1	RP2	RP3
1.5	0.13	0.08	-0.31	0.12	-0.01	0
5.5	0.35	-0.04	0.03	-0.61	0.29	-0.01
8.9	0.22	-0.38	0.10	0.28	-0.23	0.02
37.2	0.11	0.27	0.09	0.05	-0.78	0.33
121	0.04	0.08	0.04	0.06	0.24	-1.57
279	0.05	0.10	0.05	0.10	0.50	1.23

Fig. S5-3 Results of target analysis of the fluorescence signals from WT' with closed RC. With each kinetic model are associated: A) decay-associated spectra (DAS) with the related lifetimes (in ps); B) species-associated emission spectra (SAES); C) time course of the population of different states; D) time-dependence of the free energy difference of the radical pairs; E) and the matrix of weighted eigenvectors, representing the amplitudes of the compartments shown in the kinetic scheme (Fig. 5-4C).

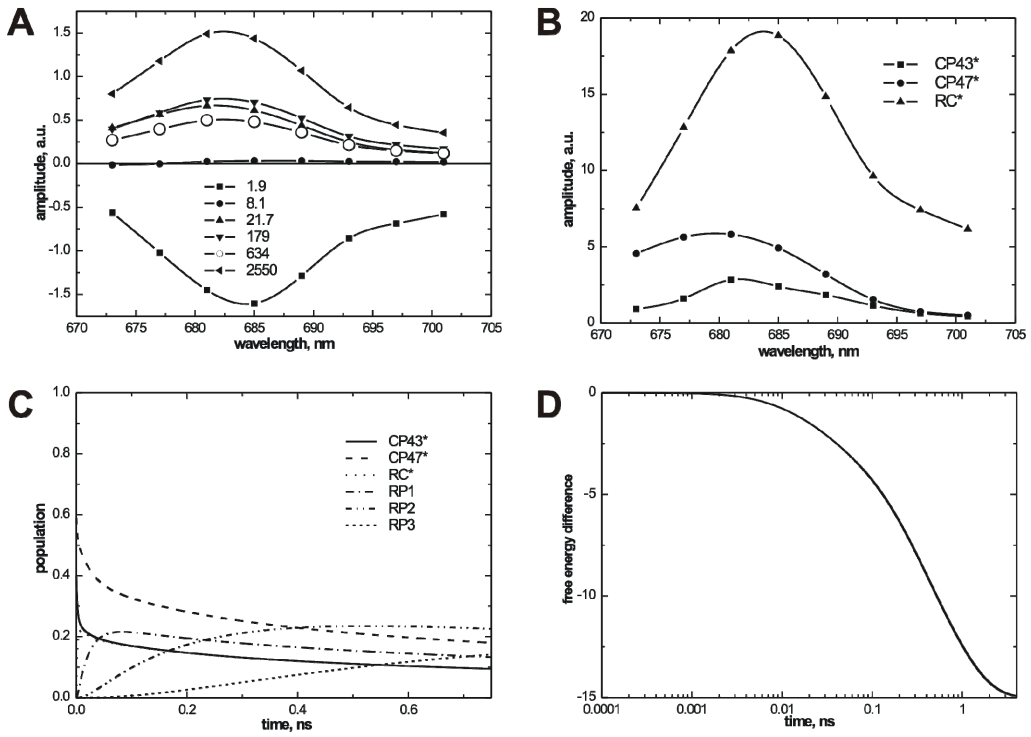

E

τ (ps)	CP43*	CP47*	RC*	RP1	RP2	RP3
1.9	0.14	0.07	-0.23	0.02	0	0
8.1	0.02	-0.02	0.01	0	0	0
21.7	0.04	0.15	0.03	-0.27	0.04	0
179	0.05	0.11	0.05	0.04	-0.36	0.14
634	0.04	0.07	0.04	0.05	0.02	-0.55
2550	0.11	0.21	0.11	0.16	0.30	0.41

Fig. S5-4 Results of target analysis of the fluorescence signals from D2-Y160F mutant with closed RC. With each kinetic model are associated: A) decay-associated spectra (DAS) with the related lifetimes (in ps); B) species-associated emission spectra (SAES); C) time course of the population of different states; D) time-dependence of the free energy difference of the radical pairs; E) and the matrix of weighted eigenvectors, representing the amplitudes of the compartments shown in the kinetic scheme (Fig. 5-4D).

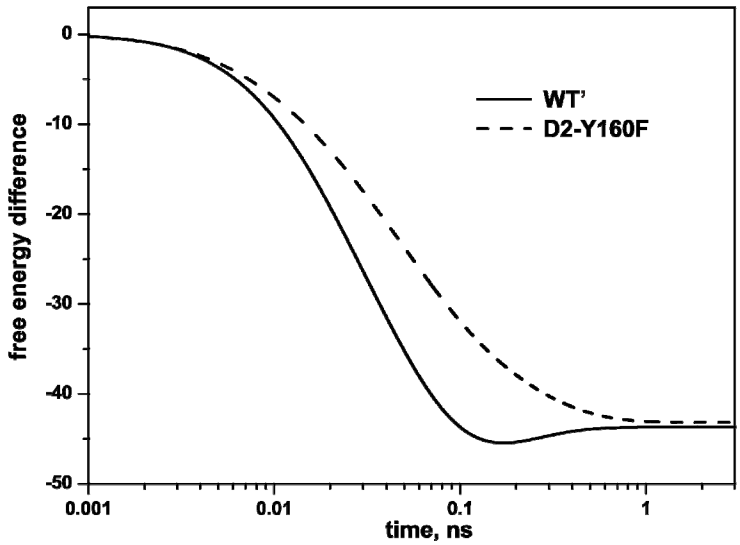

Fig. S5-5 Time-development of the sum of the free energy difference of all radical pairs, calculated for WT' and D2-Y160F PSII particles with oxidized Q_A.

6 A photoprotection mechanism involving the D_2 branch in photosystem II cores with closed reaction centers

This chapter is based on the publication: V. Martínez-Junza, M. Szczepaniak, S.E. Braslavsky, J. Sander, M. Nowaczyk, M. Rögner, A.R. Holzwarth. Photochemical & Photobiological Sciences 7 (2008), 1337-1343.

Nanosecond transient absorption spectroscopy has been used to study reaction centre (RC) chlorophyll triplet quenching by carotenoid in intact photosystem II cores from *T. elongatus* with closed RCs. We found a triplet β-carotene (^{3}Car) signal (absorption difference maximum at 530 nm) that is sensitized by the RC chlorophyll (Chl) triplet with a formation time of ca. 190 ns, has a decay time of 7 μs and is formed with a quantum yield between 10 and 20%. The ^{3}Car signal is assigned to the β-carotene on the D2 branch of the RC. We thus propose a new photoprotection mechanism operative in closed RCs where – as a consequence of the negative charge on the quinone Q_A – the triplet chlorophyll (^{3}Chl) is formed by the radical pair (RP) mechanism on the normally inactive D2 branch where it can be subsequently quenched by the D2 β-carotene. We suggest that the D2 branch becomes active when the RCs are closed under high light fluence conditions. Under these conditions the D2 branch plays a photoprotective role. This interpretation allows combining many seemingly inconsistent observations in the literature and reveals the so far missing RC triplet quenching mechanism in photosystem II. The newly proposed mechanism also explains the reason why this RC triplet quenching is not observed in isolated D1-D2-cyt *b-559* RCs. If Q_A is either not present at all (as in the isolated RC) or is not charged (as in open RCs or with doubly reduced Q_A) then the RC ^{3}Chl is formed on the D1 branch. The D1 branch ^{3}Chl can not be quenched due to the large distance to the β-carotene. This interpretation is actually in line with the well-known ^{3}RC quenching mechanism in bacterial RCs, where also the carotenoid in the (analogous to the D2 branch) B-branch of the RC becomes the quencher.

6.1 Introduction

Carotenes play an important role as photoprotectors in photosynthesis, quenching both triplet states and singlet oxygen (*14;129-131*). Despite some difficulties in the past to precisely localize the β-carotenes in the reaction centre (RC) of photosystem (PS) II (*7;59-61*), the published 3 Å resolution structure resolved two β-carotenes in the RC. The β-carotene in the D1-branch is 20 Å away from the D1-chlorophyll (Chl_{D1}) whereas the D2-carotene is only 13.2 Å away from Chl_{D2} (*cf.* Fig. 6-1) (*8*).

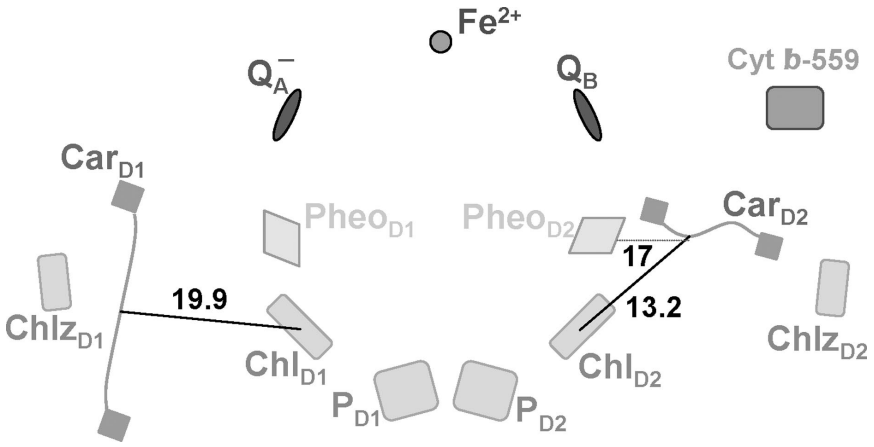

Fig. 6-1 View along the membrane plane of the cofactors present in PSII closed reaction centers. All distances are in Å. Modified from ref. (*8*). P: chlorophylls of the special pair, Chl: accessory chlorophylls, Car: carotenes, Q: quinones, Pheo: pheophytins, Cyt *b*-559: cytochrome *b-559*. Chl_Z are the peripheral Chls in the RC. D1 is the active branch, whereas D2 is the inactive branch for electron transfer under low irradiation conditions, *i.e.*, the normal functional state. Note the negative charge on Q_A for the closed RC. The suggestion from the present study is that the D2 branch becomes active in electron transfer when the RCs are closed under high light fluences. Under these conditions the D2 branch plays a photoprotective role.

The dominant and general protection mechanism of carotenoids is the quenching of triplet (bacterio)-Chls (^{3}BChl), both in photosynthetic antennae (*132;133*), and in RCs (*134-137*). In bacterial RCs a carotenoid located in the B-branch quenches RC triplet BChl (^{3}BChl) by a Dexter mechanism (*138*), producing triplet carotene (^{3}Car) (*137*) (for reviews see ref. (*135-137*)).

The photoprotective role of carotenoids in PS II has been widely studied (*139;140*) (for reviews see ref. (*14;141*)). Carotenoids act as an electron relay in conditions of over-reduction of the acceptor side in the PS II RCs, delivering electrons to the $P680^{\cdot+}$ radical from cytochrome *b-559* or/and accessory chlorophyll (Chl_Z) in D2 (*12;14;140-145*). Furthermore, the two β-carotenes also scavenge singlet oxygen before it damages the PS II RC. Singlet oxygen is an extremely damaging species produced *via* ^{3}Chl and can be quenched by carotenes producing ^{3}Car, whose decay to the ground state delivers heat (*14;139;146*). A further role of carotenoids is the protection against over-excitation of the photosynthetic unit under high radiation fluences by quenching the ^{1}Chl* states in the antenna of PS II in a range of regulation mechanisms called "non-photochemical quenching" (NPQ) (*139*).(*146-148*).

In isolated RCs of PS II, *i.e.*, the D1-D2-cyt *b-559* complex, which lacks Q_A, the forward electron transport can not proceed beyond the first two (radical pairs) RPs (*28*) and the charge-separated singlet state $P_{680}^+Pheo^-$ forms a triplet radical pair ($^3RP^{\pm}$) *via* the RP dephasing mechanism (*149*). The $^3RP^{\pm}$ then recombines to the RC ^{3}Chl state (*150;151*).

The yield of ^{3}Car in isolated D1-D2-cyt *b-559* RCs has been reported as very low (<3%) whereas the triplet yield of the primary electron donor Chl has been found to be high (ranging from 30% (*150;152*) to 50% (*153*)). Surprisingly, this $^3Chl_{D1}$ has a long lifetime of *ca.* 1 ms (*154*) and is unquenched by carotenes despite the presence of both β-carotenes in the RC (*150;155*). This led to the highly puzzling conclusion that under conditions where ^{3}Chl is formed in the RC with high yield no efficient photoprotective mechanism exists in the PS II

RC (for reviews see ref. (*14;141*)). Under aerobic conditions this ^{3}Chl state indeed leads to rapid destruction of the RC by damaging the D1 protein *via* singlet oxygen (*143;156;157*).

In contrast to the findings with isolated D1-D2-cyt *b-559* RCs, in more intact PS II particles with closed RC (*i.e.*, with singly reduced Q_A which carries a negative charge) at 20 K a much shorter lifetime of 2–20 μs was reported for the RC ^{3}Chl (quantum yield of 0.66–0.74), *i.e.*, the ^{3}RC is quenched (*158*). The yield and lifetimes of the ^{3}Chl are, however, strongly temperature dependent. Liu *et al.* (*159*) reported, for example, a yield in the range of *ca.* 10% at room temperature and a lifetime around 30 ns. These authors assigned a very small amount of an additional >1 μs lifetime component to ^{3}Car without specifying its origin.

Van Mieghem *et al.* (*158*) reported lifetimes of 30 ns and *ca.* 150 ns and a much higher yield for ^{3}Chl under conditions as above. Interestingly, intact PS II particles (PS II cores) with doubly reduced Q_A (neutral due to double protonation) show the same behavior as isolated D1-D2-cyt *b-559* RCs, *i.e.*, the RC ^{3}Chl is long-lived and is not quenched by carotenoids (*158;160*).

To explain the drastically shortened ^{3}Chl lifetime in intact PS II particles with singly reduced Q_A as compared to isolated RCs, van Mieghem *et al.* proposed a quenching mechanism where the ^{3}Chl is transferred to Pheo and subsequently an electron transfer takes place from Q_A^- to ^{3}Pheo forming the $Pheo^-$ anion. The latter would then re-reduce Q_A in the normal way (*158;161*). No direct experimental proof for this hypothesis exists, however, so far. It should be pointed out that this hypothesis implicitly assumes that the same early RPs are formed in PS II with open and closed RCs, which might not be the case (*162-164*).

Thus, an attractive alternative interpretation of the ^{3}Chl short lifetime in the case of RCs with singly reduced Q_A would be its location on a Chl different from Chl_{D1}, in agreement with EPR and optical results. Clear experimental support for different spectroscopic properties, and thus locations, of the ^{3}Chls in the two different cases has been found recently by EPR and ODMR spectroscopy (*162;164;165*). However, no assignment as to the location of the ^{3}Chl in the case of PS II with singly reduced Q_A has been made.

We note that PS II needs an efficient protection against the possible damaging effect of triplet states particularly when Q_A is reduced (closed RCs) since under this condition a high yield of long-lived ^{3}RC is formed. Thus, it would not be easily understandable that both of the carotenoids in the PS II RC would be inactive in quenching ^{3}RC.

In view of this background, we decided to search for the possible production of ^{3}Car in closed RCs, in particular the present nanosecond transient spectroscopy study analyzes the ^{3}Chl decay in intact PS II cores from *T. elongatus* and compares it with the behaviour in open RCs. We propose a photoprotective mechanism that involves ^{3}Chl to Car transfer in the D2 branch of the RC.

6.2 Materials and methods

Experiments were performed at room temperature with purified dimeric PS II core particles from *T. elongatus* with an intact oxygen evolution complex (*53*) and with isolated D1-D2-cyt *b-559* complexes from spinach isolated according to published protocols (*166*) with slight modifications (*28*). Anaerobic conditions were achieved by addition of 5 mM glucose, 0.07 mg/ml glucose oxidase and 0.07 mg/ml catalase to a 20 mM MES buffer (pH 6.5). The RCs were closed by addition of 20 μM DCMU [3-(3,4-dichlorophenyl)-1,1-dimethylurea] and weak background illumination. For measurements with open RCs, 0.8 mM potassium ferricyanide was added (*159*). The absorbance at 660 nm was around 0.6 for all samples in a 1 cm path cuvette.

The ns flash photolysis equipment already described was used in single-beam mode (*167*). Excitation at 660 and 450 nm was achieved by pumping the frequency-tripled pulse of a Nd:YAG laser (SL 456 G, 6 ns pulse duration, 355 nm, Spectron Laser Systems, Rugby, United Kingdom) into a beta barium borate optical parametric oscillator (OPO-C-355, tuning range 430–2100 nm, GWU Laser Technik Vertriebs GmbH, Erftstadt-Friesheim, Germany). The analyzing beam from a pulsed 150 W Xe arc was focused into the 1 cm optical pathlength cuvette perpendicular to the excitation after passing through a monochromator. The transmitted beam was focused into a second monochromator and detected by a Hamamatsu R3896 photomultiplier wired for rapid detection and recorded by a TDS 520A (Tektronix) transient recorder. The instrument response function is about 25–30 ns wide. Typically 100 shots were averaged for each decay. Global analysis of the data was done using either a home made program (MathCad) that also allowed convolution with the instrument function for higher resolution or the Origin program (version 7.5).

The excitation laser fluence was chosen well below the saturation level to avoid non-linear effects and artefacts due to multiple excitation of the antenna (Fig. 6-2).

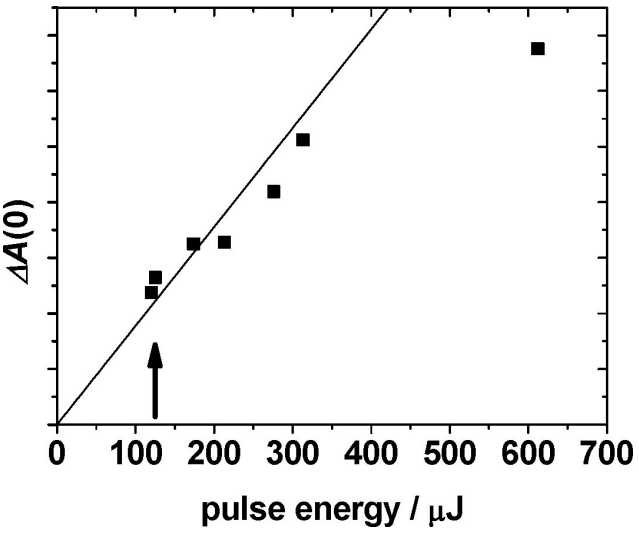

Fig. 6-2 Saturation curve obtained by plotting the pre-exponential factor of the *ca.* 7 μs lifetime component *vs.* the laser pulse energy (see Fig. 6-4B). The arrow marks the maximum laser pulse energy employed for the time-resolved measurements in the present work.

6.3 Results

Transient absorbance changes were measured for PS II with closed RCs, upon excitation at 660 nm, at eleven wavelengths between 450 and 600 nm (Fig. 6-3A) and fifteen wavelengths between 400 and 640 nm (Fig. 6-3B). The closing of the RCs was done in the mildest possible way by the addition of DCMU, thus avoiding the problems of double reduction of Q_A, easily occurring if dithionite is used to reduce Q_A such as, *e.g.*, in ref. (*159*).

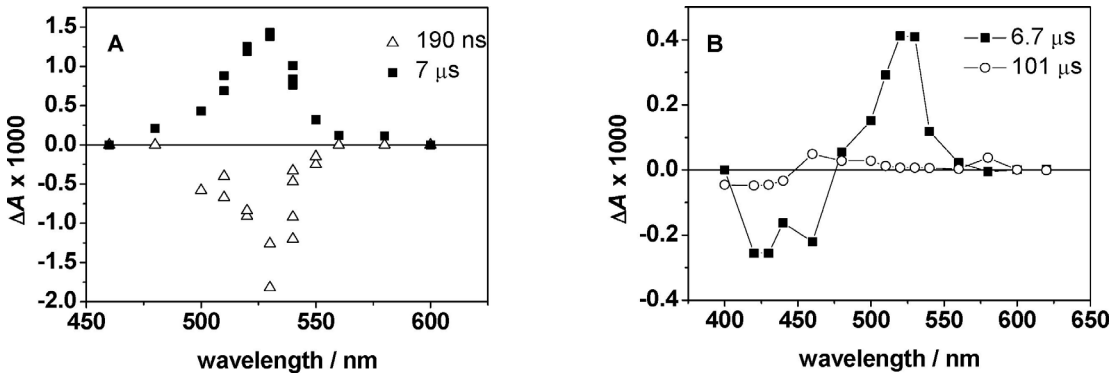

Fig. 6-3 Lifetime-associated difference spectra (LADS) upon excitation at 660 nm of PSII with closed RCs taken in two time windows. A) Higher time resolution, LADS associated with a 190 ns production of the carotene triplet state and 7 μs lifetime for its decay; B) Lower time resolution, LADS associated with a bi-exponential fit with a major component with a 6.7 μs lifetime and a very minor component with a 101 μs lifetime.

Two signals taken with a 20 and 2 ns/point resolution at 530 nm and their respective fittings obtained from a global analysis are shown in Fig. 6-4A and Fig. 6-4B, respectively. A rise time of 190 ns and a decay time of 7.3 μs were obtained when the high resolution signals (2 ns/point) were analyzed with a global analysis (Fig. 6-4B). Detailed analysis of the transient absorption signals observed at 460 nm (the ground state absorption of β-carotene, Fig. 6-4C) showed that they were well fitted with the same parameters as that at 530 nm. At the same time, a bi-exponential function fitted well the low resolution signals (20 ns/point), with a major component with a 6.7 μs lifetime and a very minor component with a 101 μs lifetime.

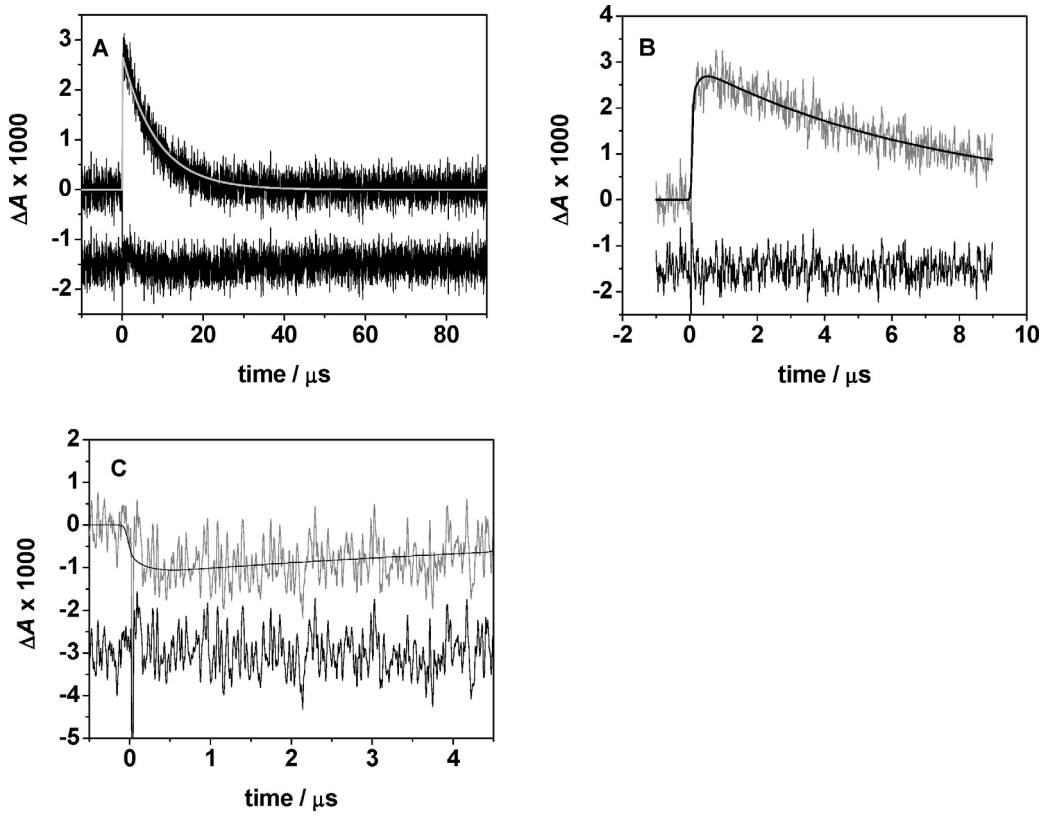

Fig. 6-4 Transient absorption signals and fittings upon excitation at 660 nm of a PSII sample with closed RCs observed at 530 nm at two time scales (A and B) and at 460 nm (C). A global analysis (15 observation wavelengths) was used to fit the signal. The fitted lifetimes for B and C are 190 ns for the appearance and 7.34 μs for the decay. The error distribution of the fitting is depicted at the bottom of each signal.

Analysis of the lifetime-associated difference spectra (LADS) for low time resolution (Fig. 6-3B) shows that the 6.7 μs component has essentially the same spectrum as the 8.5 μs component from a single-exponential fit (not shown) and the 7 μs decay component from the global analysis of the higher resolution data (Fig. 6-3A). The very small-amplitude 100 μs component (Fig. 6-3B) may originate from a very small amount of doubly reduced RCs.

Very similar data were obtained upon excitation at 450 nm (not shown). Similar transient absorbance measurements were also attempted in the 640–700 nm detection region. Unfortunately, the strong Chl fluorescence background, which blinded the photomultiplier in the early time range of several hundred ns, prevented a detection of the small signals in the time range of interest with sufficient sensitivity and thus no reasonable signals could be obtained in that range.

Fig. 6-5 shows two signals at 540 nm upon excitation at 660 nm with open and closed RCs obtained under otherwise identical conditions. The signal is absent in the PS II units with open RCs (Fig. 6-5B).

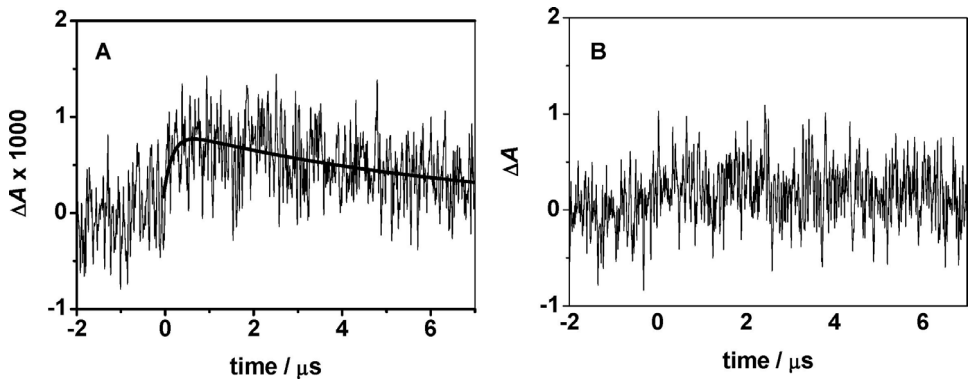

Fig. 6-5 Transient absorption signals at 540 nm upon excitation at 660 nm of two samples with: A) closed RCs; B) open RCs. The laser energy was the same in both cases and the 660 nm absorbance was matched.

Transient absorbance changes were also measured with the isolated D1-D2-cyt *b-559* complex at several wavelengths between 400 and 750 nm, upon excitation at 660 nm. Although the longest total time window available in our instrument with a pulsed analyzing beam and relatively small absorption changes was 50 μs (in view of the strong variation of the lamp output), a fitting of this long-lived signal was performed (Fig. 6-6B). The real lifetime of this transient absorbance change should be much longer (*158-160*) but can not be analyzed precisely due to too short a measuring range. Working with a non-pulsed analyzing lamp would have not improved the situation, however. The corresponding LADS of a mono-exponential decay fit of *ca.* 89 μs (Fig. 6-6A) has all features of ^{3}Chl, totally different from the 7–8 μs LADS in Fig. 6-3. The longer component observed in the closed RCs is of no significant amplitude (Fig. 6-3B) in order to make any speculation.

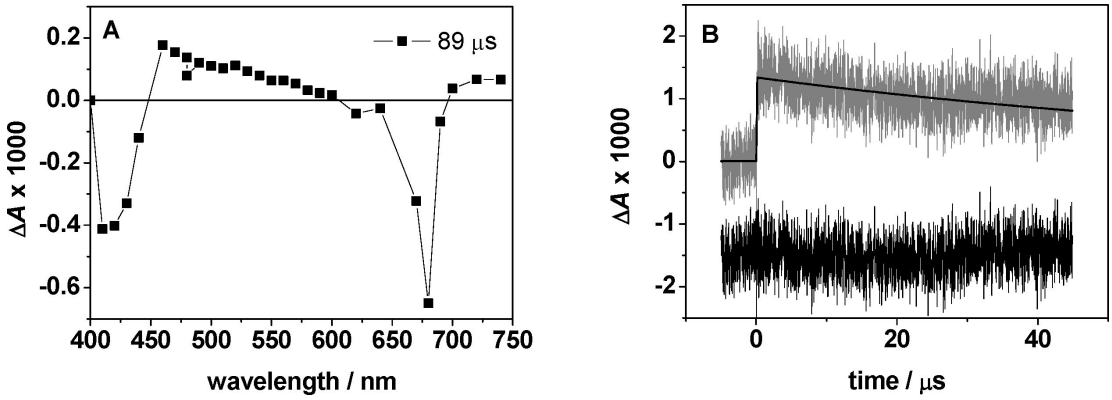

Fig. 6-6 A) Lifetime-associated difference spectra (LADS) from the mono-exponential fitting (*ca.* 90 μs) of the D1-D2-cyt *b-559* complex upon excitation at 660 nm. B) D1-D2-cyt *b-559* signal and fitting at 530 nm upon excitation at 660 nm. The error distribution of the fitting is depicted at the bottom.

6.4 Discussion

The difference spectrum associated with the appearance and decay of the transient species (190 ns rise, *ca.* 7 μs decay, Fig. 6-3A) is characteristic of a triplet carotenoid (see *e.g.* ref. (*72*)). Our transient absorption maximum at 530 nm (Fig. 6-3) is in agreement with that observed by Takahashi *et al.* (*150*) in PS II core particles but differs from the maximum of ^{3}Car in the isolated RCs (540 nm) (*150*) and in the core antenna (520 nm) (*168*). Durrant *et al.*

(*152*) reported also a maximum at 525 nm for isolated RCs similar to that previously observed by Schlodder *et al.* (*30*), who attributed the signal to ^{3}Car decay in the antenna.

The 7–8 μs decay time is in the typical range for triplet carotenoid decay in a protein (*30;169;170*). The bleaching appearance at 460 nm (Fig. 6-4C) and its recovery follow the same time behaviour as the ^{3}Car absorption and decay, respectively, supporting the assignment of this signal to a carotene accepting energy from the ^{3}Chl.

Using a molar absorption coefficient ε(Chl) = 80 000 M^{-1} cm^{-1} for Chl at 674 nm (*171*) and $\varepsilon(^3\text{Car})$ = 100 000 M^{-1} cm^{-1} at the ^{3}Car spectral maximum (*150*) and considering that there are 35 Chl per RC in our sample, a quantum yield for the formation of ^{3}Car, $\Phi(^3\text{Car})$ *ca.* 10% is estimated from the absorption signals. This value represents a minimum since in our calculation it is assumed that all RCs are excited, which is not the case. Thus, the ^{3}Car yield could be up to 20%.

The formation of ^{3}Car occurs with 190 ns rise time. The 660 nm excitation precludes a direct carotenoid excitation. But even on direct excitation ^{3}Car can not be formed efficiently due to their ultrafast singlet state decay. The only possible precursor for the observed ^{3}Car then should be a ^{3}Chl formed with substantial yield (see below).

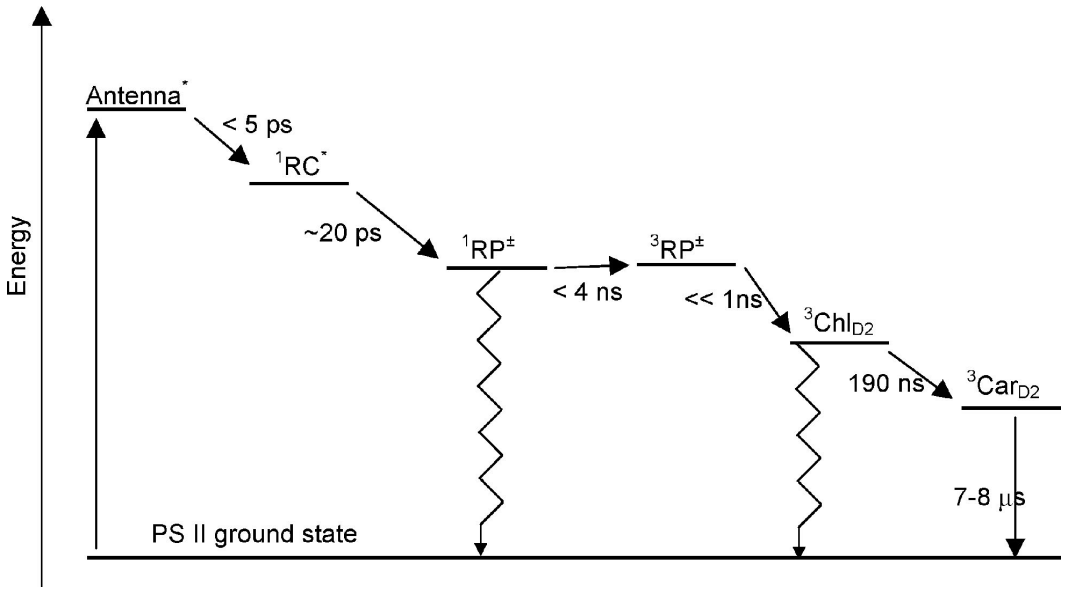

Fig. 6-7 Reaction scheme for the protection mechanism involving the D2 branch in closed PSII reaction centers. The rates of processes up to the ^{3}RP$^{\pm}$ production are taken from femtosecond transient absorption and time-resolved fluorescence experiments (*28;127*). The processes after ^{3}RP$^{\pm}$ production are assigned based on the present ns/μs flash photolysis experiments.

The question to answer is as to the actual location of the β-carotene in the complex that gets triplet sensitized. For this discussion we make use of the structural arrangement in Fig. 6-1 and the reaction scheme shown in Fig. 6-7. Two β-carotenes are located in the RC and nine in the core antenna of PS II (*8*). Direct formation of ^{3}Chl in the antenna with high yield before charge separation is very unlikely. Charge separation occurs in a time below 100 ps in PS II cores with closed RC and gives rise to a singlet RP that lives only for about 2-4 ns (*65;127*) when Q_A is singly reduced (*29*). Thus, an efficient ^{3}Chl formation can only occur *via*

the $RP^{\pm}$ dephasing mechanism in the RC on one of the RC Chls (*172*). The RC ^{3}Chl could then be quenched by one of the β-carotenes in the RC.

In isolated PS II RCs, where the ^{3}Chl has been shown to be located on Chl_{D1}, the quenching by Car_{D1} does not occur, presumably due to the long distance of 20 Å and an unfavorable arrangement of β-carotene Car_{D1} to Chl_{D1} (*8*). Since ^{3}Chl in closed (singly reduced) PS II cores has a drastically shorter lifetime than in isolated RCs, there must be a different ^{3}RC formed when Q_A is reduced in intact cores. The only other possibility for the RC ^{3}Chl quenching would be Car_{D2}, only 13 Å apart from Chl_{D2}. However, in order for this mechanism to be effective ^{3}Chl should be created on Chl_{D2} rather than on Chl_{D1} as is the case in isolated PS II RCs (*154;155*).

The above proposed mechanism would thus imply a switch in the nature of the $RP^{\pm}$ formed with closed RCs. Most likely ^{3}Chl will be formed on Chl_{D2}, rather than on Chl_{D1}. In fact, transient EPR measurements performed on PS II core crystals at low temperature could not distinguish whether the RC ^{3}Chl was formed on Chl_{D1} or on Chl_{D2} (*173*).

Our interpretation of the location of ^{3}Chl in PS II with closed RC at room temperature on Chl_{D2} would thus allow to integrate all seemingly conflicting knowledge on the spectroscopic properties and the decay of the RC ^{3}Chl (*150;155;158;160;162-164;173*).

To convince ourselves about our interpretation we need to rationalize that a distance of 13 Å between Chl_{D2} and Car_{D2} is indeed consistent with a 190 ns triplet transfer time. The Dexter transfer rate decreases exponentially with the donor–acceptor distance *R* according to eqn (6.1),

$$k = k_0 \exp(-2\alpha R) \tag{6.1}$$

where k_0 is the intrinsic Dexter rate and α gives the distance dependence.

Taking into account the data obtained for the quenching of triplet (bacterio)chlorophyll, ^{3}(B)Chl, in antenna complexes (eqn. (6.2) and (6.3)) and assuming the same Dexter quenching parameters (*i.e.*, the same intrinsic rate and distance dependence) for ^{3}RC as for antenna complexes, eqn. (6.1) can be used to evaluate the Dexter parameters. In antenna systems with a (B)Chl–Car distance typically in the range of 4–6 Å (*8;174*) ^{3}Chl are quenched within a few ns (*175*).

$$^3\text{(B)Chl}^* + {}^1\text{Car} \rightarrow {}^1\text{(B)Chl} + {}^3\text{Car}^* \tag{6.2}$$

$$^3\text{Car}^* \rightarrow {}^1\text{Car} + \text{heat} \tag{6.3}$$

This calculation shows that the proper distance dependence for the observed transfer rates in antenna on the one hand and in the PS II RC (these data) can be indeed obtained with the same set of Dexter parameters, *i.e.*, approximately k_0 = 24 ns^{-1} and α = 3.25 nm^{-1}. With these Dexter parameters and eqn. (6.1) the distance increase from 13 to 17 Å for the Chl–carotene pair in the D1 branch would result in a nearly twentyfold decrease in transfer rate. Despite being substantial, this twentyfold decrease is still too small to explain the >100 μs

lifetime of the ^{3}RC in isolated RCs and in intact PS II with Q_A doubly reduced. However, it should be noted that the D1 carotene is rotated by approximately 90° relative to the D2 carotene. This can cause a dramatic reduction in the Dexter parameter k_0 and could easily explain the very slow ^{3}RC quenching rate in the D1 branch.

The distance from accessory Chl_{D2} to Car_{D2} of 13 Å is much larger than the van der Waals distance of 4-5 Å. Why should the protecting carotenoids in RC be at relatively large distances from the ^{3}RC locations? It is quite reasonable to assume that RCs of PS II can not operate with a short distance between RC Chl and Car, since this would inevitably lead to fast electron transfer from Car to Chl, a reaction that is certainly undesirable in the RC. Thus, the long distance from Car_{D1} from the nearest RC minimizes electron transfer rate from Car to the oxidized RC Chls. Since electron transfer and the Dexter exchange mechanism for triplet transfer have, however, the same dependence on the electronic coupling, the triplet transfer rate is minimized at the same time (*176*). This then necessitates a switch of the RC branches. The D1-branch operates during normal photosynthetic electron transfer, whereas the D2 branch takes the photoprotective role in the RC. The still relatively large Chl/Car distance of 13 Å in the D2-branch clearly makes triplet transfer not impossible, but simply slows it down due to the exponential distance dependence of the Dexter mechanism. The rate is still sufficiently large to allow an efficient triplet photoprotection.

We might also consider an alternative mechanism: the $^3Chl_{D1}$ could in principle migrate to the antenna and be quenched by one of the β-carotenes located close to a Chl. Such a scenario, if realized, would also represent a photoprotection mechanism in closed PS II cores that is not known so far. Our data can not distinguish at present a β-carotene located in the RC from a β-carotene in the antenna. However, we consider this possibility as very unlikely – though not impossible – for the following reasons: in isolated PS II RCs the $^3Chl_{D1}$ does not even migrate to the peripheral Chl_z molecules, but only to the neighboring P_{D1}, located at a very short distance. All Chls of the core antenna have a similar or even larger distance to the RC Chls as compared to the Chl_{D2}–Car_{D2} distance (*8*). Therefore, such a Chl triplet–triplet migration would be even less favorable than the direct Chl_{D2}–Car_{D2} quenching. Interestingly, all antenna carotenoids are found in close distance to a Chl. Should ^{3}Chl migration over larger distances in the antenna be favourable, the large number of antenna carotenoids and their close distance to Chls would not be required for efficient triplet quenching.

We thus consider the proposed $^3Chl_{D2}$ to Car_{D2} transfer to be the most likely explanation for the ^{3}Car formed with 190 ns rise time. Our calculations show that the observed triplet transfer time of 190 ns is consistent with a Dexter mechanism. It is clearly desirable to further characterize the location and nature of the quenching β-carotene, *e.g.*, by EPR. This is, however, a difficult experiment in view of the large number of carotenoids present in PS II (*162-165;177*).

A preliminary inspection of Fig. 6-1 would suggest as a possible alternative the participation of $Pheo_{D2}$ in some step of the process leading from $^3Chl_{D2}$ to ^{3}Car formation.

However, analysis of the three-dimensional structures reveals that $Pheo_{D2}$ is at least 17 Å distant from Chl_{D2}, whereas Car_{D2} is at 13 Å from Chl_{D2}.

In conclusion, the kinetic scheme to explain the formation of this $^3Car_{D2}$ (Fig. 6-7) includes a fast energy transfer process producing the RC singlet excited state upon excitation of the antenna. From this singlet state a singlet radical pair ($^1RP^{\pm}$) is formed. The $^1RP^{\pm}$ rapidly converts to the $^3RP^{\pm}$ state and recombination takes place to yield a triplet state chlorophyll (^{3}Chl) with a high quantum yield 0.66-0.74 at 20 K (*158*). All these processes occur on a time scale faster than the resolution of the apparatus used in the present study. We can only observe the 190 ns rise time component that represents the formation of ^{3}Car upon quenching of ^{3}Chl and its decay with a lifetime of 7–8 μs. This reaction will not occur in isolated D1-D2-cyt *b-559* RCs due to the absence of Q_A. Normal charge separation occurs in the D1 branch and, therefore, no activation of the triplet protection mechanism will occur, allowing the formation of the unquenched ^{3}Chl in D1 (Fig. 6-6) (*28*).

However, if Q_A is reduced, carrying a negative charge, then the creation of an adjacent negative charge on the pheophytin in a reaction mechanism assumed identical as for open RCs (*28*) should lift up the energy of the first $RP^{\pm}$ due to the unfavorable electrostatic repulsion. As a consequence, the formation rate of this $RP^{\pm}$ would be strongly slowed down and the yield for competing slower reaction channels, which do not occur under normal conditions, could increase dramatically. Such a scenario would then indicate that the RC ^{3}Chl will be formed also on the D2 side, which would open the channel for RC ^{3}Chl protection by the D2 carotene as proposed by our experiments.

The proposed mechanism is in fact similar to the ^{3}RC quenching mechanism that has been established earlier for bacterial RCs where at low temperature the triplet transfer to the carotenes occurs with a bi-exponential kinetics with lifetimes of 150 and 500 ns (*137*). The carotenoid that quenches the ^{3}RC in bacterial RCs is located on the B-branch, structurally and functionally equivalent to the D2 branch in PS II RCs.

7 Photosystem II core complexes with open RC revisited – streak camera data

This chapter is based on the publication: M. Szczepaniak, J. Sander, C. Kley, M. Nowaczyk, M. Rögner, A.R. Holzwarth. In preparation.

7.1 Introduction

Despite the vast amount of experimental data available in the literature that discuss the energy and electron transfer processes in PSII, the agreement about the bottleneck of these processes is still not achieved (see for example a latest review (*178*)). Our recent findings (*28;33*) are still a subject of discussion in the recent literature (*128;179-181*). Coarse-grain modeling of the energy migration and the charge separation in PSII membranes (called also BBY particles), based on time-resolved fluorescence experiments (*179*), let the authors to suggest that the charge separation should be rather fast process, characterized by a significant drop in the free energy, and additionally nearly irreversible. However, in the recent report from the same group (*182*) the authors included the charge recombination process in the description of their data and this resulted in charge separation lifetime of 5.5 ps, already comparable with the one presented in our earlier paper (*33*). Furthermore the free energy drop upon charge separation and subsequent electron transfer to Q_A presented by Broess *et al.* (*182*) is similar to our finding. The femtosecond vis/mid-IR spectroscopy report on PSII core complexes (*180*) also questions our previously presented data analysis, based on the ERPE model. Nevertheless, the authors compare their findings on PSII cores, which are exposed to rather high excitation intensities that could cause reduction of Q_A (state with the so-called closed reaction center, RC) with our measurements on PSII with RC in fully open state (meaning, with Q_A in an oxidized state). In addition to this experimental data, interpreted in terms of slow energy transfer to the RC and fast charge separation, the structure-based theoretical modeling by Raszewski and Renger (*128*) also disagree with our trap-limited kinetics. Therefore, even though our studies on TyrD-less PSII showed already the necessity of the kinetics to be trap-limited to consistently describe the collected over many years data, we addressed this problem once more, and once again with the help of the time-resolved fluorescence spectroscopy. However, the experiments were performed using a streak camera setup with a single photon counting mode of detection. The biggest advantage of this setup over the previously used TCSPC setup is the much higher time resolution, of about 200 fs vs. 1-2 ps. The other improvement concerns the simultaneous detection of multiple wavelengths. In this way we expected to resolve the fast (sub)picosecond energy transfer processes in the antenna and between the antennae and the RC complexes, which was technically inaccessible in our previous fluorescence kinetics experiments. Such a fast excitation energy transfer is expected, since hole-burning, fluorescence, absorption, and fluorescence line narrowing

studies showed the presence of red-states in both PSII core antenna complexes, CP43 and CP47 (*71;72;183-187*). Actually, fast EET within these complexes was already shown in the ultrafast studies (*73;188*). For both antenna complexes, the transient absorption and fluorescence time-resolved experiments resulted in two very short lifetimes, 0.2-0.4 ps and 2-3 ps. The authors (*73*) attributed the former to the EET within a layer of chlorophylls (Chls), which is localized on the stromal side of the membrane. The slightly longer lifetime, of about 2-3 ps was assigned to the fast energy transfer from the luminal to the stromal side of CP43, and to the energy transfer to the specific lowest excitonic state in CP47, whose localization is not yet clear. Therefore, in this report we present the results from the global analysis of the time-resolved fluorescence data obtained from cyanobacterial Photosystem II core complexes.

7.2 Materials and methods

Time-resolved fluorescence kinetics has been measured at room temperature on cyanobacterial dimeric PS II core particles, isolated from *Thermosynechococcus elongatus* (*T. elongatus*). The particles were isolated and purified according to ref (*53*); the sample was characterized with high oxygen evolution rates, in the order of 3500 μmol O_2/(mg Chl*h). The sample was diluted to OD = 0.8 in the Q_y band in a following buffer: 20 mM MES (pH 6.5), 0.5 M mannitol, 10mM $CaCl_2$, 10 mM $MgCl_2$, 0.03% β-DM. Additionally, 0.4 mM ferricyanide was added to keep the RC in the F_0 state (open). The harmful anaerobic conditions were assured by bubbling the buffer with Ar and using the following oxygen-trap system: 65 μg/ml catalase, 65 μg/ml glucose oxidase and 8 mM glucose. To avoid the presence of PSII particles with closed RCs (with reduced Q_A) and to avoid multiple excitations, the sample was kept in a rotating cuvette, spun with 4000 rpm. The cuvette had a 1 mm optical path length and a diameter of 10 cm, and was moved sideways with 32 rpm. The sample was excited with laser pulses (300 fs pulse width) at 660 nm and at 4 MHz repetition rate and low laser light intensities. The laser pulses were generated by mode-locked Ti:sapphire laser operating at 82 MHz repetition rate, whose output passes through an optical parametric oscillator for the desired wavelength selection and subsequently through a pulse picker to achieve final frequency of 4 MHz.

The fluorescence signal was recorded with a synchroscan streak camera setup working in a single-photon-counting mode of detection (C5680, Hamamatsu). The emission signal passed through a polarizer set to a magic angle and through an interference cut-off filter (670 nm) to remove the scattered excitation laser beam. The time-resolved data was acquired in two time ranges: time range 1 (0-116 ps, 0.243 ps time step) and time range 2 (0-600 ps, 1.25 ps time step). The original signals are shown in Fig. 7-1. Finally, the fluorescence decays from both time ranges were simultaneously analyzed with the help of global lifetime analysis (*57*).

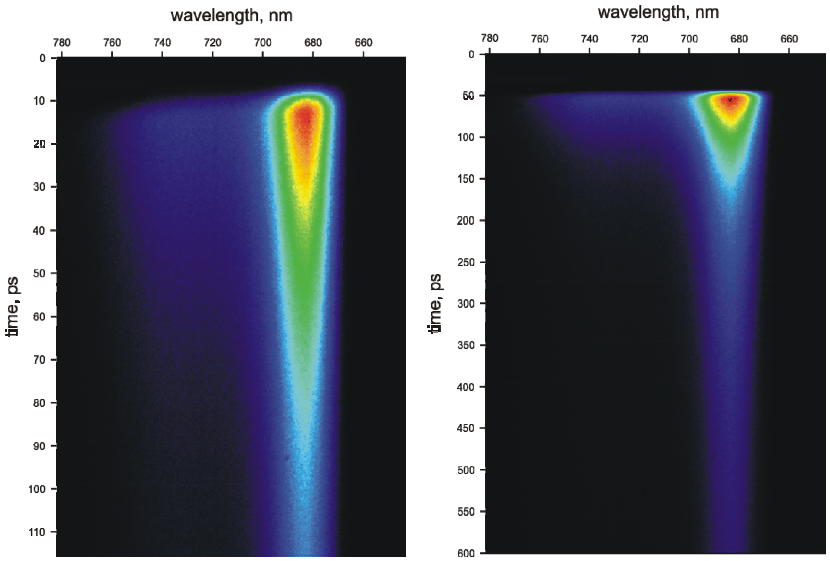

Fig. 7-1 Original fluorescence data from dimeric PSII particles with open RC: (*left*) decays measured in time range 1; (*right*) decays measured in time range 2. Note the reversed wavelength scale.

7.3 Results and discussion

The time-resolved fluorescence kinetics was analyzed in a global manner. The analysis of the data from the shortest time range suffered from many problems, mainly the obvious presence of lifetimes longer than the time range used in the experiment. Similar problems were encountered during the fitting of the second time range data alone, however in this case the major difficulty originated from the very fast processes, whose lifetimes could not be properly resolved. Therefore, global analysis was applied to the data acquired in both time ranges in a combined, simultaneous manner. This allowed to resolve both very short (< 5 ps) and medium (between 9 ps and 450 ps) lifetimes (Fig. 7-2).

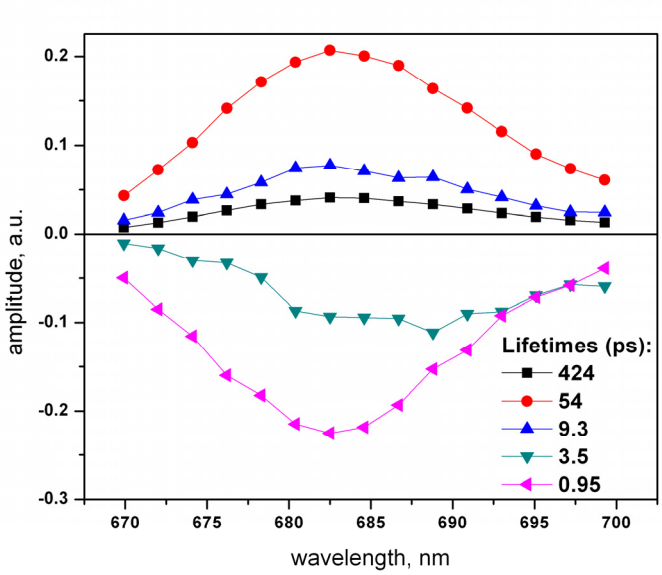

Fig. 7-2 Decay-associated spectra (DAS) of PS II core particles from *T. elongatus* excited at 660 nm resulting from the global lifetime analysis.

As shown in Fig. 7-2, the simultaneous analysis of the data sets with two different time steps resulted in five lifetimes. Additionally, a background component had to be accounted for in order to achieve a good fit. The two shortest lifetimes, 0.95 ps and 3.5 ps, are characterized with negative amplitudes, which can be attributed to the energy-transfer processes. The sub-ps lifetime has a spectrum with a negative peak at around 683 nm, whereas the 3.5 ps component has a less determined spectral shape, and seems to be red-shifted in respect to the spectrum of the shortest lifetime. The spectra of the three subsequent lifetime components, 9.3 ps, 54 ps and 424 ps, have positive amplitudes, and peak positions ~ 683 nm. The 54 ps component clearly dominates DAS. Interestingly, the global analysis of the data did not resolve lifetime much shorter than 1 ps, although with the current time resolution of the experimental setup it should be possible to determine lifetimes down to ~ 300 fs.

In our previous experiments (*33*) we resolved two short lifetimes of about 2 and 9 ps, the former with a negative amplitude over the whole measured spectral range. Due to the limited time resolution we were not able to resolve any other shorter components. At present, our improved experimental setup is already capable of distinguishing between two very short components, as can be seen in Fig. 7-2. These lifetime components can be assigned to the energy transfer processes, not only from the antenna complexes to the RC, but also between the antenna pigments. It was shown for both complexes, CP43 and CP47 that the intra-antenna energy transfer processes occur on the (sub)picosecond time-scale (*73;188*).

The remaining lifetime components are clearly associated with the charge separation and the electron transfer processes, the latter can be observed in the fluorescence signal due to the charge recombination process. In analogy to our previous results (*28;33*) the lifetime component of about 9 ps can be assigned to the charge separation process. The following lifetime of 54 ps contributes to the excited state decay with the largest positive amplitude. Similar lifetime was previously resolved (*29;32;65;66*). The longest component found in the global analysis is characterized with a relatively small amplitude and a rather long lifetime, of about 420 ps. Most probably this lifetime is a mixture of two processes, with lifetimes in the order of 100 ps and 300 ps. However, in this study the longest time range used for the signal detection (from 0 to 600 ps) allows for a reliable assignment only of the lifetimes shorter than 200 ps. Therefore, based on *a priori* estimations of the long lifetimes in PSII core complexes with open RCs we predict some contribution from both, the protein relaxation step and the electron transfer to Q_A, to the longest lifetime resolved here.

On the basis of the resolved lifetimes and their amplitudes one can calculate the average lifetime of fluorescence (see eq. 7 in section 2.3.3). For the reported here PSII core complexes with open RCs, this average lifetime is about 90 ps, which is slightly larger than the previously reported value of 65 ps (*33*). The only reason for such discrepancy lies most probably in the less precise estimation of the amplitudes and the values of the long lifetimes in the present study, due to the relatively short acquisition time window used in the experiment.

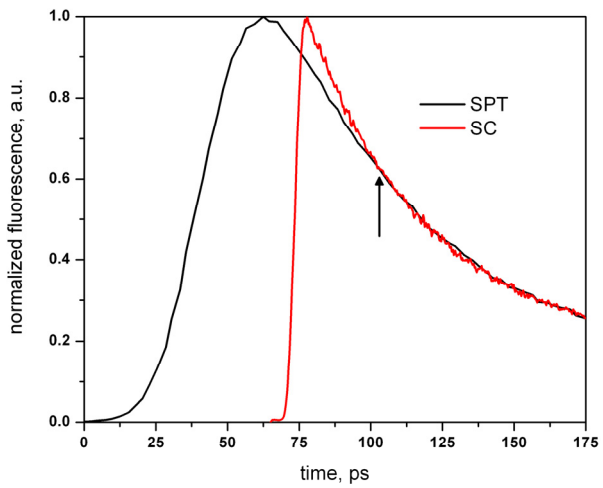

Fig. 7-3 Comparison of the original fluorescence signals recorded at 681 nm from PSII cores with oxidized Q_A. The signals were measured with SPT and SC experimental systems. In the former the PSII particles were excited at 663 nm, while in the latter at 660 nm. The time delay between the two decays is relative.

Fig. 7-3 shows two overlaid fluorescence decays measured with our two time-resolved fluorescence setups: SPT and SC. The clearly noticeable discrepancies, especially in the rise part of the signal detected by the SPT setup (data reported previously in (*33*)) are due to the much broader instrument response in the SPT experiment. However, the presented decays are actually identical, mainly beyond the position indicated with an arrow. Such a comparison is a very easy and at the same time convincing test of the compatibility of the two measurements (sample preparation, laser intensities used, *etc.*). The only difference in the sample preparation was the oxygen-trap used in the SC experiment. Though, neither DAS in Fig. 7-2, nor the fluorescence signals in Fig 7-3, show necessity of using the oxygen-scavenging system, at least along with the experimental conditions as described in section 7.2.

Since both signals in Fig. 7-3 perfectly overlap on the longer time-scale, we find it as a justification for the above assignment of the longer lifetime components found in the course of global analysis.

Additionally, Fig. 7-3 demonstrates that our SC data is capable of describing much faster processes than it was possible in our earlier SPT experiments, and thus rationalizes the resolution of a very fast, subpicosecond lifetime.

Global analysis gives only general idea about the time scales of the processes taking place in the investigated system. In order to resolve all the energy and electron transfer steps one would have to employ more elaborate data analysis procedure, based on the compartmentalization approach. This is certainly also an aim of our studies, however the specificity of the current experiment requires serious modifications of the target analysis software we usually use. For this reason, the full characterization of the processes in PSII will be presented in a future publication.

Nevertheless, on the basis of the information available in the literature on the EET in the isolated antenna complexes (*e.g.* (*73*)) one can speculate about the character of the fast

processes resolved here. Both very short lifetimes resolved in the current study can be assigned to either the energy transfer from the antenna complexes to the RC, or to the intra-antenna energy transfer. Comparison of the 0.2-0.4 ps and 2-3 ps components with the presented here 0.95 ps and 3.5 ps lifetimes shows that probably the two shortest lifetimes in Fig. 7-2 result from a mixture of the two processes. This would once again support the kinetics postulated in the earlier studies (*65*) (*28;33;34*) *i.e.* trap-limited model of the kinetics in PSII cores.

7.4 Conclusions

The present work demonstrates that with our new experimental setup we are able to reproduce the results obtained in the previous studies. Moreover, in addition to the lifetimes described in (*33*) we resolved, due to the much better time resolution of the used experimental method, one additional component in the subpicosecond range (0.95 ps). Therefore, this work confirms our earlier determination of the short lifetime components in the kinetics of the PSII core particles with open RC. The new, very fast component is preliminarily attributed to the mixture of the intra-antenna energy transfer process. This assignment is based on the global analysis of the time-resolved data. In order to describe the investigated ultrafast processes one has to perform more sophisticated data analysis. Also the analogous experiments on the isolated antenna complexes performed with the same experimental setup should bring more understanding to the EET kinetics. Nevertheless, the hypothesis about the two shortest lifetime components (0.95 ps and 3.5 ps) is given, which assumes a mixed contribution to these two components from both, the intra- and inter-complexes excitation energy transfer.

8 Conclusions

8.1 Energy and electron transfer processes

Despite the fact that time-resolved experiments on intact PSII core particles had been conducted already over 20 years ago, the energy transfer and charge separation kinetics was still discussed very controversially when the present work was started. Certainly the early measurements had much lower time resolution and therefore the analysis of the data was limited to the processes slower than 10 ps (*29;64;65*). As a result two main lifetimes were resolved at that time: A component in the order of 30-80 ps, assigned to the energy trapping by charge separation, and a longer-lived one, in the range of 300-500 ps, ascribed to the reduction of the quinone Q_A. Based on these data the "exciton/radical pair equilibrium model" (ERPE model) (*29*) was introduced to describe the energy and electron transfer kinetics in PSII. The ERPE model assumed that the energy equilibration in the PSII antenna complexes, CP 43 and CP 47, as well as between the antenna and the RC was well below the available time resolution of about 10 ps. From this hypothesis naturally emerged the assumption that the CS starts from the equilibrated excited state that spans the antenna and RC chlorophylls. Hence, a trap-limited kinetics in PSII with open RCs was proposed, that actually ignored all the energy transfer steps. Furthermore, unter recently it was believed that the mechanisms of charge separation and electron transfer in the PSII core complexes are analogous to the respective processes in the bacterial RCs (see reviews (*23;25*)). Consequently, the primarily created radical pair was supposed to consist of P_{D1} as the electron donor and $Pheo_{D1}$ as the electron acceptor ($P_{D1}^{+}Pheo_{D1}^{-}$).

Although the ERPE model was widely used for a long time to interpret time-resolved data, recent experimental and theoretical studies (*24;32;66*) criticized the fast energy equilibration hypothesis of the ERPE model. In fact, based on the fairly large distance of about 20 Å from the antenna pigments to the RC Chls (as provided by at the time available X-ray structural data (*60*)), the extreme transfer-to-the-trap limited kinetics in PSII was postulated (*24;32*). This kinetic model assumed that the rate limiting step is the energy transfer from the antenna to the RC pigments, and not the CS process, as claimed in the ERPE model. Interestingly, Vassiliev *et al.* did not resolve faster lifetimes than 60 ps in their time-resolved fluorescence studies (*66*). Nevertheless, the time-resolved absorption difference and fluorescence investigations on CP47-RC particles (*35*) finally revealed faster components, of about 2-6 ps.

In the view of the persisting disagreement on the energy and electron transfer kinetics in PSII core complexes, we decided to perform newly designed time-resolved fluorescence experiments. Our main aim was to resolve the very fast processes, inaccessible in the previous studies on PSII cores, and to clarify their character. For this we used an experimental setup with already higher available time resolution (in the order of 2 ps), and additionally PSII

samples of much higher purity and level of intactness (*53*)(see Chapter 3). In parallel to the work presented here, in our laboratory transient absorption experiments were performed on the same samples (*28*), which demonstrated the existence of the anticipated much faster components (in fact, three lifetimes below 10 ps were revealed). These findings further stimulated our motivation to further explore the trapping kinetics in PSII cores with oxidized Q_A.

In fact, our first fluorescence measurements on PSII with open RCs with the use of the SPT apparatus resulted in the determination of very fast energy transfer components. However, to describe the data in a satisfactory manner, the previously postulated ERPE model (*29*) had to be extended to include additional RPs, as well as two separate antenna compartments, CP43 and CP47. Hence, for the first time the spectrum of the excited RC was resolved (Chapter 3 and ref. (*33*)). As a consequence of the target compartment modeling we resolved a 1.5 ps lifetime component associated with the fast energy equilibration between the antenna complexes and the RC, and a slower component of 7 ps to the CS process (*28;33*). The latter is 5 times faster than assumed in the past (*65*). One additional fast lifetime was revealed (10 ps). However its nature is not clearly attributed to neither the energy nor the electron transfer processes. As in the early studies (*29;32;65;66*), the dominant excited-state decay component has a lifetime of about 42 ps. This component however clearly reflects the rise of the population of RP2 and not of RP1. RP1 and RP2 were assigned to $Chl_{accD1}^{+}Pheo_{D1}^{-}$ and $P_{D1}^{+}Pheo_{D1}^{-}$, respectively. The longest component (351 ps) included in the kinetic scheme is attributed to the electron transfer from $Pheo_{D1}^{-}$ to Q_A, in agreement with the previous studies (*29*). The additional, newly-resolved 111 ps lifetime component is suggested to arise from the protein response to the electron transfer along the RC cofactors chain. It was shown in our later studies (*127*) that the kinetic model including the relaxed form of the second RP ($RP2_{relax}$) also satisfactorily describes the fluorescence decay data. Furthermore, the longest 2.3 ns component has a very small amplitude, which proves the very high quality of the PSII core sample (usually long lifetimes in the fluorescence signal from PSII with open RCs are attributed to PSII with closed RCs and/or to uncoupled Chls, which may be related to some damaged PSII particles). The most important result however is the full agreement of the proposed model based on fluorescence data with the one based on the transient absorption studies (*28*). Moreover, detailed analysis of the total trapping time revealed a very weak dependence of the kinetics on the energy transfer rates. The calculated average excited state decay is in the order of 65 ps, including the energy and charge separation transfer contributions of 9 ps and 56 ps, respectively. The ratio of $\tau_{CS}/\tau_{et} \geq 6$ thus confirmes that the kinetics in PS II cores is strongly trap-limited. Moreover, the earlier assumption about very fast energy transfer in the ERPE model was indeed correct.

Although we were able to resolve much faster processes than it was possible before, we still could not properly separate the internal energy transfer processes in the antenna complexes from the energy transfer between the antenna and the RC. For this reason,

fluorescence measurements with the synchroscan streak camera were conducted (see Chapter 7). Since the streak camera apparatus used is characterized by a time resolution of about 300 fs, we expected to resolve even shorter lifetimes than with the SPT setup. In fact, with the new experimental setup we were able to reproduce the previously obtained results. Furthermore, in addition to the lifetimes described above we resolved, due to the much better time resolution of the used experimental method, one further component in the subpicosecond range (0.95 ps). This new, very short lifetime is attributed to a mixture of the intra-antenna energy transfer processes. Actually, based on the present time-resolved data in the literature on isolated antenna complexes (*73;188*), one would expect to observe even faster energy transfer processes. However, in order to properly describe all the processes in PSII cores one has to apply a more complex compartment target modeling. Yet, appropriate software for such analysis on the streak camera data was at the moment not available. Certainly, the high spectral overlap of the antenna pigments may cause additional difficulties in correct separating the "blue" and "red" subcompartments of the antenna. Hence, the analogous experiments on the isolated antenna complexes performed with the same experimental setup should in the future result in better understanding of the energy transfer kinetics in PSII.

In addition, our data on TyrD-less PSII (Chapter 5) also supports the trap-limited kinetics. The D2-Y160 residue was mutated to phenylalanine. Such mutation should not influence the energy transfer rates between the antenna and the RC, since this amino acid residue is not directly involved in these processes. Actually, as TyrD is supposed to influence the distribution of the positive charge on $P_{D1}P_{D2}$ pair, only the early electron transfer steps should be affected. Indeed, the mutation affects only the slower processes and consequently the fast processes are assigned to the energy transfer from the antenna complexes to the RC. Thus, these experimental findings confirm of a trap-limited kinetics in PSII core complexes and rule out a transfer-to-trap-limited kinetics..

In order to better resolve the energy transfer processes in PSII the time-resolved fluorescence measurements were performed also on PSII cores with closed RCs (see Chapter 4). There, due to the blocked electron transfer from Q_A to Q_B and the negative charge localized on Q_A, the electron transfer steps should be much slower than in the PSII with oxidized Q_A. This in turn should facilitate the separation of the energy and charge transfer processes in the time-domain. Additionally, the energy transfer processes should not be affected by the reduction of Q_A. Data analysis resulted in two kinetic schemes compatible with the data. However, we could not resolve the very fast intra-antenna energy transfer steps, once again due to the limited time-resolution of the applied experimental technique. Nevertheless, we determined the charge separation and recombination rates to be about 3 times slower than in PSII with open RCs. Moreover, we found a larger increase of the fluorescence yield and the average fluorescence lifetime (almost 10-fold in both) upon reduction of Q_A than previously reported (*30;31;34;65*). These two effects of the closing of the RCs can be explained by an

electrostatic repulsive interaction between the negative charge on Q_A and the newly ejected electron in the primary charge separation process.

8.2 Protein dynamics

Interestingly, in contrast to the reported 7-11 ns components (*30;66*), we found in PSII with closed RCs the longest lifetime to be in the order of 3-4 ns. Such a long lifetime was absent in the fluorescence decay of cyanobacterial cells with blocked electron transfer to Q_B. On the basis of pH-dependence experiments changes in the protonation state of the protein as a possible explanation was excluded. Yet, in the work presented here we were not able to determine the origin of such lifetime, present in the isolated PSII complexes but absent in the whole cells. The latter effect is most likely due to spillover to PSI and/or due to energy back transfer to phycobilisomes. However, compartmental data analysis revealed another long lifetime component (about 1 ns) that could be fitted as an additional, free-running component, but alternatively could be also included in the kinetic scheme. Such extension of the kinetic model implies the occurrence of new radical pairs. Nevertheless, taking into account the number and the mutual arrangement of the electron transfer chain cofactors in the RC, it is not very feasible for PSII with closed RCs that there should be formed more than two different RPs. This however does not exclude some potential electrostatic interactions between the charged RP cofactors and the surrounding protein. The electrostatic field created due to the charge separation process affects the protein and drives it towards a more energetically favourable subconformational state. Such an appearance of a relaxed RP will be reflected as an additional lifetime component in the fluorescence decay. Additionally, the conformational change will strongly facilitate the following electron transfer step. Similarly, each new generated RP state will interact with the protein matrix and lead to further structural reorganizations, minimizing the energy of the RP. The dependence of the energy and electron transfer rates on the protein dynamics has been already shown for the bacterial RCs (*39;41;99*) and the isolated D1-D2-cyt *b-559* (*42;43;67;101*). Moreover, after a single turnover a PSII particle does not necessarily return to the initial conformational state from which the charge separation process started. As it was previously shown by McMahon *et al.* (*36*) the structure of the proteins in bacterial RCs differs before and after the electron transfer reaction. Therefore, at least one RP state resolved in the fluorescence decay analysis in PSII with closed RC can be explained as a relaxed RP. Moreover, also the fluorescence decay data of PSII with open RCs was re-analyzed in detail and as a result a satisfactory model was established with a resolved protein relaxation step (RP3 = $RP2_{relax}$).

The results on the PSII with closed RCs, both WT' and TyrD-less mutant (see Chapter 5), show that the charge separation and the subsequent electron transfer processes are regulated and facilitated by the protein surrounding. Free energy calculations show that the total free energy loss corresponding to the steps from the charge separation to the formation of $P_{D1}^{+}Pheo_{D1}^{-}$ and the successive protein rearrangement are comparable. On this basis we

have demonstrated that although TyrD is indirectly involved in the primary processes in PSII, its absence can be efficiently overcome by the additional conformational relaxation of the protein.

8.3 Charge separation mechanism in PSII with reduced Q_A

The careful comparison of the kinetics of PSII with open and closed RCs in WT, WT' and the TyrD mutant preparation resulted in the suggestion that the charge separation mechanism is altered upon the closure of the RCs. Until now the mechanism of charge separation as well as the origin of the formed RPs in PSII with closed RCs were assumed to be identical to those with open RCs. Theoretical calculations (*96*) predicted an increase in the free energy of the first RP of about 90 meV in closed RCs as compared to PSII with open RC, due to the electrostatic repulsions between reduced Q_A and $Pheo_{D1}^-$. A similar behavior was suggested on the basis of time-resolved fluorescence and photovoltage studies (*29;83*). However, these proposals were based on the assumption that pheophytin is in fact reduced in the charge separation process. Free energy losses determined in our study does not exhibit such drastic effect due to the closure of the RCs (Chapter 5 and (*189*)). Actually, the experiments on the TyrD-less mutant show that the early RPs, especially the first one, are influenced by the absence of TyrD in PSII with closed RC. This suggests that the D2 side of the protein, with charged radical species appearing close to the TyrD radical, is involved in the charge separation process in PSII with reduced Q_A. In view of the fact that the relatively short distance to TyrD excludes $Pheo_{D1}$ and $Pheo_{D2}$ as potential partners in RP1, we suggest that P_{D1}, P_{D2}, Chl_{accD1} and Chl_{accD2} are the most probable molecules contributing to RP1 in closed state. Thus, all the results strongly suggest a switch in the CS mechanism upon closure of the RCs that does not involve pheophytin (see also Chapter 4).

Nevertheless, since fluorescence spectroscopy cannot determine the character of RPs, other experimental techniques, like *e.g.* transient absorption difference spectroscopy, should be applied to further clarify the nature of the RP intermediates formed in PSII with closed RC. Additionally, also other mutants could be used to solve this problem, and the still persistent (see (*128;179-181*) or a recent review (*178*)) trapping kinetics issue. It would be interesting from the point of view of both problems to study for example a D1-Q130 PSII point mutant, since this glutamine residue ligates $Pheo_{D1}$. Until now site-directed point mutations related to the RC cofactors were introduced only in *Synechocystis PCC 6803* (*190*), however they were lacking (fully or partially) the oxygen evolution ability, which leaves doubts concerning the intactness of the enzyme. The mutant used in the present work is the first single amino acid mutant introduced in *T. elongatus* that exhibits as high oxygen evolution as the WT preparation (*55*).

8.4 Photoprotection mechanism involves Chl triplet quenching by β-carotene

Our hypothesis concerning the switch in the mechanism of the CS requires the activation of the D2 branch of the RC. In order to further explore the events in PSII with closed RCs, nanosecond transient absorption measurements were performed (Chapter 6 and (*97*)). Since the number of likely cofactors involved in the electron transfer is limited and actually in such conditions (PSII with reduced Q_A) there is basically no possibility to dispose of the electron, the formation of a Chl triplet state seemed plausible. However, such a triplet would be harmful to the enzyme and for this reason Nature usually locates in the vicinity of potentially triplet-forming species some other molecules that have the ability to quench these triplet states. Such an arrangement is found for instance in the antenna complexes, where β-carotenes are in the proximity to some Chls, to protect the whole photosynthetic complex from oxidative damage (*132;133*). A closer look at the latest PSII RC structure (*8*) reveals the presence of a β-carotene on the D2 side (Car_{D2}), that might be involved in the quenching of the triplet Chl formed in the RC. Thus, we were aiming at resolving the potential triplet Car signal that would point to a Chl triplet quenching *via* a triplet-triplet energy transfer with a Car molecule (*97*).

Isolated D1-D2-cyt *b-559* complexes lack Q_A, and therefore the electron transport cannot proceed further than to $P_{D1}^{+}Pheo_{D1}^{-}$. In such preparations a high Chl triplet yield was detected (*150-153*)), however only a very weak signal (yield smaller than 3%) originating from ^{3}Car was found. Moreover, the Chl triplet state was characterized with very long lifetime, of about 1 ms which led to the conclusion that in the isolated PSII RC ^{3}Chl is not quenched by Car. However, in PSII with closed RC a much shorter lifetime of 2–20 μs was determined for the RC ^{3}Chl at 20 K (*158*). Whereas Liu *et al.* (*159*) reported a ^{3}Chl with ca. 10% yield and lifetime around 30 ns at room temperature. The additional, longer than 1 μs lifetime component was attributed to ^{3}Car without identifying its origin. All these findings indicate the quenching of the Chl triplet state in intact PSII with singly reduced Q_A. Interestingly, in PS II particles with doubly reduced Q_A, which is in the neutral form due to double protonation, the same behavior as in isolated D1-D2-cyt *b-559* was reported (*158;160*). In such a preparation the RC ^{3}Chl is again long-lived and is not quenched by carotenoids.

A hypothesis existing in the literature (*158*) explains the short ^{3}Chl lifetime in PSII cores with closed RC by a specific quenching mechanism in which the Chl triplet is transferred to Pheo. Consequently, electron transfer should take place from Q_A^- to ^{3}Pheo forming $Pheo^-$, which in turn would re-reduce Q_A in the usual way. However, this proposal has not been proved experimentally so far. Additionally, it has a weak point in the assumption of identical RPs formed in PSII with open and closed RCs.

In the transient absorption measurements we indeed resolved a triplet Car signal, with a maximum of the absorption difference at 530 nm. ^{3}Car is formed with a lifetime of 190 ns and

a quantum yield of 10-20%, and decays with a lifetime of 7 μs. Such signal was missing in PSII with open RC. Also theoretical estimates demonstrate that the observed triplet transfer time of 190 ns is consistent with a Dexter transfer mechanism. Nevertheless, with the applied experimental technique we were not able to definitely assign the location of the Car molecule that is involved in the RC ^{3}Chl quenching. However, migration of the triplet Chl state to the antenna complex followed by Car quenching was excluded on the basis of the results from the isolated PSII RC. There the RC Chl triplet does not even migrate to the peripheral Chl. In addition, quenching due to interactions with Car_{D1} is also highly unlikely, because of the relatively long distance of 20 Å and the unfavorable arrangement of Car_{D1} to Chl_{D1} (*8*).

In conclusion, we proposed a new photoprotection mechanism that is activated in PSII particles with reduced Q_A. Under such conditions, due to the negative charge localized on Q_A, the electron transfer is directed into the usually inactive D2 branch of the RC. Subsequently a triplet Chl is formed by a radical pair mechanism, which is finally quenched by Car_{D2}. This model explains naturally at the same time why the triplet quenching is not observed in the isolated PSII RCs. In the latter preparation Q_A is lacking, and therefore the electrostatic repulsion cannot be achieved. Thus the triplet state is formed on the D1 side of the RC. However, this ^{3}Chl cannot be quenched due to the large distance to Car_{D1}. Confirmation of this model should be possible by future EPR experiments.

9 Summary

Oxygenic photosynthesis is regarded as one of the most important biological processes given that it provides the molecular oxygen, without which life of many organisms would not be possible. Photosynthesis is an interesting and also challenging issue per se, due to its complexity and the highly evolved diverse contributing processes. Nevertheless, in the present day probably the most crucial reason for a detailed study of the photosynthetic reactions lies in the search of alternative sources of energy. Photosynthetic organisms know how to use solar energy, and the knowledge how they capture light, as well as store and utilize the absorbed energy is essential for the development of artificial systems that mimic the work of plants and algae. For this reason it is necessary to understand the primary processes taking place in the photosynthetic reaction center – the energy transfer properties, pathways, bottlenecks and limitations, as well as the details of the electron transfer processes. Moreover, one should keep in mind that all of the mentioned reactions are perfectly regulated by the surrounding medium, namely protein matrix, to achieve highest efficiencies and least losses.

In the current work the validity of the ERPE model ("exciton/radical pair equilibrium model") introduced by Schatz *et al.* (*29*) was tested in several time-resolved picosecond fluorescence experiments on intact Photosystem II (PSII) core complexes. Data analysis of the kinetics of PSII with open reaction centers (RCs) allowed resolving the very fast (~ 1.5 ps) energy transfer process from the antenna complexes, CP43 and CP47, to the RC, and the slower (7 ps) charge separation (CS) step. Compartmental modeling let us for the first time resolve the fluorescence spectrum of the excited RC and determine the two early radical pairs (RPs) formed prior to the reduction of quinone Q_A. Analysis of the data demonstrates that the kinetics in PSII is definitely trap-limited.

The experiment on PSII with open RCs performed with the synchroscan streak camera (SC) system confirms the presence of lifetimes found in the earlier study. Moreover, the higher time-resolution allowed determination of additional component in a subpicosecond range (0.95 ps) that possibly can be assigned to an even faster energy transfer in the antenna complexes.

An important outcome of the present study concerns the protein dynamics observed in PSII. Such protein relaxation steps were resolved in the PSII particles with both, open and closed RCs. We show that the protein senses the formed RPs and subsequently undergoes relaxation to an energetically more favorable state. Additionally, our studies on the PSII lacking tyrosine D (TyrD) show that the enzyme can maintain its "normal" efficiency in the absence of this amino acid residue. However, the lack of TyrD is clearly visible in the second electron transfer step in PSII with oxidized Q_A. Nevertheless, the surrounding protein balances the lack of TyrD, which is demonstrated in the comparable total losses of free energy in both, WT' (WT with attached His-tag on CP43) and TyrD-lacking PSII.

The studies on the TyrD-lacking PSII support our hypothesis that in PSII with closed RCs pheophytin is not reduced and that the CS and the electron transfer mechanism is altered upon the closure of the RCs. The comparison of the free energy levels of WT' and D2-Y160F mutant PSII suggests that the cofactors on the D2 side of the RC may be involved in electron transfer. It implies activation of the D2 branch when the RCs are closed in the high light conditions. This idea was further investigated with the nanosecond transient absorption spectroscopy. The results show the triplet β-carotene (Car) signal formed on the time scale of about 190 ns, which was assigned to the Car on the D2 branch of the RC. Thus, we propose a photoprotective function for D2 side of the RC. In the suggested mechanism the triplet chlorophyll (^{3}Chl) is formed by a radical pair mechanism on the D2 branch, and subsequently is quenched by the Car_{D2}.

To conclude, present work shows the bottleneck in the energy trapping processes, as well as the importance of the protein surrounding for the efficient performance of the enzyme. Moreover, a new protection mechanism activated in the high light conditions is proposed.

10 Zusammenfassung

Die oxygene Photosynthese wird als einer der wichtigsten biologischen Prozesse betrachtet, da sie den für zahlreiche Organismen überlebenswichtigen molekularen Sauerstoff liefert. Die Photosynthese ist aufgrund ihrer Komplexität sowie ihrer hochentwickelten Prozesse in unterschiedlichen Bereichen ein interessantes und ebenfalls herausforderndes Themengebiet. Gegenwärtig liegt wahrscheinlich der entscheidende Grund für die detaillierte Untersuchung der photosynthetischen Reaktionen jedoch in der Suche nach alternativen Energiequellen. Photosynthetische Organismen sind zur Nutzung von Solarenergie fähig und die Kenntnis darüber, wie diese Licht absorbieren und die aufgenommene Energie speichern sowie nutzbar machen, ist unerlässlich für die Entwicklung künstlicher Systeme nach dem Vorbild von Pflanzen und Algen. Aus diesem Grund ist das Verständnis der im photosynthetischen Reaktionszentrum ablaufenden primären Prozesse notwendig. Dazu gehören einerseits die Eigenschaften des Energietransfers wie beispielsweise Reaktionswege, Engpässe und Grenzen, andererseits die Details der Elektronentransferprozesse. Weiterhin ist von Bedeutung, dass die genannten Reaktionen durch das umgebende Medium, die Proteinmatrix, zur Erzielung höchster Effizienz sowie minimaler Verluste perfekt reguliert werden.

In der vorliegenden Arbeit wurde die Gültigkeit des durch Schatz *et al.* (*29*) eingeführten ERPE Modells („Exciton/Radical Pair Equilibrium Model“) mittels pikosekunden-zeitaufgelöster Fluoreszenzexperimente an intakten Photosystem II (PSII) Kernkomplexen überprüft. Die Datenanalyse der Kinetiken von PSII mit offenen Reaktionszentren (RCs) ermöglichte die Auflösung sehr schneller (~1.5 ps) Energietransferprozesse von den Antennenkomplexen CP43 und CP47 zum RC sowie die Auflösung eines langsameren (7 ps) Ladungstrennungsschrittes (Charge Separation, CS). Die Kompartmentmodellierung ermöglichte uns erstmals die Auflösung des Fluoreszenzspektrums des angeregten Reaktionszentrums sowie die Auflösung der beiden ersten Radikalpaare (RPs), die durch die Reduktion des Quinons Q_A gebildet werden.

Das mit dem Synchroscan Streak Kamera System am PSII mit geöffneten Reaktionszentren durchgeführte Experiment bestätigt die in früheren Studien gefundenen Lebensdauern. Weiterhin ermöglichte die höhere Zeitauflösung die Bestimmung einer zusätzlichen Komponente im Subpikosekunden-Bereich (0.95 ps), die wahrscheinlich dem schnellen Energietransfer in den Antennenkomplexen zugeordnet werden kann.

Eines der wichtigsten Ergebnisse dieser Arbeit bezieht sich auf die im PSII beobachtete Proteindynamik. Derartige Proteinrelaxationsschritte wurden in PSII sowohl mit offenen als auch geschlossenen Reaktionszentren aufgelöst. Wir zeigen, dass das Protein auf die Bildung der RPs reagiert und anschliessend zum energetisch günstigeren Zustand relaxiert. Zusätzlich zeigen unsere Studien am PSII ohne Tyrosin D (TyrD) im RC, dass dieser Komplex die

durchschnittliche Effizienz auch bei Abwesenheit dieses Aminosäurerestes aufweist. Jedoch ist das Fehlen von TyrD in PSII bei oxidiertem Q_A in der zweiten Elektronentransferstufe deutlich sichtbar. Dennoch gleicht die Proteinumgebung das Fehlen von TyrD aus: Dies wird belegt durch die vergleichbaren Gesamtverluste an freier Energie sowohl im WT' (WT mit angebundenem His-tag am CP43) PSII als auch im PSII ohne TyrD.

Die Studie am PSII ohne TyrD stützt unsere Hypothese, dass im PSII mit geschlossenen Reaktionszentren das Pheophytin nicht reduziert wird und dass der Mechanismus der Ladungstrennung sowie des Elektronentransfers sich durch das Schließen der Reaktionszentren ändert. Der Vergleich der Niveaus der freien Energie von WT' PSII und PSII-Mutation (D2-Y160F) deutet darauf hin, dass die Kofaktoren auf der D2-Seite des Reaktionszentrums möglicherweise an dem Elektronentransfer beteiligt sind. Dies impliziert die Aktivierung des D2-Zweiges, falls die Reaktionszentren unter Starklichtbedingung geschlossen sind. Diese Idee wurde mittels nanosekunden-transienter Absorptionsspektroskopie weiter untersucht. Die Ergebnisse zeigen, dass sich das Triplett-ß-Carotenoid (Car)-Signal in einer Zeit von etwa 190 ns bildet, welches dem Car im D2-Zweig des Reaktionszentrums zugeordnet wird. Folglich schlagen wir eine lichtschützende Funktion für die D2-Seite des Reaktionszentrums vor. Bei diesem Mechanismus entsteht durch den Radikalpaarmechanismus im D2-Zweig ein Triplett-Chlorophyll (^{3}Chl), das anschliessend durch das Car_{D2} gelöscht wird.

Die vorliegende Arbeit zeigt insgesamt sowohl den Engpass beim Energieeinfang als auch die Bedeutung der Proteinumgebung für die hohe Effizienz des Enzyms. Zusätzlich wird ein neuer Schutzmechanismus, der unter Starklichtbedingungen aktiviert wird, vorgeschlagen.

References

1. Barber, J. and Archer, M. D. (2004) in *Molecular to Global Photosynthesis* (Archer, M. D. and Barber, J., Eds.) pp 1-41, Imperial College Press, London.
2. Blankenship, R. E. Molecular mechanisms in photosynthesis. 1-321. 2002. Blackwell Publishing.
3. Hall, D. and Rao, K. K. Photosynthesis. 6nd, XIII-214. 1999. Cambridge, United Kingdom, Cambridge University Press.
4. Orr, L. and Govindjee (2007) *Photosynth. Res. 91*, 107-131.
5. Zilinskas, B. A. and Greenwald, L. S. (1986) *Photosynth. Res. 10*, 7-35.
6. Nelson, N. and Ben-Shem, A. (2004) *Nature Reviews Molecular Cell Biology 5*, 971-982.
7. Ferreira, K. N., Iverson, T. M., Maghlaoui, K., Barber, J., and Iwata, S. (2004) *Science 303*, 1831-1838.
8. Loll, B., Kern, J., Saenger, W., Zouni, A., and Biesiadka, J. (2005) *Nature 438*, 1040-1044.
9. Kern, J. and Renger, G. (2007) *Photosynth. Res. 94*, 183-202.
10. Rappaport, F. and Diner, B. A. (2008) *Coordination Chemistry Reviews 252*, 259-272.
11. Rutherford, A. W., Boussac, A., and Faller, P. (2004) *Biochim. Biophys. Acta 1655*, 222-230.
12. Hanley, J., Deligiannakis, Y., Pascal, A., Faller, P., and Rutherford, A. W. (1999) *Biochemistry 38*, 8189-8195.
13. Tracewell, C. A. and Brudvig, G. W. (2003) *Biochemistry 42*, 9127-9136.
14. Telfer, A. (2005) *Photochem. Photobiol. Sci. 4*, 950-956.
15. Kobayashi, M., Maeda, H., Watanabe, T., Nakane, H., and Satoh, K. (1990) *FEBS Lett. 260*, 138-140.
16. Eijckelhoff, C., van Roon, H., Groot, M.-L., van Grondelle, R., and Dekker, J. P. (1996) *Biochemistry 35*, 12864-12872.
17. Oren-Shamir, M., Sai, P. S. M., Edelman, M., and Scherz, A. (1995) *Biochemistry 34*, 5523-5526.
18. Müh, F., Renger, T., and Zouni, A. (2008) *Plant Physiology and Biochemistry 46*, 238-264.
19. Bricker, T. and Frankel, L. (2002) *Photosynth. Res. 72*, 131-146.
20. Yano, J., Kern, J., Irrgang, K.-D., Latimer, M. J., Bergmann, U., Glatzel, P., Pushkar, Y., Biesiadka, J., Loll, B., Sauer, K., Messinger, J., Zouni, A., and Yachandra, V. K. (2005) *Proc. Natl. Acad. Sci. 102*, 12047-12052.
21. Yano, J., Kern, J., Sauer, K., Latimer, M. J., Pushkar, Y., Biesiadka, J., Loll, B., Saenger, W., Messinger, J., Zouni, A., and Yachandra, V. K. (2006) *Science 314*, 821-825.
22. Barber, J. (2008) *Inorg. Chem. 47*, 1700-1710.
23. Diner, B. A. and Rappaport, F. (2002) *Annu. Rev. Plant Biol. 53*, 551-580.
24. Dekker, J. P. and van Grondelle, R. (2000) *Photosynth. Res. 63*, 195-208.
25. Renger, G. and Holzwarth, A. R. (2005) in *Photosystem II: The Light-Driven Water: Plastoquinone Oxidoreductase* (Wydrzynski, T. J. and Satoh, K., Eds.) pp 139-175, Springer Netherland, Berlin.
26. Prokhorenko, V. I. and Holzwarth, A. R. (1998) in *Photosynthesis: Mechanism and Effects* (Garab, G., Ed.) pp 1033-1036, Kluwer Academic Publishers, Dordrecht.
27. Groot, M.-L., Pawlowicz, N. P., van der Wilderen, L. J. G. W., Breton, J., van Stokkum, I. H. M., and van Grondelle, R. (2005) *Proc. Natl. Acad. Sci. USA 102*, 13087-13092.
28. Holzwarth, A. R., Müller, M. G., Reus, M., Nowaczyk, M., Sander, J., and Rögner, M. (2006) *Proc. Natl. Acad. Sci. USA 103*, 6895-6900.
29. Schatz, G. H., Brock, H., and Holzwarth, A. R. (1988) *Biophys. J. 54*, 397-405.
30. Schlodder, E. and Brettel, K. (1988) *Biochim. Biophys. Acta 933*, 22-34.
31. Roelofs, T. A. and Holzwarth, A. R. (1990) *Biophys. J. 57*, 1141-1153.
32. Vasil'ev, S., Orth, P., Zouni, A., Owens, T. G., and Bruce, D. (2001) *Proc. Natl. Acad. Sci. 98*, 8602-8607.
33. Miloslavina, Y., Szczepaniak, M., Müller, M. G., Sander, J., Nowaczyk, M., Rögner, M., and Holzwarth, A. R. (2006) *Biochemistry 45*, 2436-2442.
34. Roelofs, T. A., Lee, C.-H., and Holzwarth, A. R. (1992) *Biophys. J. 61*, 1147-1163.

35. Andrizhiyevskaya, E. G., Frolov, D., van Grondelle, R., and Dekker, J. P. (2004) *Phys. Chem. Chem. Phys. 6*, 4810-4819.
36. McMahon, B. H., Müller, J. D., Wraight, C. A., and Nienhaus, G. U. (1998) *Biophys. J. 74*, 2567-2587.
37. Peloquin, J. M., Williams, J. C., Lin, X., Alden, R. G., Taguchi, A. K. W., Allen, J. P., and Woodbury, N. W. (1994) *Biochemistry 33*, 8089-8100.
38. Woodbury, N. W., Peloquin, J. M., Alden, R. G., Lin, X., Lin, S., Taguchi, A. K. W., Williams, J. C., and Allen, J. P. (1994) *Biochemistry 33*, 8101-8112.
39. Holzwarth, A. R. and Müller, M. G. (1996) *Biochemistry 35*, 11820-11831.
40. Müller, M. G., Drews, G., and Holzwarth, A. R. (1996) *Chem. Phys. Lett. 258*, 194-202.
41. Wang, H. Y., Lin, S., Allen, J. P., Williams, J. C., Blankert, S., Laser, C., and Woodbury, N. W. (2007) *Science 316*, 747-750.
42. Booth, P. J., Crystall, B., Giorgi, L. B., Barber, J., Klug, D. R., and Porter, G. (1990) *Biochim. Biophys. Acta 1016*, 141-152.
43. Roelofs, T. A., Kwa, S. L. S., van Grondelle, R., Dekker, J. P., and Holzwarth, A. R. (1993) *Biochim. Biophys. Acta 1143*, 147-157.
44. O'Connor, D. V. and Phillips, D. (1984) *Time-correlated single photon counting* Academic Press, London.
45. Müller, M. G. Picosekundenuntersuchungen an Photosyntheseantennen. Schriftenreihe des MPI für Strahlenchemie Nr. 65. 1-190. 1992. ISSN 0932-5131. Thesis/Dissertation
46. Holzwarth, A. R., Müller, M. G., Niklas, J., and Lubitz, W. (2005) *J. Phys. Chem. B 109*, 5903-5911.
47. Meyer, M., Mialocq, J.-C., and Perly, B. (1990) *J. Phys. Chem. 94*, 98-104.
48. Braslavsky, S. E. (2007) *Pure and Applied Chemistry 79*, 293-465.
49. Govindjee (2004) in *Chlorophyll a Fluorescence: A Signature of Photosynthesis* (Papageorgiou, G. C. and Govindjee, Eds.) pp 1-42, Springer, Dordrecht.
50. Strasser, R. J., Srivastava, A., and Govindjee (1995) *Photochem. Photobiol. 61*, 32-42.
51. Neubauer, C. and Schreiber, U. (1987) *Z. Naturforsch. 42C*, 1246-1254.
52. Schreiber, U. and Neubauer, C. (1987) *Z. Naturforsch. 42C*, 1255-1264.
53. Kuhl, H., Kruip, J., Seidler, A., Krieger-Liszkay, A., Bunker, M., Bald, D., Scheidig, A. J., and Rögner, M. (2000) *J. Biol. Chem. 275*, 20652-20659.
54. Sugiura, M. and Inoue, Y. (1999) *Plant Cell Physiol. 40*, 1219-1231.
55. Sugiura, M., Rappaport, F., Brettel, K., Noguchi, T., Rutherford, A. W., and Boussac, A. (2004) *Biochemistry 43*, 13549-13563.
56. Schelvis, J. P. M., Germano, M., Aartsma, T. J., and van Gorkom, H. J. (1995) *Biochim. Biophys. Acta 1230*, 165-169.
57. Holzwarth, A. R. (1996) in *Biophysical Techniques in Photosynthesis. Advances in Photosynthesis Research* (Amesz, J. and Hoff, A. J., Eds.) pp 75-92, Kluwer Academic Publishers, Dordrecht.
58. van Stokkum, I. H. M., Larsen, D. S., and van Grondelle, R. (2004) *Biochim. Biophys. Acta 1657*, 82-104.
59. Biesiadka, J., Loll, B., Kern, J., Irrgang, K.-D., and Zouni, A. (2004) *Phys. Chem. Chem. Phys. 6*, 4733-4736.
60. Zouni, A., Witt, H. T., Kern, J., Fromme, P., Krauss, N., Saenger, W., and Orth, P. (2001) *Nature 409*, 739-743.
61. Kamiya, N. and Shen, J.-R. (2003) *Proc. Natl. Acad. Sci. USA 100*, 98-103.
62. Barber, J., Ferreira, K., Maghlaoui, K., and Iwata, S. (2004) *Phys. Chem. Chem. Phys. 6*, 4737-4742.
63. Rögner, M., Boekema, E. J., and Barber, J. (1996) *Trends Biochem. Sci. 21*, 44-49.
64. Nuijs, A. M., van Gorkom, H. J., Plijter, J. J., and Duysens, L. N. M. (1986) *Biochim. Biophys. Acta 848*, 167-175.
65. Schatz, G. H., Brock, H., and Holzwarth, A. R. (1987) *Proc. Natl. Acad. Sci. USA 84*, 8414-8418.
66. Vassiliev, S., Lee, C.-I., Brudvig, G. W., and Bruce, D. (2002) *Biochemistry 41*, 12236-12243.
67. Gatzen, G., Müller, M. G., Griebenow, K., and Holzwarth, A. R. (1996) *J. Phys. Chem. 100*, 7269-7278.

68. Holzwarth, A. R. (2004) in *Molecular to Global Photosynthesis* (Archer, M. D. and Barber, J., Eds.) pp 43-115, Imperial College Press, London.
69. Müller, M. G., Griebenow, K., and Holzwarth, A. R. (1992) *Chem. Phys. Lett. 199*, 465-469.
70. Müller, M. G., Drews, G., and Holzwarth, A. R. (1993) *Biochim. Biophys. Acta 1142*, 49-58.
71. Groot, M.-L., Frese, R. N., de Weerd, F. L., Bromek, K., Pettersson, A., Peterman, E. J. G., van Stokkum, I. H. M., van Grondelle, R., and Dekker, J. P. (1999) *Biophys. J. 77*, 3328-3340.
72. Groot, M.-L., Peterman, E. J. G., van Stokkum, I. H. M., Dekker, J. P., and van Grondelle, R. (1995) *Biophys. J. 68*, 281-290.
73. de Weerd, F. L., van Stokkum, I. H. M., van Amerongen, H., Dekker, J. P., and van Grondelle, R. (2002) *Biophys. J. 82*, 1586-1597.
74. Durrant, J. R., Klug, D. R., Kwa, S. L., van Grondelle, R., Porter, G., and Dekker, J. P. (1995) *Proc. Natl. Acad. Sci. USA 92*, 4798-4802.
75. Prokhorenko, V. I. and Holzwarth, A. R. (2000) *J. Phys. Chem. B 104*, 11563-11578.
76. Novoderezhkin, V. I., Andrizhiyevskaya, E. G., Dekker, J. P., and van Grondelle, R. (2005) *Biophys. J. 89*, 1464-1481.
77. van Grondelle, R. and Gobets, B. (2004) in *Chlorophyll a Fluorescence: A Signature of Photosynthesis* (Papageorgiou, G. C. and Govindjee, Eds.) pp 107-132, Springer, Dordrecht.
78. Pearlstein, R. M. (1982) in *Photosynthesis. Vol.1 Energy Conversion by Plants and Bacteria* (Govindjee, Ed.) pp 293-331, Academic Press, New York.
79. Barber, J. (2003) *Quart. Rev. Biophys. 36*, 71-89.
80. Barber, J. (2006) *Biochem. Soc. Trans. 34*, 619-631.
81. Schlodder, E., Renger, T., Raszewski, G., Coleman, W. J., Nixon, P. J., Cohen, R. O., and Diner, B. A. (2008) *Biochemistry 47*, 3143-3154.
82. Holzwarth, A. R. and Roelofs, T. A. (1992) *J. Photochem. Photobiol. B 15*, 45-62.
83. Gibasiewicz, K., Dobek, A., Breton, J., and Leibl, W. (2001) *Biophys. J. 80*, 1617-1630.
84. Van Mieghem, F. J. E., Searle, G. F. W., Rutherford, A. W., and Schaafsma, T. J. (1992) *Biochim. Biophys. Acta 1100*, 198-206.
85. Vass, I., Gatzen, G., and Holzwarth, A. R. (1993) *Biochim. Biophys. Acta 1183*, 388-396.
86. Goushcha, A. O., Kapoustina, M. T., Kharkyanen, V. N., and Holzwarth, A. R. (1997) *J. Phys. Chem. B 101*, 7612-7619.
87. Goushcha, A. O., Holzwarth, A. R., and Kharkyanen, V. N. (1999) *Phys. Rev. E 59*, 3444-3452.
88. Kleinfeld, D., Okamura, M. Y., and Feher, G. (1984) *Biochemistry 23*, 5780-5786.
89. Goushcha, A. O., Manzo, A. J., Kharkyanen, V. N., van Grondelle, R., and Scott, G. W. (2004) *J. Phys. Chem. B 108*, 2717-2725.
90. Kriegl, J. M. and Nienhaus, G. U. (2004) *Proc. Natl. Acad. Sci. USA 101*, 123-128.
91. Konermann, L., Gatzen, G., and Holzwarth, A. R. (1997) *J. Phys. Chem. B 101*, 2933-2944.
92. Hsu, B.-D., Lee, J. Y., and Pan, R. L. (1986) *Biochim. Biophys. Res. Commun. 141*, 682-688.
93. Wraight, C. A. (1981) *Isr. J. Chem. 21*, 348-354.
94. Arsköld, S. P., Prince, B. J., Krausz, E., Smith, P. J., Pace, R. J., Picorel, R., and Seibert, M. (2004) *J. Luminesc. 108*, 97-100.
95. Müller, M. G., Niklas, J., Lubitz, W., and Holzwarth, A. R. (2003) *Biophys. J. 85*, 3899-3922.
96. Ishikita, H., Biesiadka, J., Loll, B., Saenger, W., and Knapp, E.-W. (2006) *Angew. Chem. ,Int. Ed. 45*, 1964-1965.
97. Martinez-Junza, V., Szczepaniak, M., Braslavsky, S. E., Sander, J., Nowaczyk, M., Rögner, M., and Holzwarth, A. R. (2008) *Photochem. Photobiol. Sci. 7*, 1337-1343.
98. Ehrenberg, A. (2004) *Biochim. Biophys. Acta 1655*, 231-234.
99. Woodbury, N. W. T. and Parson, W. W. (1984) *Biochim. Biophys. Acta 767*, 345-361.

100. Katiliene, Z., Katilius, E., and Woodbury, N. W. (2003) *Biophys. J. 84*, 3240-3251.
101. Barter, L. M. C. and Klug, D. R. (2005) *Chem. Phys. 319*, 308-315.
102. Barter, L. M. C., Schilstra, M. J., Barber, J., Durrant, J. R., and Klug, D. R. (2001) *J. Photochem. Photobiol. A 142*, 127-132.
103. Parak, F. and Frauenfelder, H. (1993) *Physica A 201*, 332-345.
104. Nienhaus, G. U., Mourant, J. R., and Frauenfelder, H. (1992) *Proc. Natl. Acad. Sci. USA 89*, 2902-2906.
105. Frauenfelder, H., Sligar, S. G., and Wolynes, P. G. (1991) *Science 254*, 1598-1603.
106. Papageorgiou, G., Tsimilli-Michael, M., and Stamatakis, K. (2007) *Photosynth. Res.*
107. Maxwell, K. and Johnson, G. N. (2000) *J. Exp. Bot. 51*, 659-668.
108. Govindjee and Papageorgiou, G. C. (1971) in *Photophysiology. 6* (Giese, A. C., Ed.) pp 1-46, Academic Press, New York.
109. Lazar, D. (1999) *Biochim. Biophys. Acta 1412*, 1-28.
110. Krause, G. H. and Weis, E. (1991) *Ann. Rev. Plant Physiol. 42*, 313-349.
111. Johnson, G. N., Boussac, A., and Rutherford, A. W. (1994) *Biochim. Biophys. Acta 1184*, 85-92.
112. Rutherford, A. W. and Faller, P. (2003) *Phil. Trans. R. Soc. Lond. B 358*, 245-253.
113. Kim, S., Liang, J., and Barry, B. A. (1997) *Proc. Natl. Acad. Sci. USA 94*, 14406-14411.
114. Babcock, G. T., Barry, B. A., Debus, R. J., Hoganson, C. W., Atamian, M., McIntosh, L., Sithole, I., and Yocum, C. F. (1989) *Biochemistry 28*, 9557-9565.
115. Hienerwadel, R., Boussac, A., Breton, J., Diner, B. A., and Berthomieu, C. (1997) *Biochemistry 36*, 14712-14723.
116. Boerner, R. J. and Barry, B. A. (1993) *J. Biol. Chem. 268*, 17151-17154.
117. Barry, B. A. and Babcock, G. T. (1987) *Proceedings of the National Academy of Sciences of the United States of America 84*, 7099-7103.
118. Un, S., Boussac, A., and Sugiura, M. (2007) *Biochemistry 46*, 3138-3150.
119. Hienerwadel, R., Diner, B. A., and Berthomieu, C. (2008) *Biochimica et Biophysica Acta (BBA) - Bioenergetics 1777*, 525-531.
120. Buser, C. A., Thompson, L. K., Diner, B. A., and Brudvig, G. W. (1990) *Biochemistry 29*, 8977-8985.
121. Faller, P., Debus, R. J., Brettel, K., Sugiura, M., Rutherford, A. W., and Boussac, A. (2001) *Proc. Natl. Acad. Sci. USA 98*, 14368-14373.
122. Styring, S. and Rutherford, A. W. (1987) *Biochemistry 26*, 2401-2405.
123. Boerner, R. J., Bixby, K. A., Nguyen, A. P., Noren, G. H., Debus, R. J., and Barry, B. A. (1993) *J. Biol. Chem. 268*, 1817-1823.
124. Jeans, C., Schilstra, M. J., Ray, N., Husain, S., Minagawa, J., Nugent, J. H. A., and Klug, D. R. (2002) *Biochemistry 41*, 15754-15761.
125. Diner, B. A., Bautista, J. A., Nixon, P. J., Berthomieu, C., Hienerwadel, R., Britt, R. D., Vermaas, W. F. J., and Chisholm, D. A. (2004) *Phys. Chem. Chem. Phys. 6*, 4844-4850.
126. Kirilovsky, D. L., Boussac, A. G. P., Van Mieghem, F. J. E., Setif, P. R., Ducruet, J.-M. R. C., Yu, J., Vermaas, W. F. J., and Rutherford, A. W. (1992) *Biochemistry 31* , 2099-2107.
127. Szczepaniak, M., Sander, J., Nowaczyk, M., Müller, M. G., Rögner, M., and Holzwarth, A. R. (2009) *Biophys. J. In press*.
128. Raszewski, G. and Renger, T. (2008) *J. Am. Chem. Soc. 130*, 4431-4446.
129. Demmig-Adams, B., Gilmore, A. M., and Adams, W. W. (1996) *FASEB J. 10*, 403-412.
130. Frank, H. A. (1999) in *The Photochemistry of Carotenoids* (Frank, H. A., Young, A. J., Britton, G., and Cogdell, R. J., Eds.) pp 235-244, Kluwer Academic Publihers, Dordrecht.
131. Paulsen, H. (1999) in *The Photochemistry of Carotenoids* (Frank, H. A., Young, A. J., Britton, G., and Cogdell, R. J., Eds.) pp 123-135, Kluwer Academic Publishers, Dordrecht.
132. Cogdell, R. J. and Frank, H. A. (1987) *Biochim. Biophys. Acta 895*, 63-79.

133. Naqvi, K. R., Melo, T. B., Raju, B. B., Javorfi, T., Simidjiev, I., and Garab, G. (1997) *Spectrochim. Acta A 53*, 2659-2667.
134. Krasnovsky, A. A. (1982) *Photochem. Photobiol. 36*, 733-741.
135. Frank, H. A. and Cogdell, R. J. (1996) *Photochem. Photobiol. 63*, 257-264.
136. Frank, H. A. and Violette, C. A. (1989) *Biochim. Biophys. Acta 976*, 222-232.
137. Cogdell, R. J., Howard, T. D., Bittl, R., Schlodder, E., Geisenheimer, I., and Lubitz, W. (2000) *Phil. Trans. R. Soc. Lond. B 355*, 1345-1349.
138. Dexter, D. L. (1953) *J. Chem. Phys. 21*, 836-850.
139. Telfer, A., Dhami, S., Bishop, S. M., Phillips, D., and Barber, J. (1994) *Biochemistry 33*, 14469-14474.
140. Tracewell, C. A. (2004) *Structure 12*, 733-734.
141. Telfer, A., Moore, T. A., Styring, S., Rutherford, A. W., Fromme, P., Aro, E. M., and Brudvig, G. W. (2002) *Phil. Trans. R. Soc. Lond. B 357*, 1431-1440.
142. Ishikita, H., Loll, B., Biesiadka, J., Kern, J., Irrgang, K.-D., Zouni, A., Saenger, W., and Knapp, E.-W. (2007) *Biochim. Biophys. Acta 1767*, 79-87.
143. De Las Rivas, J., Telfer, A., and Barber, J. (1993) *Biochim. Biophys. Acta 1142*, 155-164.
144. Faller, P., Pascal, A., and Rutherford, A. W. (2001) *Biochemistry 40*, 6431-6440.
145. Deligiannakis, Y., Hanley, J., and Rutherford, A. W. (2000) *J. Am. Chem. Soc. 122*, 400-401.
146. Telfer, A., Oldham, T. C., Phillips, D., and Barber, J. (1999) *J. Photochem. Photobiol. B 48*, 89-96.
147. Horton, P. and Ruban, A. V. (2005) *J. Exp. Bot. 56*, 365-373.
148. Holt, N. E., Fleming, G. R., and Niyogi, K. K. (2004) *Biochemistry 43*, 8281-8289.
149. Hoff, A. J., Rademaker, H., van Grondelle, R., and Duysens, L. N. M. (1977) *Biochim. Biophys. Acta 460*, 547-554.
150. Takahashi, Y., Hansson, Ö., Mathis, P., and Satoh, K. (1987) *Biochim. Biophys. Acta 893*, 49-59.
151. Groot, M.-L., Peterman, E. J. G., van Kan, P. J. M., van Stokkum, I. H. M., Dekker, J. P., and van Grondelle, R. (1994) *Biophys. J. 67*, 318-330.
152. Durrant, J. R., Giorgi, L. B., Barber, J., Klug, D. R., and Porter, G. (1990) *Biochim. Biophys. Acta 1017*, 167-175.
153. Yruela, I., Churio, M. S., Gensch, T., Braslavsky, S. E., and Holzwarth, A. R. (1994) *J. Phys. Chem. 98*, 12789-12795.
154. Kamlowski, A., Frankemöller, L., van der Est, A. J., Stehlik, D., and Holzwarth, A. R. (1996) *Ber. Bunsenges. Phys. Chem. 100*, 2045-2051.
155. Van Mieghem, F. J. E., Satoh, K., and Rutherford, A. W. (1991) *Biochim. Biophys. Acta 1058*, 379-385.
156. Noguchi, T. (2002) *Plant Cell Physiol. 43*, 1112-1116.
157. Seibert, M., Picorel, R., Rubin, A. B., and Connolly, J. S. (1988) *Plant Physiol. 87*, 303-306.
158. van Mieghem, F., Brettel, K., Hillmann, B., Kamlowski, A., Rutherford, A. W., and Schlodder, E. (1995) *Biochemistry 34*, 4798-4813.
159. Liu, B., Napiwotzki, A., Eckert, H.-J., Eichler, H.-J., and Renger, G. (1993) *Biochim. Biophys. Acta 1142*, 129-138.
160. Hillmann, B., Brettel, K., van Mieghem, F., Kamlowski, A., Rutherford, A. W., and Schlodder, E. (1995) *Biochemistry 34*, 4814-4827.
161. Deligiannakis, Y. and Rutherford, A. W. (1998) *Biochim. Biophys. Acta 1365*, 354-362.
162. Feikema, W. O., Gast, P., Klenina, I. B., and Proskuryakov, I. I. (2005) *Biochim. Biophys. Acta 1709*, 105-112.
163. Bosch, M. K., Proskuryakov, I. I., Gast, P., and Hoff, A. J. (1996) *J. Phys. Chem. 100*, 2384-2390.
164. Santabarbara, S., Bordignon, E., Jennings, R. C., and Carbonera, D. (2002) *Biochemistry 41*, 8184-8194.
165. Santabarbara, S., Jennings, R. C., and Carbonera, D. (2003) *Chem. Phys. 294*, 257-266.

166. van Leeuwen, P. J., Nieveen, M. C., van de Meent, E. J., Dekker, J. P., and van Gorkom, H. J. (1991) *Photosynth. Res. 28*, 149-153.
167. Schmidt, P., Gensch, T., Remberg, A., Gärtner, W., Braslavsky, S. E., and Schaffner, K. (1998) *Photochem. Photobiol. 68*, 754-761.
168. Mathis, P., Butler, W. L., and Satoh, K. (1979) *Photochem. Photobiol. 30*, 603-614.
169. Peterman, E. J. G., Dukker, F. M., van Grondelle, R., and van Amerongen, H. (1995) *Biophys. J. 69*, 2670-2678.
170. Lampoura, S. S., Barzda, V., Owen, G. M., Hoff, A. J., and van Amerongen, H. (2002) *Biochemistry 41*, 9139-9144.
171. Porra, R. J., Thompson, W. A., and Kriedemann, P. E. (1989) *Biochim. Biophys. Acta 975*, 384-394.
172. Ogrodnik, A., Volk, M., and Michel-Beyerle, M. E. (1988) in *The Photosynthetic Bacterial Reaction Center. 149* (Breton, J. and Vermeglio, A., Eds.) pp 177-183, Plenum Press, New York.
173. Kammel, M., Kern, J., Lubitz, W., and Bittl, R. (2003) *Biochim. Biophys. Acta 1605*, 47-54.
174. Liu, Z., Yan, H., Wang, K., Kuang, T., Zhang, J., Gui, L., An, X., and Chang, W. (2004) *Nature 428*, 287-292.
175. Croce, R., Mozzo, M., Morosinotto, T., Romeo, A., Hienerwadel, R., and Bassi, R. (2007) *Biochemistry 46*, 3846-3855.
176. You, Z. Q., Hsu, C. P., and Fleming, G. R. (2006) *J. Chem. Phys. 124*, 044506-1-054506-10.
177. Santabarbara, S., Agostini, G., Heathcote, P., and Carbonera, D. (2005) *Photosynth. Res. 86*, 283-296.
178. Vassiliev, S. and Bruce, D. (2008) *Photosynth. Res. 97*, 75-89.
179. Broess, K., Trinkunas, G., van der Weij-de Wit, C. D., Dekker, J. P., van Hoek, A., and van Amerongen, H. (2006) *Biophys. J. 91*, 3776-3786.
180. Pawlowicz, N. P., Groot, M. L., van Stokkum, I. H. M., Breton, J., and van Grondelle, R. (2007) *Biophys. J. 93*, 2732-2742.
181. Di Donato, M., Cohen, R. O., Diner, B. A., Breton, J., van Grondelle, R., and Groot, M. L. (2008) *Biophys. J. 94*, 4783-4795.
182. Broess, K., Trinkunas, G., van Hoek, A., Croce, R., and van Amerongen, H. (2008) *Biochimica et Biophysica Acta (BBA) - Bioenergetics 1777*, 404-409.
183. de Weerd, F. L., Palacios, M. A., Andrizhiyevskaya, E. G., Dekker, J. P., and van Grondelle, R. (2002) *Biochemistry 41*, 15224-15233.
184. Hughes, J. L., Picorel, R., Seibert, M., and Krausz, E. (2006) *Biochemistry 45*, 12345-12357.
185. Zazubovich, V. and Jankowiak, R. (2007) *Journal of Luminescence 127*, 245-250.
186. Dang, N. C., Zazubovich, V., Reppert, M., Neupane, B., Picorel, R., Seibert, M., and Jankowiak, R. (2008) *J. Phys. Chem. B 112*, 9921-9933.
187. Reppert, M., Zazubovich, V., Dang, N. C., Seibert, M., and Jankowiak, R. (2008) *J. Phys. Chem. B 112*, 9934-9947.
188. Di Donato, M., van Grondelle, R., van Stokkum, I. H. M., and Groot, M. L. (2007) *J. Phys. Chem. B 111*, 7345-7352.
189. Szczepaniak, M., Sugiura, M., and Holzwarth, A. R. (2008) *Biochimica Biophysica Acta, 1777*, 1510-1517.
190. Diner, B. A., Schlodder, E., Nixon, P. J., Coleman, W. J., Rappaport, F., Lavergne, J., Vermaas, W. F. J., and Chisholm, D. A. (2001) *Biochemistry 40*, 9265-9281.

List of publications

Publications:

Y. Milaslavina, M. Szczepaniak, M.G. Müller, J. Sander, M. Nowaczyk, M. Rögner, A.R. Holzwarth (2006) "Charge separation kinetics in intact photosystem II core particles is trap-limited. A picosecond fluorescence study." Biochemistry, **45**: 2436-2442.

M. Szczepaniak, M. Sugiura, A.R. Holzwarth (2008) "The role of TyrD in the electron transfer kinetics in photosystem II." Biochimica et Biophysica Acta, **1777**: 1510-1517.

V. Martínez-Junza, M. Szczepaniak, S.E. Braslavsky, J. Sander, M. Nowaczyk, M. Rögner, A.R. Holzwarth (2008) "A new photoprotection mechanism in photosystem II cores with closed reaction center." Photochemical & Photobiological Sciences, **7**: 1337-1343.

M. Szczepaniak, J. Sander, M. Nowaczyk, M.G. Müller, M. Rögner, A.R. Holzwarth (2009) "Charge separation, stabilization, and protein relaxation in photosystem II core particles with closed reaction center." Biophysical Journal, **96**: 621-631.

Conference proceedings:

M. Szczepaniak, J. Sander, M. Nowaczyk, M.G. Müller, M. Rögner, A.R. Holzwarth (2007) "Influence of the protein environment on the regulation of the Photosystem II activity - a time resolved fluorescence study" in: *14th International Congress of Photosynthesis*, Glasgow. Springer Netherlands.

V. Martinez-Junza, M. Szczepaniak, S.E. Braslavsky, J. Sander, M. Rögner, A.R. Holzwarth (2007) "Triplet photocprotection by carotenoid in in intact photosystem II cores" in: *14th International Congress of Photosynthesis*, Glasgow. Springer Netherlands.

Oral presentations:

"Charge separation and protein relaxation in closed photosystem II cores" Intro2 network workshop, 2005, Loosdrecht, Netherlands.

"Ultrafast spectroscopic studies on cyanobacterial and plant photosystems: PSI and PSII" Workshop „Emergent dynamic properties of photosynthetis organisms", 2006, Nove Hrady, Czech Republic.

"Charge separation and protein relaxation in cyanobacterial PSII core complexes studied in closed state" 15. Photosynthese Workshop Nord-West, 2006, Aachen, Germany.
"Other parts of the PSII puzzle" Intro2 network symposium "Role of Photosystem II", 2006, Prague, Czech Republic.

"Time-resolved fluorescence kinetics of Photosystem II" Intro2 network symposium, 2008, Lanzarote, Spain.

Poster presentations:

"Charge separation and protein relaxation in Photosystem II core complexes" Gordon Research Conference in Photosynthesis, 2006, Smithfield, US.

"psbA3 vs. WT – is there any difference in the primary processes?" SFB663 meeting, 2007, Bad Münstereifel, Germany.

"Electron transfer processes in cyanobacterial Photosystem II In the light of protein relaxation" 16. Photosynthese Workshop Nord-West, 2007, Mülheim, Germany.

"Influence of the redox-active tyrosine D on the electron transfer kinetics in cyanobacterial Photosystem II" PS2007 Light-Harvesting Systems Workshop, 2007, Drymen, United Kingdom.

"Influence of the protein environment on the regulation of the Photosystem II activity – a time-resolved fluorescence study" Photosynthesis Congress 2007, Glasgow, United Kingdom.

"A study of the electron transfer pathways in PSII with oxidized/reduced Q_A" 17. Photosynthese Workshop Nord-West, 2008, Bochum, Germany.

Acknowledgments

First of all I would like to thank the whole ultrafast group from BAC MPI. I would like to express my appreciation especially to my supervisor, Prof. Alfred Holzwarth, for giving me the opportunity to join his group. Dr Marc Müller is acknowledged for his assistance with laser systems, data analysis software and help with the translation of the Summary in this work. Michael Reus was always there, never refusing to help even with the silliest problems one can encounter in the lab. I would like to thank also my supervisor from Düsseldorf University, Prof. Georg Pretzler, for his support and willingness to discuss problems and questions that arose during my studies, even though photosynthesis does not lie in the immediate field of his research. I am grateful to all our collaborators for providing us kindly with the samples, especially to Julia Sander from Bochum University for nearly unlimited PSII supply. I also owe a lot to my friend, Chavdar Slavov, who brought not only a lot of fun, joy and music in my life and in the office we used to share; I am thankful to Chavdar for all the scientific discussions we had, the advises he gave me when needed, and most importantly for his permanent support. Thanks to all the group members for sharing the affection for spicy food and great cocktails, especially to Christopher, who helped with the translation into/from German many important documents, including Summary chapter in this thesis. I should not forget to thank the 'Catan team' for our battles for sheep and wood, usually lasting from dusk till dawn. And at last, but not least, I want to express my gratitude to my mother for her belief in me.